THE
PHYSICAL
SOCIETY

MEMOIRS

OF THE

COLLEGE OF SCIENCE

UNIVERSITY OF KYOTO

SERIES A

VOL. XXVIII, No. 4

May, 1958

KYOTO

Memoirs of the College of Science, University of Kyoto, Series A,
Vol. XXVIII, No. 4, Article 1, 1958.

THE EFFECT OF ELECTRIC FIELD UPON THE STRUCTURE OF THIN FILMS OF SOME DIPOLAR LONG-CHAIN MOLECULES

BY

Kensuke HARADA and Tōru SAKAI

(Received November 29, 1957)

ABSTRACT

The effect of static electric field applied to thin films of stearic acid and octadecyl alcohol upon the structure of the films was investigated by the method of electron diffraction. The electric field was applied when the films were formed by evaporation of solution or by melting. In the case of stearic acid, some definite relation between the orientation of the crystals in the film and the direction of the applied field was found. While, in the case of octadecyl alcohol, the applied field affected the lattice dimension of the crystals.

1. Introduction

The investigation of crystal structure of long-chain compound was initiated by A. Müller (**1**) in his X-ray diffraction analysis of a paraffin. Later, C. A. Murison (**2**), J. J. Trillat and H. Motz (**3**), C. H. MacGillavry (**4**) and others examined, by the method of electron diffraction, the molecular arrangement in thin films of some long-chain compounds formed on solid substrates. The structure of built-up films and polymorphism of these substances were also investigated by L. H. Germer and K. H. Storks (**5**) and P. A. Thiessen and T. Schoon (**8**) respectively. Temperature dependence of the molecular structure of such films were observed by K. Tanaka (**6**). Y. Kakiuchi (**7**) and M. Ida (**9**) have examined the crystal arrangement in the specimen of some long-chain compounds prepared by cooling from molten state under the presence of strong electric field. In the following, some results of observation on the effect of electric field applied upon the molecular arrangement in the films of stearic acid and octadecyl alcohol.

2. Experimental method

As the specimen holder, we prepared a narrow parallel slit of 0.2~0.3 mm width and 8 mm length with two metal plates, and covered it with thin film of Formbar. Static electric field of about 9 kV/cm was applied between these two metal plates. Various test specimens were prepared by dropping a drop of freshly prepared benzene

solution of the compound on the holder and then letting it to evaporate, or by melting a small piece of the compound on the holder. The specimens thus prepared were investigated by the transmission method of electron diffraction. The applied voltage to the electron-gun was about 40 kV.

3. Results and discussion

Case of stearic acid

(a) *Thin films prepared by evaporation of benzene solution*

Diffraction patterns of thin films prepared from benzene solution in the absence of an electric field are shown in Plates 1 and 2, while those of films prepared under the presence of an electric field are shown in Plates 3, 4 and 5, as examples. Thin films prepared in the absence of an electric field have different structures according to some condition of preparation. In most cases the film consists of two crystal groups: one with their c-axes inclined to the surface of the film, while in the other the said axes are nearly parallel to the same surface.

It is known that there are various types of structure of the crystal. In the present case the crystals in the film seemed to be somewhat deformed from the known ε_2-type whose monoclinic unit cell has the dimensions of $a=9.12$ Å, $b=4.94$ Å and $\beta=56°11'$. The observed lattice spacings for various thin films examined are tabulated in Table 1 in the columns 1~4. The values in the sixth column are the spacings

Table 1. (Å-unit)

1	2	3	4	5	ε_2-type
	4.56 s				4.57(112)
		4.46 s			
4.35 s	4.35 s	4.35m	4.30 s		4.36(111)
4.17 s					4.17(201)
4.13 ss	4.12 ss	4.12 ss	4.12 ss	4.15 s	4.12(110)
		3.75m		3.78 s	3.79(200)
3.35m			3.31m		3.33(019)
3.27m		3.22w	3.23m		3.25(114)
3.17m					3.15(201)
2.48 s	2.49 s	2.48 s	2.47 s	2.47w	2.47(020)
2.38m	2.375w		2.38w		2.38(01, 15)
2.33m			2.34m		2.34(120)
2.16w	2.17w		2.16w		2.18(222)
2.05m	2.06m	2.06m	2.04m		2.06(220)
	1.63w		1.61w		
1.59m					
1.44w					1.44(510)
1.28w					1.24(430)

calculated for ε_2-type. Some of these thin films show relatively simple diffraction patterns as shown in Plate 2. The observed spacings for such a film are shown in the fifth column. This crystal is considered as the elementary type, i. e. the crystal having the unit cell of $a=4.94$ Å, $b=7.58$ Å and $\beta=90°$ assumed by T. Schoon. In each case, the crystals in the thin film cannot be considered as to be composed of crystals of a single type.

When thin films of stearic acid are prepared under the presence of an electric field, the small crystals in the film have a general tendency of definite orientation in which the b-axis or the a-axis of the crystal is arranged perpendicularly to the applied electric field. The values of the lattice spacings observed in the cases of

Table 2. (Å-unit)

1	2	3	Müller	Germer
		4.35m		
		4.07m		
3.86 s	3.87m	3.87m		3.88(200)
	3.67m	3.70m	3.69(020)	
4.16 s	4.16 s	4.16 s		4.18(110)
	4.12 s	4.12 s	4.12(110)	
	2.96m	2.97m	2.96(120)	
2.47m	2.48 s	2.47m	2.48(200)	2.48(020)
		2.33w		
2.05w		2.13w	2.11(220)	2.09(220)
1.61w		1.60w	1.61(310)	1.62(130)

Plates 3, 4 and 5 are shown in Table 2 in the columns 1, 2 and 3 respectively. From the observed spacings, the crystals in a film which has comparatively regular arrangement of crystals as shown in Plate 3 are considered to be similar to those found by Germer and Storks in a built-up film of stearic acid, which was investigated by them in detail. The values in the fourth and the fifth columns in Table 2 are respectively the calculated spacings for the values $a=5.546$ Å, $b=7.38$ Å, $c=48.84$ Å and $\beta=63°38'$, which were given to the unit cell of a single crystal of stearic acid by Müller as the result of his X-ray examination, and those calculated for the unit cell of the crystal in the built-up film, whose dimensions were given by Germer and Storks as $a=8.27$Å, $b=4.96$Å, $c=49.0$Å and $\beta=63°38'$. As can be seen in Table 2, a lattice plane having a spacing 3.87Å is found in all diffraction patterns examined and the plane is perpendicular to the applied electric field. And a lattice plane 3.7Å also appears perpendicularly to the field. Occasionally, lattice planes 4.05Å and 4.35Å appeared.

From these observations it can be seen that the crystals in a thin film prepared in an electric field have tendencies to lie in such a manner that their b-axes are

perpendicular to the applied field when the crystals are of Müller type, while their *a*-axes are perpendicular to the field when the crystals are of Germer type. Frequently, these two types of crystals appeared in a film. In every case, the axes of the long-chain molecules have a tendency to arrange themselves perpendicularly to the applied field.

(b) *Thin films prepared by melting*

Plates 6 and 7 show diffraction patterns of specimens prepared by heating a film of stearic acid on the holder up to about 85°C in air and by succesive cooling-down to room temperature without an applied electric field. These specimens show ring patterns as shown in Plate 6 and rarely single crystal patterns as shown in Plate 7. The lattice spacings observed in Plates 6 and 7 are shown in Table 3. The spacings obtained from Plate 6 coincide well with those obtained from Plate 7. But, both of these spacings do not coincide with the spacings of crystals prepared by evaporation of benzene solution in the absence of applied field. These films consist of mixtures of two kinds of crystals with slightly different cross-sections. In the case of Plate 7, the *c*-axes of both crystals are parallel to each other and their (100) and (010) planes are also parallel to each other respectively. The cross-section of one kind of crystals is shown in Fig. 1. Ring pattern in Plate 6 shows that the film has fibrous structures of two kinds of crystal appeared in Plate 7 and each of them has its *c*-axis as fiber axis.

Table 3. (Å-unit)

Plate 6	Plate 7
7.86 w	
4.83 w w	
4.50 m	4.58 s (spot)
4.42 s	4.42 w (ring)
4.32 s (diffuse)	4.38 s (spot)
4.12 m	4.12 w (ring)
	4.11 s (spot)
3.93 w	3.95 w (spot)
3.84 s	3.83 s (spot)
	3.81 w (ring)
3.77 s (diffuse)	3.79 w (ring)
3.67 s	3.65 s (spot)
2.48 w	2.56 s (spot)

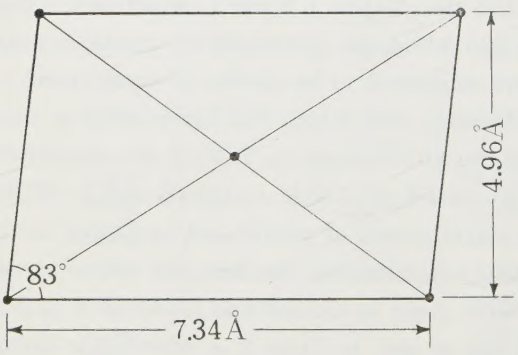

Fig. 1

A pattern such as shown in Plate 8 is always obtained for specimens prepared under an applied electric field of about 9 kV/cm. From this, it is considered that the crystals grown under an electric field always arrange themselves in fibrous structure. As can be seen in Fig. 2, the schematic representation of Plate 8, the pattern consists of spots on parallel lines with equal distances of two groups (K

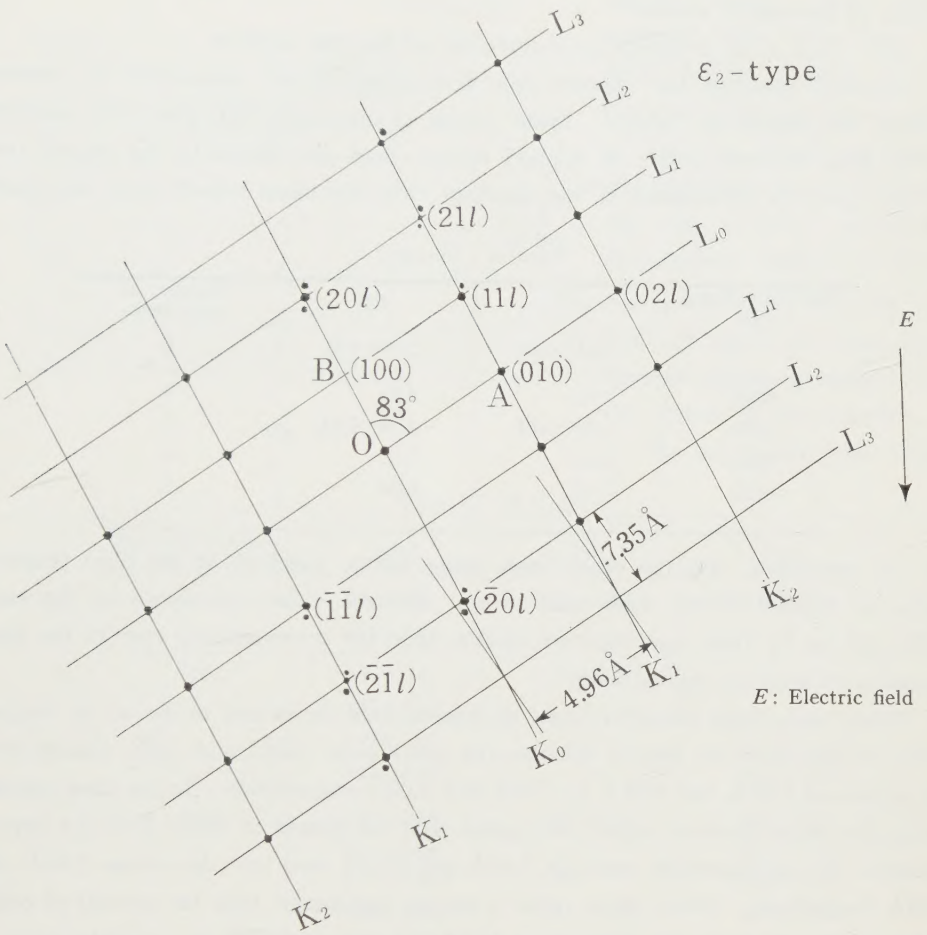

Fig. 2

and L). Each spot on the intersection of these lines is split up into several spots in the direction of applied electric field. In Fig. 2, the spacings corresponding to the lengths of OA and OB are 4.96Å and 7.35Å respectively. And the angle between K-lines and L-lines is about 83°. Therefore, the film contains mostly the crystals of the same dimensions as that shown in Fig. 1 and except them there are a few kinds of crystals with slightly different dimensions as can be seen from the splitting-up of the spots. The orientations of the microcrystals of these kinds are not parallel to each other but distributed in the angular range of about 10°. But there could not be found any definite relation between the orientation of the crystal around its c-axis and the direction of the applied electric field excepting that the splitting-up of each spot always occurred in the direction of the applied field.

Case of octadecyl alcohol

(a) *Thin films prepared by evaporation of benzene solution*

Observed spacings for various thin films prepared by evaporation of benzene solution are shown in Table 4. Mean values of observed (100) and (010) spacings for six films prepared under no applied electric field are shown in the second row. In this case, the differences of the spacings from the mean values were very small

Table 4. (Å-unit)

Applied voltage V/cm	(100)	(010)	Number of specimens
0	7.44±0.04	5.05±0.02	6
9000	7.21	4.93	1
9000	7.26±0.04	4.95±0.04	4
6000	7.36	5.02	5
6000	7.44	5.04	2

for six specimens. On the other hand, these lattice spacings of the films prepared under an applied electric field took several different values as shown in the same table and all of these spacings are smaller than the corresponding ones of the films prepared without an applied field.

When these films prepared under an applied field are heated in air at an temperature of about 40°C for several minutes, the spacings of (100) and (101) change from the values of 7.26Å and 4.95Å to 7.34Å and 5.03Å respectively. In the same manner, when the films prepared under no applied field are heated at about 50°C for several minutes, the corresponding spacings 7.44Å and 5.03Å turn into the values 7.34Å and 5.03Å respectively. From these facts it can be considered that the crystal of orthorhombic system with the dimensions $a=7.34$Å and $b=5.03$Å is a stable form of octadecyl alcohol in such films. Plate 9 is an example of the diffraction patterns of thin films prepared under an electric field.

(b) *Thin films prepared by melting*

Plates 10 and 11 are examples of diffraction patterns of thin films prepared by melting without and with an applied electric field respectively. Figs. 3 and 4 are the schematic representations of these plates. In each case, the film contains

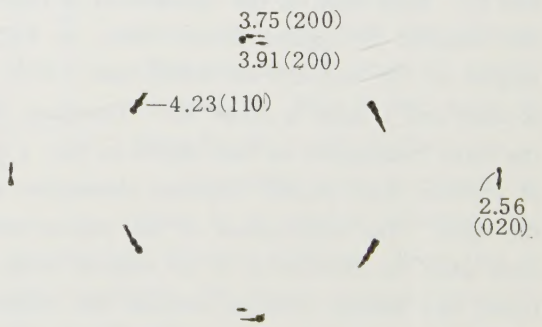

Fig. 3

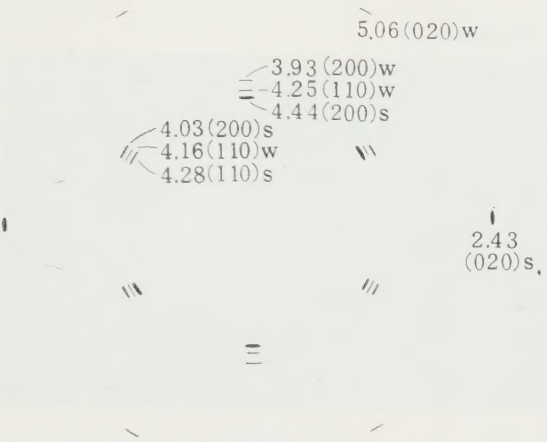

Fig. 4

several crystal forms slightly different from each other. The mean lattice spacings observed for many specimens are tabulated in Table 5. These spacings are different from those observed in the case of films prepared by evaporation. Plate 12 is a reflection pattern of a film and shows that all molecular axes in the film are nearly perpendicular to the surface of the substrate.

As can be seen from Table 5,

Table 5. (Å-unit)

Applied voltage V/cm	(100)	(010)	(110)
0	7.5 ±0.1	5.1 ±0.04	4.22±0.06
	7.92±0.12	〃	〃
5000	7.3 ±0.04	5.05±0.07	4.16±0.03
	7.48±0.04	〃	〃
	7.72±0.04	〃	〃
	8.12±0.04	〃	4.33±0.02
9000	7.3 ±0.04	4.87±0.02	4.05±0.03
	7.9 ±0.04	〃	4.16±0.02
	8.1 ±0.06	5.06	4.26±0.03
	8.94±0.06	4.87±0.02	4.26±0.03

there are many kinds of crystal forms in the case of applied field and they have larger spacings than those formed under no applied field. It seems from Fig. 4 that the orientations of the orthorhombic crystals are such that they are formed a single high temperature hexagonal crystal through the transition point of the compound. Though we could not find any definite relation between the orientation of the crystals in the film and the direction of the applied electric field as in the case of stearic acid, the variation of the lattice dimensions seems to be caused by the applied field, since the latter affects the interaction between polar molecules of the alcohol when the crystal is formed.

In conclusion, the writers wish to express their sincere thanks to Prof. K. Tanaka for his kind guidance throughout the present research.

REFERENCES

1. A. MÜLLER, Proc. Roy. Soc., A **120** (1928), 437.
2. C. A. MURISON, Phil. Mag., **17** (1934), 201.
3. J. J. TRILLAT and H. MOTZ, Trans. Faraday Soc., **31** (1935), 1127; Z. Krist., **91** (1935), 248.
4. C. H. MACGILLAVRY, Z. Krist., **98** (1938), 407.
5. L. H. GERMER and K. H. STORKS, Proc. Nat. Acad., **23** (1937), 390; J. Chem. Phys., **6** (1938), 280.
6. K. TANAKA, Memoirs Coll. Sci., Kyoto Univ., **21** (1938), 21; **22** (1939), 377; **23** (1941), 195.
7. Y. KAKIUCHI, Sci. Pap. I. P. C. R., **40** (1943), 189.
8. P. A. THIESEN and T. SCHOON, Z. Phys. Chem., B **3** (1937), 216.
9. M. IDA, J. Phys. Soc. Japan, **10** (1955), 318.

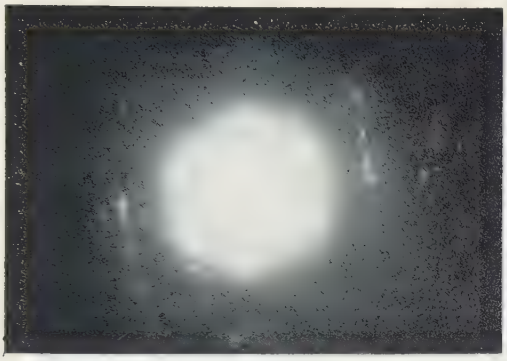

Plate 1

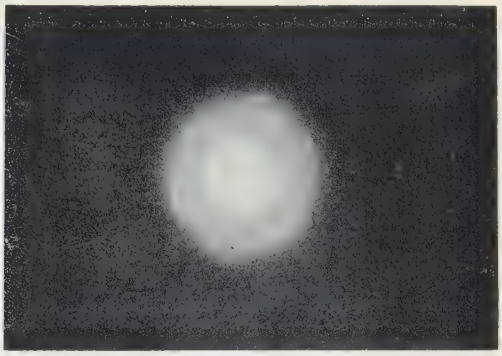

Plate 2

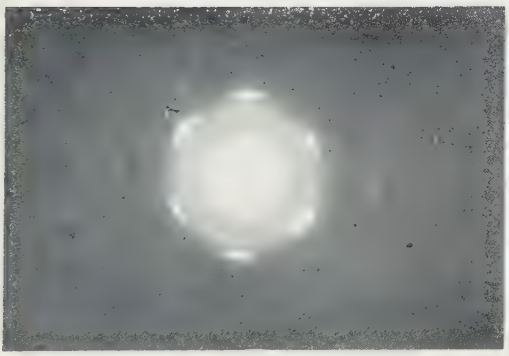

Plate 3

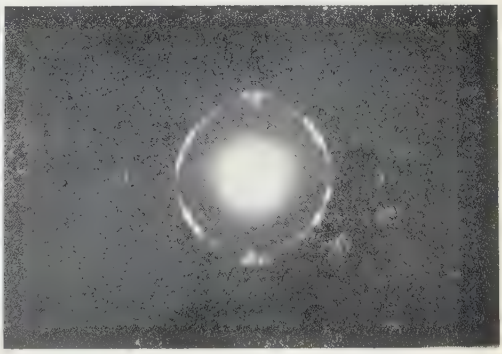

Plate 4

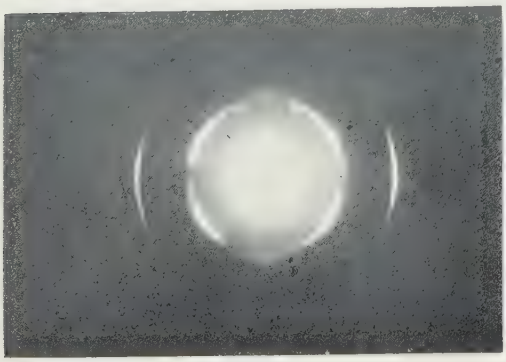

Plate 5

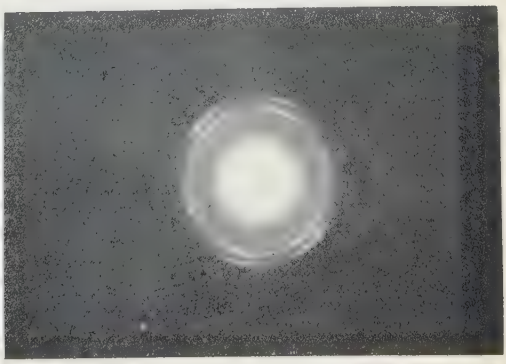

Plate 6

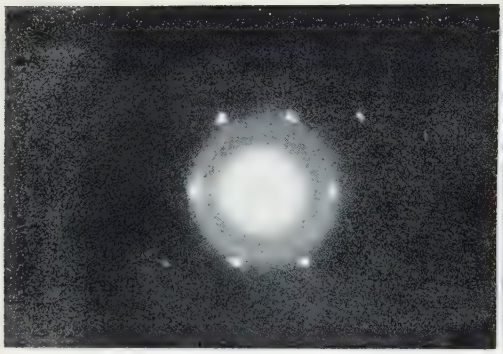

Plate 7

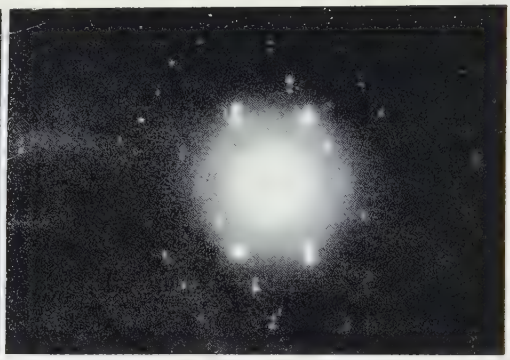

Plate 8

Plate 9

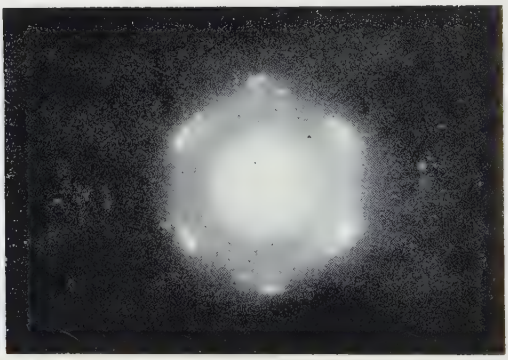

Plate 10

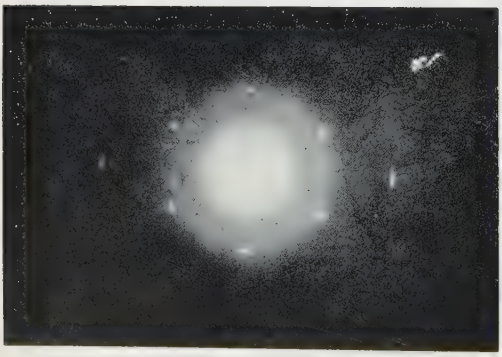

Plate 11

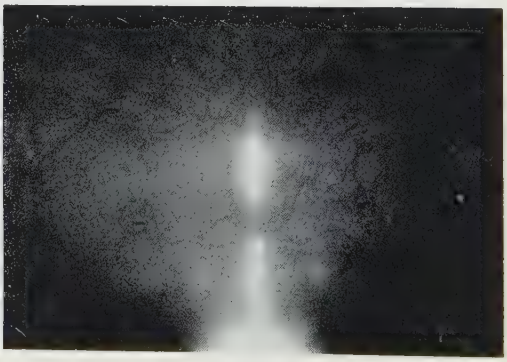

Plate 12

Memoirs of the College of Science, University of Kyoto, Series A,
Vol. XXVIII, No. 4, Article 2, 1958.

INTRODUCTION OF THE TRANSLATIONAL OPERATOR IN FREQUENCY DOMAIN AND TREATMENT OF CERTAIN LINEAR DIFFERENTIAL EQUATIONS, I.

BY

Tadashi WATANABE

(*Received December 5, 1957*)

ABSTRACT

In this paper, the author describes a method of solving the ordinary linear differential equation whose coefficients are E-type functions, i. e. sums of exponential functions of independent variable by introducing the translational operator in frequency domain. And further, the Maxwell equations in the medium whose material constants are E-type functions of time, are reformulated in the frequency domain.

1. Introduction

It is well known that the ordinary linear differential equation with constant coefficients can be easily solved by applying the Laplace transform. Pipes (**1**) attempted to solve the ordinary linear differential equation whose coefficients are arbitrary functions of independent variable, by applying the Laplace transform. He tried to obtain the solution in the form of power series of parameter. But he derived only a few initial terms in the series for an example given by him though he obtained the complete solution in the case when the original differential equation is an ordinary linear differential equation of the first order.

The author attempts to obtain the solution of the linear differential equation by applying the Laplace transform, under the restriction that the coefficients are expressed by periodic functions* of independent variable, or more generally, expressed by the sums** of exponentials of independent variable. Such a function as the latter is called E-type function in the following. When the coefficients are restricted to E-type functions, we can introduce the author's translational operator in frequency domain into the transformed equation and derive, in the frequency domain, the general term in the series of the solution that has not been derived by Pipes. Furthermore, without the trouble of directly obtaining the solution, various ideas such as impedance, reflection coefficient, etc. in the linear fixed electrical network*** can be naturally

* It is assumed that they can be expanded in Fourier series.

** The infinite series may be included, if the convergency is assured.

*** A linear electrical network whose circuit elements are constant in time.

extended to the linear varying electrical network*.

In part I, the author considers the method of solving the ordinary linear differential equation whose coefficients are of E-type, by introducing the translational operator. And further, the operator is introduced into the Maxwell equations in the medium where the material constants ε (dielectric constant) and μ (magnetic permeability)** are E-type functions of the time.

And it is discussed how the propagation of the electromagnetic waves in the wave guide filled with a material of fixed constants is extended to the case of a material of varying constants.

In part II, it will be discussed how the various ideas in the linear fixed electrical network are extended to the linear varying electrical network.

2. Introduction of the translational operator into the ordinary linear differential equations with E-type coefficients

The E-type function has the form:

$$a_i(t) = \sum_{\alpha=0}^{\nu} \sum_{k=-Ni,\alpha}^{Ni,\alpha} A_k^{(i)}(\alpha)\, e^{ik\omega_\alpha t},$$

and the ordinary linear differential equation with such coefficients as $a_i(t)$ has the following form:

$$\sum_{i=0}^{n} a_i(t) \frac{d^{n-i}}{dt^{n-i}} y(t) = x(t). \tag{2.1}$$

Taking the Laplace transforms of both sides of (2.1), we obtain:

$$L\left(\sum_{i=0}^{n} a_i(t) \frac{d^{n-i}}{dt^{n-i}} y(t) \right) = L(x(t)).***$$

Then, putting $p_{k,\alpha} = p - ik\omega_\alpha$, it can be reduced to:

$$\sum_{i=0}^{n} \sum_{\alpha=0}^{\nu} \sum_{k=-Ni,\alpha}^{Ni,\alpha} A_k^{(i)}(\alpha) \left\{ p_{k,\alpha}^{n-i}\, Y(p_{k,\alpha}) - \sum_{j=0}^{n-i-1} p_{k,\alpha}^{n-(i+j+1)}\, y^{(j)}(0) \right\} = X(p), \tag{2.2}$$

where

$$\left.\begin{aligned} X(p) &= L(x(t)), \\ Y(p) &= L(y(t)), \end{aligned}\right\} \qquad y^{(j)}(0) = \left\{ \frac{d^j y(t)}{dt^j} \right\}_{t=0}.$$

* A linear electrical network whose circuit elements are varying in time. In the present paper, the consideration is restricted only to a network whose circuit elements can be expressed by E-type functions.

** In the dispersive medium, ε and μ cannot be defined in the time domain, but can be defined in the frequency domain (3). They sometimes depend on the external electric and magnetic fields as well as on the frequency as parameters. The time variation of ε and μ means that these parameters are varying in time. The description "ε and μ are E-type functions of time" means that the above-mentioned parameters are so varying as to be expressed by E-type functions of the time.

*** L and L^{-1} denote respectively Laplace transform and its inverse.

Further, putting

$$X'(p) = X(p) + \sum_{i=0}^{n} \sum_{\alpha=0}^{\nu} \sum_{k=-Ni,\alpha}^{Ni,\alpha} A_k^{(i)}(\alpha) \sum_{j=0}^{n-i-1} p_{k,\alpha}^{n-(i+j+1)} y^{(j)}(0) , \tag{2.3}$$

the expression (2.2) becomes:

$$\sum_{i=0}^{n} \sum_{\alpha=0}^{\nu} \sum_{k=-Ni,\alpha}^{Ni,\alpha} A_k^{(i)}(\alpha) p_{k,\alpha}^{n-i} Y(p_{k,\alpha}) = X'(p) . \tag{2.4}$$

Now, when $f(p)$ is an arbitrary function of p, the author introduces the operator $T(\omega_\alpha)$ defined by the following expression, and calls it the translational operator in frequency domain:

$$T(\omega_\alpha) f(p) = f(p - i\omega_\alpha) . \tag{2.5}$$

Substituting this operator into (2.4), we obtain:

$$\{ \sum_{i=0}^{n} \sum_{\alpha=0}^{\nu} \sum_{k=-Ni,\alpha}^{Ni,\alpha} A_k^{(i)}(\alpha) T^k(\omega_\alpha) p^{n-i} \} Y(p) = X'(p) , \tag{2.6}$$

where

$$X'(p) = X(p) + \sum_{i=0}^{n} \sum_{\alpha=0}^{\nu} \sum_{k=-Ni,\alpha}^{Ni,\alpha} A_k^{(i)}(\alpha) \sum_{j=0}^{n-i-1} T^k(\omega_\alpha) p^{n-(i+j+1)} y^{(j)}(0) . \tag{2.7}$$

When the factor to $Y(p)$ is denoted by $S(T, p)$*, the equation becomes:

$$S(T, p) Y(p) = X'(p) , \tag{2.8}$$

or with an inverse operator $S^{-1}(T, p)$,

$$Y(p) = S^{-1}(T, p) X'(p) . \tag{2.8'}$$

Thus, if $S^{-1}(T, p)$ is found, $Y(p)$ can easily be obtained by (2.8') and then the solution of the original equation can be derived by taking the inverse Laplace transform of $Y(p)$.

Next, we can easily extend the above discussion to the simultaneous ordinary linear differential equations whose coefficients are E-type functions. The simultaneous differential equations are given as follows:

$$\sum_{m=1}^{M} \sum_{i=0}^{n_{lm}} a_{l;lm}(t) \frac{d^{n_{lm}-i}}{dt^{n_{lm}-i}} y_m(t) = x_l(t) , \tag{2.9}$$

$$a_{l;lm}(t) = \sum_{\alpha=0}^{\nu} \sum_{k=-Ni,\alpha;lm}^{Nl,\alpha;lm} A_k^{(l;lm)}(\alpha) e^{ik\omega_\alpha t} , \quad l = 1, 2, \cdots M. \tag{2.10}$$

Taking the Laplace transforms of both sides of (2.9) and then introducing the translational operator into the resulting expressions, we obtain the following expression:

$$\{ \sum_{m=1}^{M} \sum_{i=0}^{n_{lm}} \sum_{\alpha=0}^{\nu} \sum_{k=-Ni,\alpha;lm}^{Ni,\alpha;lm} A_k^{(l;lm)}(\alpha) T^k(\omega_\alpha) p^{n_{lm}-i} \} Y_m(p) = X_l'(p) , \tag{2.11}$$

* The notation $S(T, p)$ is used in order to show that it contains the translational operator as well as p.

with

$$X_l'(p) = X_l(p) + \sum_{m=1}^{M} \sum_{i=0}^{n_{lm}} \sum_{\alpha=0}^{\nu} \sum_{k=-N_{i;lm}}^{Ni,\alpha;lm} A_k^{(i;lm)}(\alpha) T^k(\omega_\alpha) \sum_{j=0}^{n_{lm}-i-1} p^{n_{lm}-(i+j+1)} y_m^{(j)}(0), \quad l = 1, 2, \cdots M, \tag{2.12}$$

where

$$Y_m(p) = L(y_m(t)), \quad X_l(p) = L(x_l(t)),$$
$$y_m^{(j)}(0) = \left\{ \frac{d^j y_m(t)}{dt^j} \right\}_{t=0}.$$

If the factor to $Y_m(p)$ in (2.11) is represented by $S_{lm}(T, p)$, we can rewrite (2.11) as follows:

$$\sum_{m=1}^{M} S_{lm}(T, p) Y_m(p) = X_l'(p). \tag{2.13}$$

The equation (2.13) can be written in a matrix form. Namely,

$$[S(T, p)][Y(p)] = [X_l'(p)], \tag{2.13'}$$

where

$$[Y(p)] = \begin{pmatrix} Y_1(p) \\ Y_2(p) \\ \vdots \\ Y_M(p) \end{pmatrix}, \quad [X'(p)] = \begin{pmatrix} X_1'(p) \\ X_2'(p) \\ \vdots \\ X_M'(p) \end{pmatrix}, \tag{2.14}$$

$$[S(T, p)] = \begin{pmatrix} S_{11} & S_{12} & \cdots\cdots & S_{1M} \\ S_{21} & S_{22} & \cdots\cdots & S_{2M} \\ \cdots\cdots & \cdots\cdots & \cdots\cdots & \cdots\cdots \\ S_{M1} & S_{M2} & \cdots\cdots & S_{MM} \end{pmatrix}. \tag{2.15}*$$

The above equation has the same form as (2.8). And to solve the original simultaneous equations, (2.9) reduces to obtaining the inverse matrix $[S(T, p)]^{-1}$ of $[S(T, p)]$. The circuit equations of the linear varying electrical network are included in the cases when $n_{lm} \leq 2$. They will be discussed in detail later on.

3. Some properties of the translational operator

The translational operator $T(\omega_\alpha)$ has been defined by (2.5) for an arbitrary function $f(p)$ of p. So, the following expressions (3.1) and (3.2) can easily be shown to be true:

$$T^k(\omega_\alpha) f(p) = f(p - ik\omega_\alpha), \tag{3.1}$$

$$\begin{aligned} T^{k_1}(\omega_\alpha) T^{k_2}(\omega_\alpha) f(p) &= T^{k_2}(\omega_\alpha) T^{k_1}(\omega_\alpha) f(p) \\ &= f(p - i(k_1 + k_2)\omega_\alpha) \\ &= T^{k_1+k_2}(\omega_\alpha) f(p), \end{aligned} \tag{3.2}$$

* The matrix element S_{lm} is an abbreviated form of $S_{lm}(T, p)$.

where k_1 and k_2 represent negative or positive integers including zero.

From (3.2) we obtain:

$$T^{k_1}(\omega_\alpha)T^{k_2}(\omega_\alpha) = T^{k_2}(\omega_\alpha)T^{k_1}(\omega_\alpha) = T^{k_1+k_2}(\omega_\alpha)\,. \tag{3.2'}$$

For two functions $f_1(p)$ and $f_2(p)$,

$$\begin{aligned} T^{k_1}(\omega_\alpha)f_1(p)T^{k_2}(\omega_\alpha)f_2(p) &= f_1(p-ik_1\omega_\alpha)T^{k_1+k_2}(\omega_\alpha)f_2(p) \\ &= f_1(p-ik_1\omega_\alpha)f_2(p-i(k_1+k_2)\omega_\alpha)\,. \end{aligned} \tag{3.3}$$

Further, if $f(p)$ is analytic at p, the operator $T(\omega_\alpha)$ can be explicitly expressed as follows:

$$T(\omega_\alpha) = \sum_{n=0}^{\infty}{}' (-1)^n \frac{(i\omega_\alpha)^n}{n!}\frac{d^n}{dp^n} = \exp\left(-i\omega_\alpha\frac{d}{dp}\right).$$

Now, we assume that $F(T(\omega_\alpha))$ is a function of $T(\omega_\alpha)$ and does not include p and that it can be formally expanded into a power series of $T(\omega_\alpha)$, i.e.

$$F(T(\omega_\alpha)) = \sum_n C_n T^n(\omega_\alpha)\,. \tag{3.4}$$

Operating $F(T(\omega_\alpha))$ on a function $pf(p)$, we obtain, by (3.4), the following expression:

$$F(T(\omega_\alpha))pf(p) = \{p(\sum_n C_n T^n(\omega_\alpha)) - i\omega_\alpha(\sum_n nC_n T^n(\omega_\alpha))\}f(p)\,.$$

From the relation

$$\sum_n nC_n T^n(\omega_\alpha) = T(\omega_\alpha)\frac{\partial}{\partial T(\omega_\alpha)}F(T(\omega_\alpha))\,,$$

we obtain:

$$F(T(\omega_\alpha))pf(p) = \left\{pF(T(\omega_\alpha)) - i\omega_\alpha T(\omega_\alpha)\frac{\partial}{\partial T(\omega_\alpha)}F(T(\omega_\alpha))\right\}f(p)\,. \tag{3.5}$$

For the two translational operators $T(\omega_\alpha)$ and $T(\omega_\beta)$, we can easily show

$$\begin{aligned} T^k(\omega_\alpha)T^{k'}(\omega_\beta)f(p) &= T^k(\omega_\alpha)f(p-ik'\omega_\beta) \\ &= f(p-i(k\omega_\alpha+k'\omega_\beta)) \\ &= T^{k'}(\omega_\beta)T^k(\omega_\alpha)f(p)\,, \end{aligned} \tag{3.6}$$

i.e.

$$T^k(\omega_\alpha)T^{k'}(\omega_\beta) = T^{k'}(\omega_\beta)T^k(\omega_\alpha)\,, \tag{3.7}$$

where both k and k' represent positive or negative integers including zero.

Next, algebraical properties of $T^k(\omega_\alpha)$ are considered, though they will not be used explicitly in later paragraphs.

When k passes through all positive and negative integers including zero, with ω_α fixed, we obtain an ensemble of $T^k(\omega_\alpha)$. If $\mathfrak{M}$ denotes the above ensemble, we can show that the element $T^k(\omega_\alpha)$ of $\mathfrak{M}$ satisfies the following conditions.

When k_1, k_2 and k_3 are positive or negative integers (zero inclusive), the following four relations are obtained by (3.2′).

$$T^{k_1}(\omega_\alpha)T^{k_2}(\omega_\alpha) = T^{k_1+k_2}(\omega_\alpha)\,,$$

i.e.

$$T^{k_1+k_2}(\omega_\alpha) \in \mathfrak{M}\,; \tag{3.8}$$

$$\begin{aligned} &T^{k_1}(\omega_\alpha)(T^{k_2}(\omega_\alpha)T^{k_3}(\omega_\alpha)) \\ &= T^{k_1}(\omega_\alpha)T^{k_2+k_3}(\omega_\alpha) = T^{k_1+k_2+k_3}(\omega_\alpha)\,; \\ &(T^{k_1}(\omega_\alpha)T^{k_2}(\omega_\alpha))T^{k_3}(\omega_\alpha) \\ &= T^{k_1+k_2}(\omega_\alpha)T^{k_3}(\omega_\alpha) = T^{k_1+k_2+k_3}(\omega_\alpha)\,, \end{aligned} \tag{3.9}$$

so that

$$T^{k_1}(\omega_\alpha)(T^{k_2}(\omega_\alpha)T^{k_3}(\omega_\alpha)) = (T^{k_1}(\omega_\alpha)T^{k_2}(\omega_\alpha))T^{k_3}(\omega_\alpha)\,.$$

And then

$$T^0(\omega_\alpha)T^k(\omega_\alpha) = T^k(\omega_\alpha)T^0(\omega_\alpha) = T^k(\omega_\alpha)\,, \tag{3.10}$$

i.e. $T^0(\omega_\alpha)$ is the unit element belonging to $\mathfrak{M}$.

$$T^{-k}(\omega_\alpha)T^k(\omega_\alpha) = T^k(\omega_\alpha)T^{-k}(\omega_\alpha) = T^0(\omega_\alpha)\,, \tag{3.11}$$

i.e. $T^{-k}(\omega_\alpha)$ is the inverse of $T^k(\omega_\alpha)$ and belongs to $\mathfrak{M}$.

From the relations (3.8) to (3.11), we understand that $\mathfrak{M}$ is a group and that it is an Abelian group by (3.2′).

4. Solution of the ordinary linear differential equation of the first order with *E*-type coefficients

The ordinary linear differential equation of the first order can be generally solved in the time domain by introducing an integrating factor. Here it is discussed on an example, whether the process corresponding to the integrating factor exists or not. For example, we try to solve the following equation:

$$\frac{dy}{dt} + a_1(t)y = e^{i\omega t}\,, \tag{4.1}$$

$$a_1(t) = A_0^{(1)} + 2A_1^{(1)}\cos\omega_0 t\,. \tag{4.2}$$

Corresponding to (2.8), the following expressions are given:

$$S(T,\ p)Y(p) = X'(p)\,, \tag{4.3}$$

$$\left.\begin{aligned} S(T,\ p) &= p + A_0^{(1)} + A_1^{(1)}(T(\omega_0) + T^{-1}(\omega_0))\,, \\ X'(p) &= (p - i\omega)^{-1} + y(0)\,. \end{aligned}\right\} \tag{4.4}$$

Substituting the expression:

$$F(T(\omega_0)) = \exp\{\beta(T(\omega_0) - T^{-1}(\omega_0))\}$$

into (3.5), the following relation is obtained:

$$\exp\{\beta(T(\omega_0)-T^{-1}(\omega_0))\}p$$
$$= p\exp\{\beta(T(\omega_0)-T^{-1}(\omega_0))\}-i\omega_0\beta(T(\omega_0)+T^{-1}(\omega_0))\exp\{\beta(T(\omega_0)-T^{-1}(\omega_0))\}.$$

Further, putting $\beta = A_1^{(1)}/i\omega_0$ and $U(T(\omega_0)) = \exp\left\{\frac{A_1^{(1)}}{i\omega_0}(T(\omega_0)-T^{-1}(\omega_0))\right\}$, we can show from the above relation that the expression (4.3) becomes:

$$\{U(T(\omega_0))S(T,p)U^{-1}(T(\omega_0))\}U(T(\omega_0))Y(p) = U(T(\omega_0))X'(p),$$

where

$$U(T(\omega_0))S(T,p)U^{-1}(T(\omega_0)) = p+A_0^{(1)}.$$

Therefore, we obtain:

$$Y(p) = U^{-1}(T(\omega_0))(p+A_0^{(1)})^{-1}U(T(\omega_0))X'(p).$$

When $U(T(\omega_0))$ and $U^{-1}(T(\omega_0))$ are expressed in such power series of $T(\omega_0)$ as

$$\left.\begin{aligned} U(T(\omega_0)) &= \sum_{k'} C_{k'}^{(+)}T^{k'}(\omega_0), \\ U^{-1}(T(\omega_0)) &= \sum_{k} C_{k}^{(-)}T^{k}(\omega_0), \end{aligned}\right\} \tag{4.5}$$

we obtain

$$\begin{aligned} Y(p) = &\sum_{k,k'} C_k^{(-)}C_{k'}^{(+)}T^k(\omega_0)(p+A_0^{(1)})^{-1}T^{k'}(\omega_0)(p-i\omega)^{-1} \\ &+y(0)\sum_{k,k'} C_k^{(-)}C_{k'}^{(+)}T^k(\omega_0)(p+A_0^{(1)})^{-1}. \end{aligned} \tag{4.6}$$

The relations

$$\begin{aligned} &L^{-1}\{T^k(\omega_0)(p+A_0^{(1)})^{-1}T^{k'}(\omega_0)(p-i\omega)^{-1}\} \\ &= (e^{i\omega_0 t})^k e^{-A_0^{(1)}t}\int_0^t e^{(A_0^{(1)}+i\omega)t'}(e^{i\omega_0 t'})^{k'}dt', \\ &L^{-1}\{T^{k'}(\omega_0)(p+A_0^{(1)})^{-1}\} = e^{-A_0^{(1)}t}(e^{i\omega_0 t})^k \end{aligned}$$

can easily be shown to be true.

Taking the inverse Laplace transform of (4.6), and utilizing the above relations, we obtain:

$$\begin{aligned} y(t) = &\sum_{k,k'} C_k^{(-)}(e^{i\omega_0 t})^k e^{-A_0^{(1)}t}\int_0^t e^{(A_0^{(1)}+i\omega)t'}C_{k'}^{(+)}(e^{i\omega_0 t'})^{k'}dt' \\ &+y(0)\sum_{k,k'} C_k^{(-)}(e^{i\omega_0 t})^k e^{-A_0^{(1)}t}C_{k'}^{(+)}. \end{aligned}$$

Then, using (4.5), the above expression becomes:

$$\begin{aligned} y(t) = &U^{-1}(e^{i\omega_0 t})e^{-A_0^{(1)}t}\int_0^t e^{(A_0^{(1)}+i\omega)t'}U(e^{i\omega_0 t'})dt' \\ &+y(0)U^{-1}(e^{i\omega_0 t})e^{-A_0^{(1)}t}U(1). \end{aligned} \tag{4.7}$$

From the above descriptions, it follows that when $a_1(t)$ takes a more general form:

$$a_1(t) = \sum_k A_k^{(1)}e^{ik\omega_0 t},$$

the solution of (4.1) is given in the same form as (4.7) in which, however, $U(T(\omega_0))$ defined by the following expressions is used:

$$\left.\begin{aligned} G(T(\omega_0)) &= \sum_k{}' A_k^{(1)} T^k(\omega_0)\,, \\ U(T(\omega_0)) &= \exp\left\{\frac{1}{i\omega_0}\int^{T(\omega_0)} \frac{G(T)}{T}\,dT\right\}, \end{aligned}\right\} \tag{4.8}$$

where the dash in $\sum_k{}'$ means that $k=0$ is excluded from the summation.

5. Derivation of Hill's determinantal equation in the frequency domain

Hill's determinantal equation has been derived from the consideration in the time domain (**2**). In this paragraph, the derivation in the frequency domain is considered. Hill's equation is given by

$$\left.\begin{aligned} &\frac{d^2y}{dt^2} + \sum_{k=-\infty}^{\infty} A_k^{(2)} e^{ik\omega_0 t}\, y = 0\,, \\ &A_k^{(2)} = A_{-k}^{(2)}\,. \end{aligned}\right\} \tag{5.1}$$

This is transformed into the frequency domain:

$$S(T,\ p)\,Y(p) = X'(p)\,, \tag{5.2}$$

with

$$\left.\begin{aligned} S(T,\ p) &= p^2 + \sum_k A_k^{(2)} T^k(\omega_0)\,, \\ X'(p) &= py(0) + y'(0)\,. \end{aligned}\right\} \tag{5.3}$$

When

$$Y(p) = \sum_{n=-\infty}^{\infty} \frac{b_n}{p-(\mu+in\omega_0)} + \sum_{n=-\infty}^{\infty} \frac{b_n'}{p-(\mu'+in\omega_0)} \tag{5.4}$$

is substituted into (5.3), we obtain:

$$\begin{aligned} &p\Big(\sum_n b_n + \sum_n b_n'\Big) + \Big\{\sum_n (\mu+in\omega_0)b_n + \sum_n (\mu'+in\omega_0)b_n'\Big\} \\ &+ \sum_n (p-(\mu+in\omega_0))^{-1}\Big\{b_n(\mu+in\omega_0)^2 + \sum_m A_m^{(2)} b_{n-m}\Big\} \\ &+ \sum_n (p-(\mu'+in\omega_0))^{-1}\Big\{b_n'(\mu'+in\omega_0)^2 + \sum_m A_m^{(2)} b_{n-m}'\Big\} \\ &= py(0) + y'(0)\,. \end{aligned} \tag{5.3'}$$

Dividing both sides of (5.3′) by p and making $p\to\infty$, we obtain:

$$\sum_n b_n + \sum_n b_n' = y(0)\,, \tag{5.5}$$

and when this is substituted, (5.3′) becomes:

$$\begin{aligned} &\Big\{\sum_n (\mu+in\omega_0)b_n + \sum_n (\mu'+in\omega_0)b_n'\Big\} \\ &+ \sum_n (p-(\mu+in\omega_0))^{-1}\Big\{b_n(\mu+in\omega_0)^2 + \sum_m A_m^{(2)} b_{n-m}\Big\} \\ &+ \sum_n (p-(\mu'+in\omega_0))^{-1}\Big\{b_n'(\mu'+in\omega_0)^2 + \sum_m A_m^{(2)} b_{n-m}'\Big\} \\ &= y'(0)\,. \end{aligned} \tag{5.3''}$$

The above expression becomes with $p \to \infty$:

$$\sum_n (\mu + in\omega_0) b_n + \sum_n (\mu' + in\omega_0) b'_n = y'(0) . \tag{5.6}$$

Further, substituting (5.6) into (5.3″), and multiplying the rest by $p-(\mu+in\omega_0)$ or $p-(\mu'+in\omega_0)$, and then making $p \to \mu+in\omega_0$ or $p \to \mu'+in\omega_0$ respectively, we obtain:

$$b_n(\mu+in\omega_0)^2 + \sum_m A_m^{(2)} b_{n-m} = 0 , \tag{5.7}$$

$$b'_n(\mu'+in\omega_0)^2 + \sum_m A_m^{(2)} b'_{n-m} = 0 . \tag{5.7'}$$

Eliminating b_n (or b'_n) from (5.7) (or (5.7′)), we obtain the equation for determining μ (or μ'), i.e. Hill's determinantal equation.

6. Method of series expansion

If the inverse of $S(T, p)$ in (2.8) or that of $[S(T, p)]$ in (2.13′) is obtained, the solution of the original differential equation can easily be obtained, but it is difficult to obtain the inverse in a compact form except in the case of ordinary differential equations of the first order. In such cases, it is useful to obtain the inverse $S^{-1}(T, p)$ or $[S(T, p)]^{-1}$ in a series form by expansion, as will be described in the following lines. However, the validity of the solution in a series form depends on the convergency of the series.

First, we consider the ordinary linear differential equation. Putting

$$\sum_{i=0}^{n} \sum_{\alpha=0}^{\nu} A_0^{(i)}(\alpha) p^{n-i} = H^{(0)}(p) , \tag{6.1}$$

$$\sum_{i=0}^{n} \sum_{\alpha=0}^{\nu} \sum_{k=-Ni,\alpha}^{Ni,\alpha}{}' A_0^{(i)}(\alpha) T^k(\omega_\alpha) p^{n-i} = H^{(1)}(T, p) , \tag{6.2}$$

(2.6) can be rewritten as follows:

$$\{H^{(0)}(p) + H^{(1)}(T, p)\} Y(p) = X'(p) . \tag{6.3}$$

With the notations:

$$(H^{(0)}(p))^{-1} X'(p) = X''(p) ,$$
$$(H^{(0)}(p))^{-1} H^{(1)}(T, p) = h(T, p) ,$$

(6.3) is further rewritten:

$$\{1 + h(T, p)\} Y(p) = X''(p) ,$$

from which we obtain:

$$Y(p) = \sum_{n=0}^{\infty} (-1)^n \{h(T, p)\}^n X''(p) . \tag{6.4}$$

The simultaneous ordinary linear differential equations can be treated in a similar way to the above. Namely, we write:

$$\left.\begin{aligned} S_{lm}(T,\ p) &= H^{(0)}_{lm}(p)+H^{(1)}_{lm}(T,\ p)\,,\\ H^{(0)}_{lm}(p) &= \sum_{i=0}^{n_{lm}}\sum_{\alpha=0}^{\nu} A_0^{(i;lm)}(\alpha)p^{n_{lm}-i}\,,\\ H^{(1)}_{lm}(T,\ p) &= \sum_{i=0}^{n_{lm}}\sum_{\alpha=0}^{\nu}\sum_{k=-Ni,\alpha;lm}^{Ni,\alpha;lm}{}' A_k^{(i;lm)}(\alpha)T^k(\omega_\alpha)p^{n_{lm}-i}\,, \end{aligned}\right\} \tag{6.5}$$

$$[H^{(0)}(p)] = \begin{pmatrix} H^{(0)}_{11} & H^{(0)}_{12} & \cdots\cdots & H^{(0)}_{1M}\\ H^{(0)}_{21} & H^{(0)}_{22} & \cdots\cdots & H^{(0)}_{2M}\\ \cdots\cdots & \cdots\cdots & \cdots\cdots & \cdots\cdots\\ \cdots\cdots & \cdots\cdots & \cdots\cdots & \cdots\cdots\\ H^{(0)}_{M1} & H^{(0)}_{M2} & \cdots\cdots & H^{(0)}_{MM} \end{pmatrix}, \tag{6.6}$$

$$[H^{(1)}(T,\ p)] = \begin{pmatrix} H^{(1)}_{11} & H^{(1)}_{12} & \cdots\cdots & H^{(1)}_{1M}\\ H^{(1)}_{21} & H^{(1)}_{22} & \cdots\cdots & H^{(1)}_{2M}\\ \cdots\cdots & \cdots\cdots & \cdots\cdots & \cdots\cdots\\ \cdots\cdots & \cdots\cdots & \cdots\cdots & \cdots\cdots\\ H^{(1)}_{M1} & H^{(1)}_{M2} & \cdots\cdots & H^{(1)}_{MM} \end{pmatrix}, \tag{6.6'}$$

where $H^{(0)}_{lm}=H^{(0)}_{lm}(p)$ and $H^{(1)}_{lm}=H^{(1)}_{lm}(T,\ p)$. Using (6.6) and (6.6′), we obtain:

$$[Y(p)] = \{\sum_{n=0}^{\infty}(-1)^n[h(T,\ p)]^n\}[X''(p)]\,,$$

where

$$[H^{(0)}(p)]^{-1}[H^{(1)}(T,\ p)] = [h(T,\ p)]\,,$$
$$[H^{(0)}(p)]^{-1}[X'(p)] = [X''(p)]\,.$$

As a first example, we consider the equation:

$$\frac{d^2y}{dt^2}+(A_0^{(1)}+2A_1^{(1)}\cos\omega_0 t)\frac{dy}{dt}+A_0^{(2)}y = e^{i\omega t}\,, \tag{6.7}$$

where it is assumed that $A_0^{(1)}$, $A_1^{(1)}$, $A_0^{(2)}$, ω and ω_0 are all real.

Transforming it to the representation in the frequency domain and taking into account the following expressions:

$$\left.\begin{aligned} X'(p) &= (p-i\omega)^{-1}\ \{py(0)+(A_0^{(1)}+2A_1^{(1)})y(0)+y'(0)\}\,,\\ h(T,\ p) &= A_1^{(1)}(p^2+A_0^{(1)}p+A_0^{(2)})^{-1}(T(\omega_0)+T^{-1}(\omega_0))p\,, \end{aligned}\right\} \tag{6.8}$$

we obtain the $(n+1)$th term of (6.4) as follows:

$$\begin{aligned} &\frac{A_1^{(1)n}}{p^2+A_0^{(1)}p+A_0^{(2)}}\left\{(T(\omega_0)+T^{-1}(\omega_0))\frac{p}{p^2+A_0^{(1)}p+A_0^{(2)}}\right\}^n X'(p)\\ &\quad=\frac{A_1^{(1)n}}{p^2+A_0^{(1)}p+A_0^{(2)}}\mathfrak{S}_n\left\{T^{\varepsilon_1}(\omega_0)\frac{p}{p^2+A_0^{(1)}p+A_0^{(2)}}T^{\varepsilon_2}(\omega_0)\frac{p}{p^2+A_0^{(1)}p+A_0^{(2)}}\right.\\ &\qquad\left.\times\cdots\cdots T^{\varepsilon_n}(\omega_0)\frac{p}{p^2+A_0^{(1)}p+A_0^{(2)}}\right\}X'(p)\,, \end{aligned}$$

where each of $\varepsilon_1, \varepsilon_2, \cdots$, and ε_n can take only 1 or -1 and $\mathfrak{S}_n$ means the sum taken

over all the combinations of ε_1, ε_2, $\cdots$, and ε_n. Further, the above expression can be modified as follows:

$$\frac{A_1^{(1)n}}{p^2+A_0^{(1)}p+A_0^{(2)}}\mathfrak{S}_n\prod_{l=1}^{n}\frac{(p-i\varepsilon_{1,2,\dots,l}\omega_0)X'(p-i\varepsilon_{1,2,\dots,l}\omega_0)}{\{(p-i\varepsilon_{1,2,\dots,l}\omega_0)^2+A_0^{(1)}(p-i\varepsilon_{1,2,\dots,l}\omega_0)+A_0^{(2)}\}}, \tag{6.9}$$

where $\varepsilon_{1,2,3,\dots,n}=\varepsilon_1+\varepsilon_2+\cdots\cdots+\varepsilon_n$.

Substituting (6.9) into (6.4) and taking the inverse Laplace transform of the resulting expression, we collect the terms that have the time factor $e^{i\omega t}$. Then, we obtain the following expression which may be called the steady state part of the solution:

$$\begin{aligned} y_{\text{steady}}(t) &= \frac{e^{i\omega t}}{A_0^{(2)}+i\omega A_0^{(1)}-\omega^2} \\ &\quad+e^{i\omega t}\sum_{n=1}^{\infty}(-i)^nA_1^{(1)n}\mathfrak{S}_nB(\varepsilon_1,\varepsilon_2,\cdots,\varepsilon_n)e^{i\varepsilon_{1,2,\dots,n}\omega_0 t}, \end{aligned} \tag{6.10}$$

where

$$\begin{aligned} B(\varepsilon_1,\varepsilon_2,\cdots,\varepsilon_n) &= \omega\{\omega+\varepsilon_{1,2,\dots,n}\omega_0\}^{-1}\{A_0^{(2)}+i\omega A_0^{(1)}-\omega^2\}^{-1} \\ &\quad\times\prod_{l=1}^{n}\frac{(\omega+\varepsilon_{1,2,\dots,l}\omega_0)}{\{A_0^{(2)}+i(\omega+\varepsilon_{1,2,\dots,l}\omega_0)A_0^{(1)}-(\omega+\varepsilon_{1,2,\dots,l}\omega_0)^2\}}. \end{aligned} \tag{6.11}$$

We can easily show that $y_{\text{steady}}(t)$ is absolutely convergent, when $|2A_1^{(1)}/A_0^{(1)}|<1$.*

As a second example, we consider the following equation:

$$\frac{d^2y}{dt^2}+(A_0^{(2)}+A_1^{(2)}e^{-\alpha t})y=0 \quad (\alpha>0). \tag{6.12}$$

Now putting $A_0^{(2)}=\omega_L^2$ and $A_1^{(2)}/A_0^{(2)}=\kappa$, $h(T,p)$ and $X''(p)$ are given as follows:

$$\left.\begin{aligned} h(T,p) &= (\kappa\omega_L^2/(p^2+\omega_L^2))T(i\alpha), \\ X''(p) &= (p^2+\omega_L^2)^{-1}(py(0)+y'(0)), \end{aligned}\right\} \tag{6.13}$$

where we assume that ω_L and κ are real.

By (6.4) we obtain:

$$\begin{aligned} Y(p) &= X''(p)+y(0)\sum_{n=1}^{\infty}(-1)^n(\omega_L^2\kappa)^n(p+n\alpha)\prod_{l=0}^{n}\{(p+l\alpha)^2+\omega_L^2\}^{-1} \\ &\quad+y'(0)\sum_{n=1}^{\infty}(-1)^n(\omega_L^2\kappa)^n\prod_{l=0}^{n}\{(p+l\alpha)^2+\omega_L^2\}^{-1}. \end{aligned}$$

Then, defining $A_n(p)$ and $B_n(p)$ by the following expression:

$$\begin{aligned} Y(p) &= X''(p)+y(0)\sum_{n=1}^{\infty}(-1)^n\left(\frac{\omega_L^2\kappa}{\alpha^2}\right)^nA_n(p) \\ &\quad+y'(0)\sum_{n=1}^{\infty}(-1)^n\left(\frac{\omega_L^2\kappa}{\alpha^2}\right)^nB_n(p), \end{aligned} \tag{6.14}$$

and denoting the inverse Laplace transform of $A_n(p)$ and $B_n(p)$ by $A_n(t)$ and $B_n(t)$ respectively, we obtain:

* Reference should be made to Appendix.

$$
\begin{aligned}
y(t) &= y(0)\cos\omega_L t+\omega_L^{-1}y'(0)\sin\omega_L t \\
&\quad + y(0)\sum_{n=1}^{\infty}(-1)^n\left(\frac{\omega_L^2\kappa}{\alpha^2}\right)^n A_n(t) \\
&\quad + y'(0)\sum_{n=1}^{\infty}(-1)^n\left(\frac{\omega_L^2\kappa}{\alpha^2}\right)^n B_n(t)\,,
\end{aligned}
\tag{6.15}
$$

where $A_n(t)$ and $B_n(t)$ are given by the following expressions:

$$
\left.
\begin{aligned}
A_n(t) &= \mathrm{Im}\left\{ ie^{i\omega_L t}\sum_{k=0}^{n} e^{-\alpha k t}\,\frac{\left|\Gamma\left(1+\frac{i}{x^2}\right)\right|^2}{\Gamma(k+1)\Gamma(n-k+1)\Gamma\left(k+1-\frac{i}{x^2}\right)\Gamma\left(n-k+1+\frac{i}{x^2}\right)}\right. \\
&\quad \left. -e^{i\omega_L t}\left(\frac{\alpha}{\omega_L}\right)\sum_{k=0}^{n-1} e^{-\alpha k t}\,\frac{\left|\Gamma\left(1+\frac{i}{x^2}\right)\right|^2}{\Gamma(k+1)\Gamma(n-k)\Gamma\left(k+1-\frac{i}{x^2}\right)\Gamma\left(n-k+1+\frac{i}{x^2}\right)}\right\}, \\
B_n(t) &= \mathrm{Im}\left\{ \frac{e^{i\omega_L t}}{\omega_L}\sum_{k=0}^{n} e^{-\alpha k t}\,\frac{\left|\Gamma\left(1+\frac{i}{x^2}\right)\right|^2}{\Gamma(k+1)\Gamma(n-k+1)\Gamma\left(k+1-\frac{i}{x^2}\right)\Gamma\left(n-k+1+\frac{i}{x^2}\right)}\right\}. \\
x &= \left(\frac{\alpha}{2\omega_L}\right)^{1/2} \qquad n\geq 1\,.
\end{aligned}
\right\}
\tag{6.16}
$$

We can also easily show that (6.5) is absolutely convergent*.

7. Formulation of Maxwell equations in the medium whose material constants ε and μ are E-type functions of time

In the frequency domain, we will formulate Maxwell equations in such a medium that the material constants (dielectric constant ε and magnetic permeability μ) are E-type functions of time t, by introducing the translational operator. We can write the phenomenological electromagnetic field equations as follows, in M. K. S. units:

$$
\left.
\begin{aligned}
&\nabla\times\mathbf{E}(\mathbf{r},\,t)+\frac{\partial\mathbf{B}(\mathbf{r},\,t)}{\partial t}=0\,, \\
&\nabla\times\mathbf{H}(\mathbf{r},\,t)-\frac{\partial\mathbf{D}(\mathbf{r},\,t)}{\partial t}=\mathbf{J}(\mathbf{r},\,t)\,, \\
&\nabla\cdot\mathbf{D}(\mathbf{r},\,t)=\rho(\mathbf{r},\,t)\,, \\
&\nabla\cdot\mathbf{B}(\mathbf{r},\,t)=0\,.
\end{aligned}
\right\}
\tag{7.1}
$$

Taking the Laplace transforms of equations (7.1), we obtain:

$$
\left.
\begin{aligned}
&\nabla\times\mathbf{E}(\mathbf{r},\,p)+p\mathbf{B}(\mathbf{r},\,p)=\mathbf{B}(\mathbf{r},\,0)\,, \\
&\nabla\times\mathbf{H}(\mathbf{r},\,p)-p\mathbf{D}(\mathbf{r},\,p)=\mathbf{J}(\mathbf{r},\,p)-\mathbf{D}(\mathbf{r},\,0)\,, \\
&\nabla\cdot\mathbf{D}(\mathbf{r},\,p)=\rho(\mathbf{r},\,p)\,, \\
&\nabla\cdot\mathbf{B}(\mathbf{r},\,p)=0\,.
\end{aligned}
\right\}
\tag{7.2}
$$

* Reference should be made to Appendix.

The Laplace transforms of the quantities which appear in (7.1), are represented by the corresponding symbols in which t is replaced by p. Thus, for instance,

$$L(\mathbf{E}(\mathbf{r}, t)) = \mathbf{E}(\mathbf{r}, p),$$
$$L(\mathbf{H}(\mathbf{r}, t)) = \mathbf{H}(\mathbf{r}, p), \quad \text{etc.}$$

$\mathbf{B}(\mathbf{r}, 0)$ and $\mathbf{D}(\mathbf{r}, 0)$ mean $\lim_{t\to 0}\mathbf{B}(\mathbf{r}, t)$ and $\lim_{t\to 0}\mathbf{D}(\mathbf{r}, t)$ respectively. We will derive connections between $\mathbf{D}(\mathbf{r}, p)$ and $\mathbf{E}(\mathbf{r}, p)$, and $\mathbf{B}(\mathbf{r}, p)$ and $\mathbf{H}(\mathbf{r}, p)$ by introducing the material constants and the electric and the magnetic polarization $\mathbf{P}(\mathbf{r}, t)$ and $\mathbf{M}(\mathbf{r}, t)$. From

$$\left.\begin{aligned}\mathbf{D}(\mathbf{r}, t) &= \varepsilon_0\mathbf{E}(\mathbf{r}, t)+\mathbf{P}(\mathbf{r}, t),\\ \mathbf{B}(\mathbf{r}, t) &= \mu_0\{\mathbf{H}(\mathbf{r}, t)+\mathbf{M}(\mathbf{r}, t)\},\end{aligned}\right\} \tag{7.3}$$

we obtain, by taking Laplace transforms:

$$\left.\begin{aligned}\mathbf{D}(\mathbf{r}, p) &= \varepsilon_0\mathbf{E}(\mathbf{r}, p)+\mathbf{P}(\mathbf{r}, p),\\ \mathbf{B}(\mathbf{r}, p) &= \mu_0\{\mathbf{H}(\mathbf{r}, p)+\mathbf{M}(\mathbf{r}, p)\},\end{aligned}\right\} \tag{7.4}$$

and

$$\left.\begin{aligned}\mathbf{P}(\mathbf{r}, p) &= \varepsilon_0\vec{\chi}_e(T, p)\cdot\mathbf{E}(\mathbf{r}, p),\\ \mathbf{M}(\mathbf{r}, p) &= \vec{\chi}_m(T, p)\cdot\mathbf{H}(\mathbf{r}, p),\end{aligned}\right\} \tag{7.5}*$$

where $\vec{\chi}_e(T, p)$ and $\vec{\chi}_m(T, p)$ are tensors of the second rank and may be called the electric susceptibility operator and the magnetic susceptibility operator. The ij-components of $\vec{\chi}_e(T, p)$ and $\vec{\chi}_m(T, p)$ can be written as follows:

$$\left.\begin{aligned}(\vec{\chi}_e)_{ij} &= \sum_{\alpha=0}^{\nu}\sum_{k=-Nij;\alpha e}^{Nij;\alpha e}\chi_{e,ij}^{(k)}(p;\alpha)T^k(\omega_\alpha),\\ (\vec{\chi}_m)_{ij} &= \sum_{\alpha=0}^{\nu}\sum_{k=-Nij;\alpha m}^{Nij;\alpha m}\chi_{m,ij}^{(k)}(p;\alpha)T^k(\omega_\alpha),\end{aligned}\right\} \tag{7.6}$$

where i and j represent x, y and z.

When the medium is isotropic, $\vec{\chi}_e(T, p)$ and $\vec{\chi}_m(T, p)$ reduce to the simple scalar operators, which we will denote by $\chi_e(T, p)$ and $\chi_m(T, p)$, respectively and we obtain:

$$\left.\begin{aligned}\mathbf{D}(\mathbf{r}, p) &= \varepsilon_0\{1+\chi_e(T, p)\}\mathbf{E}(\mathbf{r}, p),\\ \mathbf{B}(\mathbf{r}, p) &= \mu_0\{1+\chi_m(T, p)\}\mathbf{H}(\mathbf{r}, p).\end{aligned}\right\} \tag{7.7}$$

Now, putting

$$\left.\begin{aligned}\varepsilon(T, p) &= \varepsilon_0(1+\chi_e(T, p)),\\ \mu(T, p) &= \mu_0(1+\chi_m(T, p)),\end{aligned}\right\} \tag{7.8}$$

* Here are introduced the relations between $\mathbf{P}(\mathbf{r}, p)$ and $\mathbf{E}(\mathbf{r}, p)$, and $\mathbf{M}(\mathbf{r}, p)$ and $\mathbf{H}(\mathbf{r}, p)$, since ε and μ, and accordingly χ_e and χ_m are generally dependent on the frequency. Reference should be made to the footnote to the Introduction.

and assuming that $\mathbf{B}(\mathbf{r}, 0)=0$, $\mathbf{D}(\mathbf{r}, 0)=0$, and $\rho(\mathbf{r}, t)=0$, $\mathbf{J}(\mathbf{r}, t)=0$, the equations (7.2) become as follows:

$$\left.\begin{aligned} \nabla\times\mathbf{E}(\mathbf{r}, p)+p\mu(T, p)\mathbf{H}(\mathbf{r}, p) &= 0, \\ \nabla\times\mathbf{H}(\mathbf{r}, p)-p\varepsilon(T, p)\mathbf{E}(\mathbf{r}, p) &= 0, \\ \nabla\cdot\mathbf{E}(\mathbf{r}, p) &= 0, \\ \nabla\cdot\mathbf{H}(\mathbf{r}, p) &= 0. \end{aligned}\right\} \tag{7.9}$$

Next we consider the propagation of the electromagnetic waves in the hollow metallic (perfectly conducting) tube filled with such a medium that the equations (7.9) are valid. When we take the z-axis along the pipe axis and the x, y axes in a plane perpendicular to the pipe axis, we can express in the frequency domain the propagation modes as follows:

For the TE waves ($E_z(\mathbf{r}, t)=0$), $H_z(\mathbf{r}, p)$ is given by

$$H_z(\mathbf{r}, p) = \psi_n(x, y)e^{\mp\gamma_z(T, p)z}F(p), \tag{7.10}$$

where $\psi_n(x, y)$ is defined by

$$\left(\frac{\partial^2}{\partial x^2}+\frac{\partial^2}{\partial y^2}+k_n^2\right)\psi_n(x, y) = 0,$$

subject to the boundary condition $\dfrac{\partial\psi_n}{\partial n}=0$ at the wall and

$$\left.\begin{aligned} \gamma^2(T, p) &= \gamma_z^2(T, p)-k_n^2, \\ \gamma^2(T, p) &= p\varepsilon(T, p)p\mu(T, p). \end{aligned}\right\} \tag{7.10'}$$

The other field components are expressed as follows:

$$\left.\begin{aligned} H_x(\mathbf{r}, p) &= \mp k_n^{-2}\gamma_z(T, p)\frac{\partial}{\partial x}H_z(\mathbf{r}, p), \\ H_y(\mathbf{r}, p) &= \mp k_n^{-2}\gamma_z(T, p)\frac{\partial}{\partial y}H_z(\mathbf{r}, p), \\ E_x(\mathbf{r}, p) &= -k_n^{-2}p\mu(T, p)\frac{\partial}{\partial y}H_z(\mathbf{r}, p), \\ E_y(\mathbf{r}, p) &= k_n^{-2}p\mu(T, p)\frac{\partial}{\partial x}H_z(\mathbf{r}, p), \end{aligned}\right\} \tag{7.11}$$

where $F(p)$ is an arbitrary function of p.

For TM waves ($H_z(\mathbf{r}, t)=0$), $E_z(\mathbf{r}, p)$ is given by

$$E_z(\mathbf{r}, p) = \phi_n(x, y)e^{\mp\gamma_z'(T, p)z}G(p), \tag{7.12}$$

where $\phi_n(x, y)$ is defined by

$$\left(\frac{\partial^2}{\partial x^2}+\frac{\partial^2}{\partial y^2}+k_n'^2\right)\phi_n(x, y) = 0$$

subject to the boundary condition $\phi_n(x, y)=0$ at the wall and

$$\left.\begin{aligned}\gamma'^2(T,\ p) &= \gamma_z'^2(T,\ p) - k_n'^2\,,\\ \gamma'^2(T,\ p) &= p\mu(T,\ p)p\varepsilon(T,\ p)\,.\end{aligned}\right\} \tag{7.12'}$$

The other field components are given by the following expressions:

$$\left.\begin{aligned}H_x(\mathbf{r},\ p) &= k_n'^{-2}p\varepsilon(T,\ p)\frac{\partial}{\partial y}E_z(\mathbf{r},\ p)\,,\\ H_y(\mathbf{r},\ p) &= -k_n'^{-2}p\varepsilon(T,\ p)\frac{\partial}{\partial x}E_z(\mathbf{r},\ p)\,,\\ E_x(\mathbf{r},\ p) &= \mp k_n'^{-2}\gamma_z'(T,\ p)\frac{\partial}{\partial x}E_z(\mathbf{r},\ p)\,,\\ E_y(\mathbf{r},\ p) &= \mp k_n'^{-2}\gamma_z'(T,\ p)\frac{\partial}{\partial y}E_z(\mathbf{r},\ p)\,,\end{aligned}\right\} \tag{7.13}$$

where $G(p)$ is an arbitrary function of p. From (7.10)$\sim$(7.13), it is evident that in the frequency domain, the propagation mode takes the same form as that in the medium of fixed material constants, except that the propagation constant operator $\gamma_z(T,\ p)$ or $\gamma_z'(T,\ p)$ and the material constant operator $\mu(T,\ p)$ or $\varepsilon(T,\ p)$ include the translational operator.

8. Conclusion

Summarizing we may say that the descriptions in the preceding paragraphs could be an answer for the following problem. How can the method of solving the ordinary linear differential equation with constant coefficients be extended by the Laplace transform to the case of the ordinary linear differential equation with E-type coefficients? As shown in § 2, to solve the ordinary linear differential equations (2.1) and (2.9) is reduced to obtaining the inverses of $S(T,\ p)$ and $[S(T,\ p)]$.

In the special cases shown in § 4, the inverse of $S(T,\ p)$ was easily obtained in a compact form, but in the general case it will be difficult to obtain the inverse in a compact form. Then, in such a case, the method of the series expansion should be used. Though in § 6 the geometrical series expansion was utilized, it is hoped that the more powerful expansion method will be devised.

Acknowledgements

The author wishes to thank Professor S. Tomotika and Professor I. Takahashi for their kind guidance and persistent encouragement.

Appendix

It will be shown that (6.10) and (6.15) are absolutely convergent. First, the convergency of (6.10) is examined. By (6.11), we obtain the following inequality

$$|B(\varepsilon_1, \varepsilon, \cdots, \varepsilon_n)| < \left| \frac{\omega}{A_0^{(2)} + i\omega A_0^{(1)} - \omega^2} \right| |A_0^{(1)}|^{-(n-1)}$$
$$\times |A_0^{(2)} + iA_0^{(1)}(\omega + \varepsilon_{1,2,\cdots,n}\omega_0) - (\omega + \varepsilon_{1,2,\cdots,n}\omega_0)^2|^{-1}.$$

We represent the minimum of $|\omega + \varepsilon_{1,2,\cdots,n}\omega_0|$ for all the values of n, by ω_m.

Now putting

$$\left.\begin{aligned} &\omega_m |A_0^{(1)}| = m, && \text{when} \quad \omega_m \neq 0, \\ &\text{min.}\,(|A_0^{(2)}|, |\omega_0 A_0^{(1)}|) = m, && \text{when} \quad \omega_m = 0, \end{aligned}\right\}$$

we obtain:

$$|A_0^{(2)} + i(\omega + \varepsilon_{1,2,\cdots,n}\omega_0)A_0^{(1)} - (\omega + \varepsilon_{1,2,\cdots,n}\omega_0)^2|^{-1} < \frac{1}{m},$$

$$\therefore \quad |B(\varepsilon_1, \varepsilon_2, \cdots, \varepsilon_n)| < \frac{1}{m} |A_0^{(1)}|^{-n}.$$

Since in $\mathfrak{S}_n B(\varepsilon_1, \varepsilon_2, \cdots, \varepsilon_n)$ are included 2^n of $B(\varepsilon_1, \varepsilon_2, \cdots, \varepsilon_n)$'s,

$$|\mathfrak{S}_n B(\varepsilon_1, \varepsilon_2, \cdots, \varepsilon_n)| < \frac{1}{m} \left| \frac{2}{A_0^{(1)}} \right|^n.$$

Therefore $$|(-i)^n A_1^{(1)n} \mathfrak{S}_n B(\varepsilon_1, \varepsilon_2, \cdots, \varepsilon_n) e^{i\varepsilon_{1,2,\cdots,n}\omega_0 t}| < \frac{1}{m} \left| \frac{2A_1^{(1)}}{A_0^{(1)}} \right|^n,$$

$$\therefore \quad \left| y_{\text{steady}}(t) - \frac{e^{i\omega t}}{A_0^{(2)} + i\omega A_0^{(1)} - \omega^2} \right| < \frac{1}{m} \sum_{n=1}^{\infty} \left| \frac{2A_1^{(1)}}{A_0^{(1)}} \right|^n.$$

From the above inequalities, we see that $y_{\text{steady}}(t)$ is absolutely convergent when $|2A_1^{(1)}/A_0^{(1)}| < 1$ i.e. $|2A_1^{(1)}| < |A_0^{(1)}|$, under the assumption that $A_0^{(1)}$, $A_0^{(2)}$ and ω_0 are so taken that $m \neq 0$.

Next the convergency of (6.5) is examined. Putting $L^{-1}(X''(p)) = x''(t)$ and $\Delta y(t) = y(t) - x''(t)$, we consider the convergency of $\Delta y(t)$. We can easily show the following inequalities:

$$\left| \frac{\Gamma\left(1 - \frac{i}{x^2}\right)}{\Gamma\left(k + 1 - \frac{i}{x^2}\right)} \right| < (x^2)^k = \left(\frac{\alpha}{2\omega_L}\right)^k \quad (\omega_L > 0)$$

and

$$\left| \frac{\Gamma\left(1 + \frac{i}{x^2}\right)}{\Gamma\left(n - k + 1 + \frac{i}{x^2}\right)} \right| < \left(\frac{\alpha}{2\omega_L}\right)^{n-k},$$

$$\therefore \quad \left| \sum_{k=0}^{n} e^{-\alpha k t} \frac{\left|\Gamma\left(1 + \frac{i}{x^2}\right)\right|^2}{\Gamma(k+1)\Gamma(n-k+1)\Gamma\left(k+1-\frac{i}{x^2}\right)\Gamma\left(n-k+1+\frac{i}{x^2}\right)} \right|$$
$$< \left(\frac{\alpha}{2\omega_L}\right)^n \frac{1}{n!} \sum_{k=0}^{n} \frac{n!}{k!\,(n-k)!} e^{-\alpha k t} = \left(\frac{\alpha}{2\omega_L}\right)^n \frac{1}{n!} (1 + e^{-\alpha t})^n.$$

Similarly

$$\left|\left(\frac{\alpha}{\omega_L}\right)\sum_{k=1}^{n-1} e^{-\alpha kt}\frac{\left|\Gamma\left(1+\frac{i}{x^2}\right)\right|^2}{\Gamma(k+1)\Gamma(n-k)\Gamma\left(k+1-\frac{i}{x^2}\right)\Gamma\left(n-k+1+\frac{i}{x^2}\right)}\right|$$

$$\leq \frac{\alpha}{\omega_L}\left(\frac{\alpha}{2\omega_L}\right)^n \frac{1}{(n-1)!}(1+e^{-\alpha t})^{n-1}.$$

Therefore, the following inequalities are established:

$$\left|1-n\left(\frac{\omega_L^2\kappa}{\alpha^2}\right)^2 A_n(t)\right| \leq \frac{1}{n!}\left|\frac{\omega_L\kappa}{2\alpha}\right|^n (1+e^{-\alpha t})^n$$

$$+\frac{\alpha}{\omega_L}\frac{1}{(n-1)!}\left|\frac{\omega_L\kappa}{2\alpha}\right|^n (1+e^{-\alpha t})^{n-1},$$

$$\left|1-n\left(\frac{\omega_L^2\kappa}{\alpha^2}\right)^2 B_n(t)\right| \leq \frac{1}{\omega_L}\frac{1}{n!}\left|\frac{\omega_L\kappa}{2\alpha}\right|^n (1+e^{-\alpha t})^n.$$

Finally

$$\Delta y(t) \leq |y(0)|\sum_{n=1}^{\infty}\frac{1}{n!}\left\{\left|\frac{\omega_L\kappa}{2\alpha}\right|(1+e^{-\alpha t})\right\}^n$$

$$+\frac{\alpha}{\omega_L}|y(0)|\sum_{n=1}^{\infty}\frac{1}{(n-1)!}\left\{\left|\frac{\omega_L\kappa}{2\alpha}\right|(1+e^{-\alpha t})\right\}^{n-1}$$

$$+\frac{1}{\omega_L}|y'(0)|\sum_{n=1}^{\infty}\frac{1}{n!}\left\{\left|\frac{\omega_L\kappa}{2\alpha}\right|(1+e^{-\alpha t})\right\}^n$$

$$\leq |y(0)|e^{\left|\frac{\omega_L\kappa}{2\alpha}\right|(1+e^{-\alpha t})}+\frac{\alpha}{\omega_L}|y(0)|e^{\left|\frac{\omega_L\kappa}{2\alpha}\right|(1+e^{-\alpha t})}$$

$$+\frac{|y'(0)|}{\omega_L}e^{\left|\frac{\omega_L\kappa}{2\alpha}\right|(1+e^{-\alpha t})}$$

$$=\left(|y(0)|+\frac{\alpha}{\omega_L}|y(0)|+\frac{|y'(0)|}{\omega_L}\right)e^{\left|\frac{\omega_L\kappa}{2\alpha}\right|(1+e^{-\alpha t})}.$$

Thus it has been shown that $\Delta y(t)$ is absolutely convergent and so is also $y(t)$.

REFERENCES

1. L. A. Pipes, Phil. Mag. [7] **25** (1938) 585.
2. E. T. Whittaker and G. N. Watson, *A Course of Modern Analysis* (Cambridge Univ. Press, 4th ed 1935), p. 413.
3. J. H. Van Vleck, *The Theory of Electric and Magnetic Susceptibility* (Clarendon Press, Oxford, 1932), p. 1.

Memoirs of the College of Science, University of Kyoto, Series A,
Vol. XXVIII, No. 4, Article 3, 1958.

INTRODUCTION OF THE TRANSLATIONAL OPERATOR IN FREQUENCY DOMAIN AND TREATMENT OF CERTAIN LINEAR DIFFERENTIAL EQUATIONS, II.

BY

Tadashi WATANABE

(*Received December 5, 1957*)

ABSTRACT

In this paper, by introducing the translational operator in frequency domain defined in part I, the theory of the linear fixed electrical network is extended to the linear network containing circuit elements which are expressed by E-type functions of time described in part I.

Also the treatment of transmission lines with the above-mentioned network inserted is discussed and especially the extensions of reflection coefficient and transmission coefficient are described.

1. Introduction

As to the linear varying electrical network whose elements might not necessarily be of E-type, only special cases were discussed by several authors, e.g. J. R. Carson (**1**), J. Neufeld (**2**) and L. A. Pipes (**3**).

In this country, M. Akiyama (**4**, **5**, **6**) and Z. Kiyasu (**11**) discussed the theory of the linear periodically varying electrical network.

Recently, L. A. Zadeh (**7**, **8**, **9**, **10**) established the general theory of the linear varying electrical network by introducing the system function. But in order to derive system functions, we generally have to solve higher order linear differential equations with the coefficients which are functions of time. And further it seems generally difficult to know how the impedance and the admittance, i.e. the system functions are constructed by circuit elements.

In the present paper the author deals with principally the linear varying network which includes real circuit elements* varying periodically in time. The consideration can be extended, with a little modification, to the case of the linear varying network whose circuit elements can be expressed by E-type functions**.

2. Linear fixed electrical network

We shall begin with a review of the linear fixed electrical network.

---

* They are restricted to the functions which can be expanded in Fourier series.

** Reference should be made to part I.

If the degrees of freedom of the network under consideration be N, we can express the circuit equations of the network in the time domain as follows:

$$\left.\begin{aligned} &\sum_{k=1}^{N} \bar{Z}_{jk} i_k(t) = e_j(t)\,, \\ &\bar{Z}_{jk} = DL_{jk} + R_{jk} + S_{jk}\frac{1}{D}\,, \\ &D = \frac{d}{dt}\,, \quad \frac{1}{D} = \int^{t}\,, \end{aligned}\right\} \tag{2.1}$$

where $i_k(t)$ is the mesh current flowing along the k-th mesh and $e_j(t)$ the algebraic sum of e.m.f. involved in the j-th mesh.

The positive sense of the current $i_k(t)$ is selected uniquely over all meshes, e.g. clockwise, while the positive sense of $e_j(t)$ is taken so as to increase the mesh current $i_j(t)$.

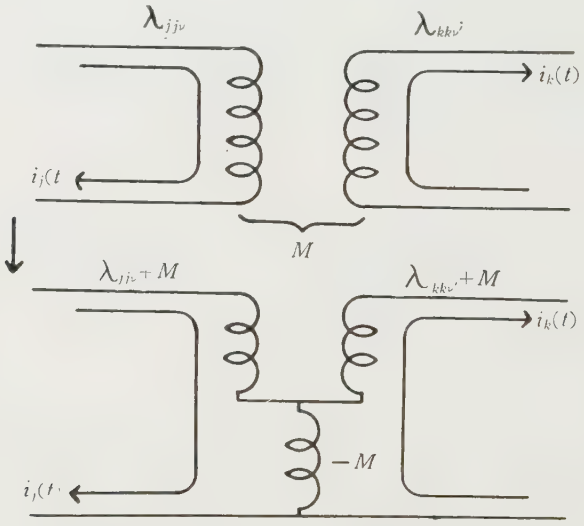

Fig. 1

Next we consider the constructions of L_{jk}, R_{jk} and S_{jk}. When $j \neq k$, $-L_{jk}$ is the sum of all self-inductive coefficients $-\lambda_{jk\kappa}$'s involved in the branch common to the j-th and the k-th meshes. When the j-th and the k-th meshes include coupling by mutual induction, we replace the coupling part by the equivalent circuit as shown in Fig. 1, where M is the mutual inductive coefficient, and then we take the sum described above. Thus:

$$L_{jk} = \sum_{\kappa} \lambda_{jk\kappa}\,. \tag{2.2}$$

Similarly R_{jk} and S_{jk} are obtained by taking sums of all resistances $-\rho_{jk\mu}$'s and all elastive coefficients $-\sigma_{jk\nu}$'s respectively, included in the branch common to the

j-th and the k-th meshes and changing the signs.

Namely:

$$R_{jk} = \sum_{\mu} \rho_{jk\mu} \qquad (j \neq k), \tag{2.3}$$

$$S_{jk} = \sum_{\nu} \sigma_{jk\nu} \qquad (j \neq k). \tag{2.4}$$

When the inductive coefficients, resistances and elastive coefficients which belong to the j-th mesh but not to the other meshes are represented by $\lambda_{jj\kappa}$'s, $\rho_{jj\mu}$'s and $\sigma_{jj\nu}$'s respectively, the expressions L_{jj}, R_{jj} and S_{jj} are given as follows:

$$L_{jj} = \sum_{\kappa} \lambda_{jj\kappa} - \sum_{l}{}' \sum_{\kappa} \lambda_{jl\kappa}, \tag{2.2'}$$

$$R_{jj} = \sum_{\mu} \rho_{jj\mu} - \sum_{l}{}' \sum_{\mu} \rho_{jl\mu}, \tag{2.3'}$$

$$S_{jj} = \sum_{\nu} \sigma_{jj\nu} - \sum_{l}{}' \sum_{\nu} \sigma_{jl\nu}, \tag{2.4'}$$

where the dash in $\sum'$ indicates that terms for which $l=j$ are excluded from the summation. As will easily be seen, we have

$$L_{jk} = L_{kj}, \quad R_{jk} = R_{kj}, \quad S_{jk} = S_{kj},$$

so that we obtain:

$$\bar{Z}_{jk} = \bar{Z}_{kj} \qquad \text{(reciprocity relation)}. \tag{2.5}$$

Also we can express (2.1) in a matrix form:

$$[\bar{Z}][i(t)] = [e(t)], \tag{2.1'}$$

where

$$[e(t)] = \begin{bmatrix} e_1(t) \\ e_2(t) \\ \vdots \\ e_N(t) \end{bmatrix}, \quad [i(t)] = \begin{bmatrix} i_1(t) \\ i_2(t) \\ \vdots \\ i_N(t) \end{bmatrix}, \quad [\bar{Z}] = \begin{bmatrix} \bar{Z}_{11} & \bar{Z}_{12} \cdots \bar{Z}_{1N} \\ \bar{Z}_{21} & \bar{Z}_{22} \cdots \bar{Z}_{2N} \\ \cdots\cdots\cdots\cdots \\ \cdots\cdots\cdots\cdots \\ \bar{Z}_{N1} & \bar{Z}_{N2} \cdots \bar{Z}_{NN} \end{bmatrix}.$$

Taking the Laplace transform of (2.1'), we obtain:

$$[Z(p)][I(p)] = [E'(p)], \tag{2.1''}$$

where $[Z(p)]$ is $[\bar{Z}]$ with D replaced by p, $[I(p)]$ the Laplace transform of $[i(t)]$, and $[E'(p)]$ the Laplace transform of $[e(t)]$ added with the terms which include the initial values of currents $[i(t)]$ and charges $[q(t)]$, where $q_j(t) = \int^t i_j(t')\,dt'$.

3. Circuit equations of linear varying network whose elements are expressed by real periodic functions of time*

We assume that $\lambda_{jk\kappa}$, $\rho_{jk\mu}$ and $\sigma_{jk\nu}$ are periodic functions of time with the periods $\omega_{jk\kappa}$, $\omega_{jk\mu}$ and $\omega_{jk\nu}$, respectively:

* Read in part before the joint meetings of Kansai branches of three Electrical Societies, Oct., 18, 1952 and Oct., 17, 1953 (**12, 13**).

$$\left.\begin{aligned}\lambda_{jk\kappa} &= \sum_{n=-\infty}^{\infty} \lambda_{jk\kappa}^{(n)} e^{in\omega_{jk\kappa}t}, \\ \rho_{jk\mu} &= \sum_{n=-\infty}^{\infty} \rho_{jk\mu}^{(n)} e^{in\omega_{jk\mu}t}, \\ \sigma_{jk_\nu} &= \sum_{n=-\infty}^{\infty} \sigma_{jk\nu}^{(n)} e^{in\omega_{jk_\nu}t}.\end{aligned}\right\} \tag{3.1}$$

Since the circuit constants are real, the following relations are obtained:

$$\left.\begin{aligned}\widetilde{\lambda_{jk\kappa}^{(n)}} &= \lambda_{jk\kappa}^{(-n)}, \\ \widetilde{\rho_{jk\mu}^{(n)}} &= \rho_{jk\mu}^{(-n)}, \\ \widetilde{\sigma_{jk\nu}^{(n)}} &= \sigma_{jk\nu}^{(-n)},\end{aligned}\right\} \tag{3.2}$$

where the quantities with $\sim$ represent the complex conjugates of the corresponding quantities. In this case, the circuit equations in the time domain are the same as (2.1), except that DL_{jk} and $S_{jk}\frac{1}{D}$ should both be kept unchanged in order.

Next, considering that L_{jk}, R_{jk} and S_{jk} are constructed by $\lambda_{jk\kappa}$, $\rho_{jk\mu}$ and $\sigma_{jk\nu}$ as shown in (3.1) respectively*, we take the Laplace transforms of (2.1) in which, however, L_{jk}, R_{jk} and S_{jk} are constructed by linear varying circuit elements given by (3.1).

Then we obtain:

$$\left.\begin{aligned}&\sum_k \sum_n \Big[\sum_\kappa \{p\lambda_{jk\kappa}^{(n)}(I_k(p-in\omega_{jk\kappa})-I_j(p-in\omega_{jk\kappa})\,\delta_{jk}')\} \\ &\quad+\sum_\mu \{\rho_{jk\mu}^{(n)}(I_k(p-in\omega_{jk\mu})-I_j(p-in\omega_{jk\mu})\,\delta_{jk}')\} \\ &\quad+\sum_\nu \{\sigma_{jk\nu}^{(n)}(p-in\omega_{jk_\nu})^{-1}(I_k(p-in\omega_{jk_\nu})-I_j(p-in\omega_{jk_\nu})\,\delta_{jk}')\}\Big] \\ &\quad= E_j'(p), \\ &E_j'(p) = E_j(p)+\sum_k \{L_{jk}(0)\,i_k(0)-p^{-1}S_{jk}(p)\,q_k(0)\}^{**},\end{aligned}\right\} \tag{3.3}$$

where

$$\left.\begin{aligned}&E_j(p) = L(e_j(t)), \quad I_j(p) = L(i_j(t)), \\ &q_j(t) = \int^t i_j(t')\,dt', \quad \delta_{jk}' = \begin{cases}0 & (j=k), \\ 1 & (j\neq k),\end{cases} \\ &S_{jk}'(p) = p\{\sum_\nu \sum_n \sigma_{jk\nu}^{(n)}(p-in\omega_{jk_\nu})^{-1}\} \qquad (j\neq k), \\ &S_{jj}(p) = p\{\sum_\nu \sum_n \sigma_{jj\nu}^{(n)}(p-in\omega_{jj_\nu})^{-1}-\sum_l{}' \sum_\nu \sum_n \sigma_{jl\nu}^{(n)}(p-in\omega_{jl_\nu})^{-1}\}.\end{aligned}\right\} \tag{3.4}$$

When we can solve $I_k(p)$'s from the fundamental equations (3.3), $i_k(t)$'s can be obtained as inverse Laplace transforms of $I_k(p)$'s.

Further, since it is difficult to make (3.3) in this form correspond to (2.1″), we must introduce the translational operator in frequency domain into (3.3).

---

* The processes of the constructions are the same as in § 2.

** $L_{jk}(0)=L_{jk}(t)\big|_{t=0}$.

As described in part I, when $f(p)$ is a function of p, the translational operator is defined as follows:

$$T(\omega)\, f(p) = f(p - i\omega)\,. \tag{3.5}$$

Using the operator, we can rewrite (3.3) and (3.4) as follows:

$$\begin{aligned}\sum_k \sum_n \Big[&\sum_\kappa \{p\lambda^{(n)}_{jk\kappa} T^n(\omega_{jk\kappa})(I_k(p) - I_j(p)\,\delta'_{jk})\} \\ &\sum_\mu \{\rho^{(n)}_{jk\mu} T^n(\omega_{jk\mu})(I_k(p) - I_j(p)\,\delta'_{jk})\} \\ &\sum_\nu \left\{\sigma^{(n)}_{jk\nu} T^n(\omega_{jk\nu})\,\frac{1}{p}\,(I_k(p) - I_j(p)\,\delta'_{jk})\right\} \\ = E'_j(p)\,,\end{aligned} \tag{3.6}$$

$$\left.\begin{aligned} S'_{jk}(p) &= p\left\{\sum_\nu \sum_n \sigma^{(n)}_{jk\nu} T^n(\omega_{jk\nu})\,\frac{1}{p}\right\} \qquad (j \neq k)\,, \\ S'_{jj}(p) &= p\{\sum_\nu \sum_n \sigma^{(n)}_{jj\nu} T^n(\omega_{jj\nu}) - \sum'_l \sum_\nu \sum_n \sigma^{(n)}_{jl\nu} T^n(\omega_{jl\nu})\}\,\frac{1}{p}\,. \end{aligned}\right\} \tag{3.7}$$

Now, when $L_{jk}(T, p)$, $R_{jk}(T, p)$ and $S_{jk}(T, p)$ are defined by the following expressions:

$$\left.\begin{aligned} L_{jk}(T, p) &= \{\sum_\kappa \sum_n \lambda^{(n)}_{jk\kappa} T^n(\omega_{jk\kappa})\} - \{\sum'_l \sum_\kappa \sum_n \lambda^{(n)}_{jl\kappa} T^n(\omega_{jl\kappa})\}\,\delta_{jk}\,, \\ R_{jk}(T, p) &= \{\sum_\mu \sum_n \rho^{(n)}_{jk\mu} T^n(\omega_{jk\mu})\} - \{\sum'_l \sum_\mu \sum_n \rho^{(n)}_{jl\mu} T^n(\omega_{jl\mu})\}\,\delta_{jk}\,, \\ S_{jk}(T, p) &= \{\sum_\nu \sum_n \sigma^{(n)}_{jk\nu} T^n(\omega_{jk\nu})\} - \{\sum'_l \sum_\nu \sum_n \sigma^{(n)}_{jl\nu} T^n(\omega_{jl\nu})\}\,\delta_{jk}\,, \end{aligned}\right\} \tag{3.8}$$

the equations (3.6) and (3.7) becomes as follows:

$$\sum_k \left(pL_{jk}(T, p) + R_{jk}(T, p) + S_{jk}(T, p)\,\frac{1}{p}\right) I_k(p) = E'_j(p)\,, \tag{3.6'}$$

$$S'_{jk}(p) = pS_{jk}(T, p)\,\frac{1}{p}\,. \tag{3.7'}$$

Equation (3.6′) is further rewritten:

$$\sum_k Z_{jk}(T, p)\, I_k(p) = E'_j(p)\,, \tag{3.6''}$$

with

$$Z_{jk}(T, p) = pL_{jk}(T, p) + R_{jk}(T, p) + S_{jk}(T, p)\,\frac{1}{p}\,. \tag{3.9}$$

(3.6″) is expressed in a matrix form:

$$[Z(T, p)][I(p)] = [E'(p)]\,, \tag{3.6'''}$$

where

$$[I(p)] = \begin{bmatrix} I_1(p) \\ I_2(p) \\ \vdots \\ I_N(p) \end{bmatrix}, \quad [E'(p)] = \begin{bmatrix} E'_1(p) \\ E'_2(p) \\ \vdots \\ E'_N(p) \end{bmatrix},$$

$$[Z(T, p)] = \begin{bmatrix} Z_{11} & Z_{12} \cdots\cdots Z_{1N} \\ Z_{21} & Z_{22} \cdots\cdots Z_{2N} \\ \cdots\cdots\cdots\cdots\cdots \\ \cdots\cdots\cdots\cdots\cdots \\ Z_{N1} & Z_{N2} \cdots\cdots Z_{NN} \end{bmatrix}^{*}.$$

Representing the inverse matrix of $[Z(T, p)]$ by $[Y(T, p)]$, we obtain:

$$[I(p)] = [Y(T, p)][E'(p)]. \tag{3.10}$$

We will call $[Z(T, p)]$ and $[Y(T, p)]$ generalized impedance operator matrix and generalized admittance operator matrix respectively. From (3.10), we see that it reduces to the discovery of the inverse matrix $[Y(T, p)]$, to obtain $i_k(t)$'s.

We can easily show that Kirchhoff's laws, the principle of superposition, Thévenin-Ho's theorem and the duality of network are valid in the varying network.

Next we derive the nodal equations of the linear varying network by setting the following correspondence:

inductance	(L)	capacitance (C)
resistance	(R)	conductance (G)
elastance	(S)	reciprocal inductance (Γ)
mesh current		nodal voltage
mesh voltage		nodal current
mesh		node.

From the above duality relations, the nodal equations corresponding to (3.6′) are obtained:

$$\sum_k \left(pC_{jk}(T, p) + G_{jk}(T, p) + \Gamma_{jk}(T, p)\frac{1}{p} \right) E_k(p) = I'_j(p), \tag{3.11}$$

where

$$I'_j(p) = I_j(p) + \sum_k \left\{ C_{jk}(0)\, e_k(0) - \Gamma_{jk}(T, p)\, \frac{1}{p}\, \phi_k(0) \right\},^{**}$$

$$\phi_k(t) = \int^t e_k(t')\, dt'.$$

Putting

$$Y_{jk}(T, p) = pC_{jk}(T, p) + G_{jk}(T, p) + \Gamma_{jk}(T, p)\, \frac{1}{p} \tag{3.12}$$

and defining the generalized admittance operator by the following matrix:

$$[Y(T, p)] = \begin{bmatrix} Y_{11} & Y_{12} \cdots\cdots Y_{1N} \\ Y_{21} & Y_{22} \cdots\cdots Y_{2N} \\ \cdots\cdots\cdots\cdots\cdots \\ \cdots\cdots\cdots\cdots\cdots \\ Y_{N1} & \cdots\cdots\cdots Y_{NN} \end{bmatrix}^{***},$$

* The matrix element Z_{lm} is an abbreviation of $Z_{lm}(T, p)$.

** $C_{jk}(0) = C_{jk}(t)|_{t=0}$.

*** Y_{lm} is an abbreviation of $Y_{lm}(T, p)$.

we can rewrite (3.11) as follows:

$$[Y(T, p)][E(p)] = [I'(p)], \tag{3.11'}$$

which corresponds to (3.6‴).

We will call (3.6‴) and (3.11′) generalized mesh equations and generalized nodal equations respectively.

From (3.6‴), (3.9), (3.11′) and (3.12), we can see that in our treatment, the circuit equations of linear fixed network are naturally extended to the linear varying network where the elements are expressed by periodic functions of time.

In Kiyasu's theory, impedances are expressed by infinite dimensional matrices and so it seems to the author that the author's method utilizing the translational operator is more convenient.

The procedure described can evidently be extended to the case when $\lambda_{jk\kappa}$, $\rho_{jk\mu}$ and $\sigma_{jk\nu}$ are varying with the following angular frequencies:

$$\left.\begin{aligned} &\omega_{jk\kappa}^{(1)}, \ \omega_{jk\kappa}^{(2)}, \ \cdots\cdots\cdots, \ \omega_{jk\kappa}^{(l)} \quad \text{for} \quad \lambda_{jk\kappa}, \\ &\omega_{jk\mu}^{(1)}, \ \omega_{jk\mu}^{(2)}, \ \cdots\cdots\cdots, \ \omega_{jk\mu}^{(m)} \quad \text{for} \quad \rho_{jk\mu}, \\ &\omega_{jk\nu}^{(1)}, \ \omega_{jk\nu}^{(2)}, \ \cdots\cdots\cdots, \ \omega_{jk\nu}^{(n)} \quad \text{for} \quad \sigma_{jk\nu}. \end{aligned}\right\} \tag{3.13}$$

And when $\omega_{jk\kappa}^{(l)}$, $\omega_{jk\mu}^{(l)}$ and $\omega_{jk\nu}^{(l)}$ are complex quantities, the above process can be adapted by making the following modification. Namely, in order that the circuit elements may be expressed by real functions, (3.1) are modified as follows*:

$$\left.\begin{aligned} \lambda_{jk\kappa} &= \lambda_{jk\kappa}^{(0)} + \sum_{n=1}^{\infty} \lambda_{jk\kappa}^{(n)} e^{in\omega_{jk\kappa}t} + \sum_{n=1}^{\infty} \lambda_{jk\kappa}^{(-n)} \widetilde{e^{in\omega_{jk\kappa}t}}, \\ \rho_{jk\mu} &= \rho_{jk\mu}^{(0)} + \sum_{n=1}^{\infty} \rho_{jk\mu}^{(n)} e^{in\omega_{jk\mu}t} + \sum_{n=1}^{\infty} \rho_{jk\mu}^{(-n)} \widetilde{e^{in\omega_{jk\mu}t}}, \\ \sigma_{jk\nu} &= \sigma_{jk\nu}^{(0)} + \sum_{n=1}^{\infty} \sigma_{jk\nu}^{(n)} e^{in\omega_{jk\nu}t} + \sum_{n=1}^{\infty} \sigma_{jk\nu}^{(-n)} \widetilde{e^{in\omega_{jk\nu}t}}. \end{aligned}\right\} \tag{3.1'}$$

The relations (3.2) remain to be valid. From (3.1′), it is evident that (3.8) and (3.7) have only to be modified as follows. Namely, while the translational operators behind the factors, $\lambda_{jk\kappa}^{(n)}$, $\rho_{jk\mu}^{(n)}$ and $\sigma_{jk\nu}^{(n)}$ $(n>0)$ are left unchanged, the operators behind $\lambda_{jk\kappa}^{(-n)}$, $\rho_{jk\mu}^{(-n)}$ and $\sigma_{jk\nu}^{(-n)}$ $(n>0)$ are replaced by the following operators:

$$\widetilde{T(\omega_{jk\kappa})}, \quad \widetilde{T(\omega_{jk\mu})}, \quad \widetilde{T(\omega_{jk\nu})}$$

respectively, with the power indices of the translational operator remaining unchanged.

Similar extensions are possible for the nodal equations.

---

* Here is considered the case when $l=m=n=1$ in (3.13) and $\omega_{jk\kappa}^{(1)}$, $\omega_{jk\mu}^{(1)}$ and $\omega_{jk\nu}^{(1)}$ are represented by $\omega_{jk\kappa}$, $\omega_{jk\mu}$ and $\omega_{jk\nu}$ respectively. It is easy to extend the discussion to the case when l, m and n are all greater than unity.

4. Linear varying network whose circuit elements vary periodically with one common period

The case shown in the title corresponds to conditions that

$$T(\omega_{jk\kappa}) = T(\omega_{j'k'\mu}) = T(\omega_{j''k''\nu}) \tag{4.1}$$

for all (j, k, κ), (j', k', μ) and (j'', k'', ν).

Now putting

$$\omega_{jk\kappa} = \omega_{j'k'\mu} = \omega_{j''k''\nu} = \omega_0 ,$$

we obtain:

$$[Z(T, p)] = \sum_{n=-\infty}^{\infty} [Z^{(n)}(p)]\, T^n(\omega_0) . \tag{4.2}$$

$[Z^{(n)}(p)]$ is given as follows:

$$[Z^{(n)}(p)] = \begin{Vmatrix} Z_{11}^{(n)}(p) & Z_{12}^{(n)}(p) \cdots Z_{1N}^{(n)}(p) \\ Z_{21}^{(n)}(p) & Z_{22}^{(n)}(p) \cdots Z_{2N}^{(n)}(p) \\ \cdots\cdots\cdots\cdots\cdots\cdots\cdots \\ \cdots\cdots\cdots\cdots\cdots\cdots\cdots \\ Z_{N1}^{(n)}(p) & Z_{N2}^{(n)}(p) \cdots Z_{NN}^{(n)}(p) \end{Vmatrix} , \tag{4.3}$$

where

$$\left.\begin{aligned} Z_{jk}^{(n)}(p) &= p\lambda_{jk}^{(n)} + \rho_{jk}^{(n)} + p^{-1}\sigma_{jk}^{(n)\prime} , \\ p\lambda_{jk}^{(n)} &= p\{\sum_{\kappa} \lambda_{jk\kappa}^{(n)} - (\sum_{l}{}' \sum_{\kappa} \lambda_{jl\kappa})\, \delta_{jk}\} , \\ \rho_{jk}^{(n)} &= \sum_{\mu} \rho_{jk\mu}^{(n)} - (\sum_{l}{}' \sum_{\mu} \rho_{jl\mu}^{(n)})\, \delta_{jk} , \\ p^{-1}\sigma_{jk}^{(n)\prime} &= (p - in\omega_0)^{-1}\{\sum_{\nu} \sigma_{jk\nu}^{(n)} - (\sum_{l}{}' \sum_{\nu} \sigma_{jl\nu}^{(n)})\, \delta_{jk}\} . \end{aligned}\right\} \tag{4.4}$$

We can also write (4.2) as follows:

$$\left.\begin{aligned} [Z(T, p)] &= \sum_{n=-\infty}^{\infty} T^n(\omega_0)[Z^{(n)\prime}(p)] , \\ Z_{jk}^{(n)\prime}(p) &= Z_{jk}^{(n)}(p + in\omega_0) . \end{aligned}\right\} \tag{4.5}$$

In the treatment described above is included the case of the network of which only one circuit element is varying and the others are fixed. According as the varying element is an inductor or a capacitor, we obtain, using (4.2) or (4.5), the circuit equation which does not include ω_0 explicitly excepting in $T(\omega_0)$.

This is often convenient for application, e.g. when the method of series expansion is used. If the only varying element is a resistor, the same circuit equation is obtained by use of either expression.

5. Transmission lines with linear periodically varying network inserted*

The following discussion still holds when the linear periodically varying network is replaced by the E-type circuit element.

* Read in part before the joint meeting of Kansai branches of three Electrical Societies, Oct. 17, 1954 (**14**).

We consider how the reflection coefficient and the transmission coefficient are generalized, in case when the linear periodically varying network is inserted in the transmission lines such as Lecher lines, coaxial cable, wave guide, etc.

The transmission lines are assumed to be fixed. Since neither charge nor current exists in the inserted network before the arrival of the incident waves, the following are substituted into (3.6‴):

$$\left.\begin{aligned} E'_j(p) &= E_j(p) && (j = 1, 2), \\ E'_j(p) &= 0 && (j = 1, 2), \end{aligned}\right\}$$

and eliminating $I_3(p)$, $I_4(p)$,$\cdots I_N(p)$ from the resulting equations, we can easily obtain:

$$\begin{bmatrix} E_1(p) \\ E_2(p) \end{bmatrix} = \begin{bmatrix} \bar{Z}_{11}(T, p) & \bar{Z}_{12}(T, p) \\ \bar{Z}_{21}(T, p) & \bar{Z}_{22}(T, p) \end{bmatrix} \begin{bmatrix} I_1(p) \\ I_2(p) \end{bmatrix}. \tag{5.1}$$

When, as shown in Fig. 2, the semi-infinite transmission lines (I) are connected to the terminals (1, 1′) of the inserted network and the load $Z_L(p)$ to the terminals (2, 2′), we will derive the reflection coefficient in the transmission lines (I).

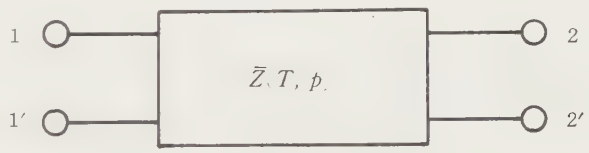

Fig. 2

Now we take the x_1-axis along the transmission lines (I), with the positive sense directed toward terminals (1, 1′). We represent the current and the voltage at the point x_1 (in the frequency domain) by $I(x_1, p)$ and $E(x_1, p)$ respectively and assume that the incident waves have the time factor $e^{i\omega t}$ in the time-domain representation. Then, in the case of constant current source the incident current and voltage are given by:

$$\left.\begin{aligned} I^{(i)}(x_1, p) &= e^{-\gamma_1(p)x_1}\{I_0 e^{-pt_0}(p-i\omega)^{-1}\}, \\ E^{(i)}(x_1, p) &= Z_0^{(1)}(p)\, e^{-\gamma_1(p)x_1}\{I_0 e^{-pt_0}(p-i\omega)^{-1}\}, \end{aligned}\right\} \tag{5.2}$$

where $\gamma_1(p)$ and $Z_0^{(1)}(p)$ are the propagation constant and the surge impedance of the transmission lines (I) in the frequency domain respectively. These expressions mean that the incident waves arrive at the inserted network at $t=t_0$, if $t_0>0$.

Next, the reflected current and voltage can be given by:

$$\left.\begin{aligned} I^{(r)}(x_1, p) &= e^{\gamma_1(p)x_1}A(T, p)\{I_0 e^{-pt_0}(p-i\omega)^{-1}\}, \\ E^{(r)}(x_1, p) &= -Z_0^{(1)}(p)\, e^{\gamma_1(p)x_1}A(T, p)\{I_0 e^{-pt_0}(p-i\omega)^{-1}\}. \end{aligned}\right\} \tag{5.3}$$

Applying the continuity conditions of the current and voltage at $x_1=0$, i.e. at the terminals $(1, 1')$, to (5.2) and (5.3), we obtain:

$$\left.\begin{aligned} &A(T, p) = \{Z_0^{(1)}(p)+\bar{Z}(T, p)\}^{-1}\{Z_0^{(1)}(p)-\bar{Z}(T, p)\}, \\ \text{where}\quad &\bar{Z}(T, p) = \bar{Z}_{11}(T, p)-\bar{Z}_{12}(T, p)\{Z_L(p)+\bar{Z}_{22}(T, p)\}^{-1}\bar{Z}_{21}(T, p). \end{aligned}\right\} \tag{5.4}$$

As $Z_L(p)$, the semi-infinite transmission lines (II) are connected to the terminals $(2, 2')$ and we take the x_2-axis along these lines, with the positive sense away from the terminals $(2, 2')$ and the origin set at the terminals $(2, 2')$.

Representing the propagation constant and the surge impedance of the transmission lines (II) in the frequency domain by $\gamma_2(p)$ and $Z_0^{(2)}(p)$ respectively, we consider the transmission coefficient in the transmission lines (II). Now the transmitted current and voltage are assumed to be given by:

$$\left.\begin{aligned} I^{(t)}(x_2, p) &= e^{-\gamma_2(p)x_2}I_2(p), \\ E^{(t)}(x_2, p) &= Z_0^{(2)}(p)\, e^{-\gamma_2(p)x_2}I_2(p). \end{aligned}\right\} \tag{5.5}$$

The following expressions are substituted into (5.1):

$$\begin{aligned} I_1(p) &= \{1+A(T, p)\}\{I_0\, e^{-pt_0}(p-i\omega)^{-1}\}, \\ E_1(p) &= Z_0^{(1)}(p)\{1-A(T, p)\}\{I_0\, e^{-pt_0}(p-i\omega)^{-1}\}, \\ E_2(p) &= -Z_0^{(2)}(p)\, I_2(p), \end{aligned}$$

where $A(T, p)$ means $A(T, p)$ which is obtained by putting

$$Z_L(p) = Z_0^{(2)}(p)$$

in (5.4).

Then

$$I_2(p) = B(T, p)\, I_0\{e^{-pt_0}(p-i\omega)^{-1}\},$$

where

$$B(T, p) = -\{Z_0^{(2)}(p)+\bar{Z}_{22}(T, p)\}^{-1}\bar{Z}_{21}(T, p)\{1+A(T, p)\}. \tag{5.6}$$

Substituting (5.6) into (5.5), we obtain:

$$\left.\begin{aligned} I^{(t)}(x_2, p) &= e^{-\gamma_2(p)x_2}B(T, p)\, I_0\{e^{-pt_0}(p-i\omega)^{-1}\}, \\ E^{(t)}(x_2, p) &= Z_0^{(2)}(p)\, e^{-\gamma_2(p)x_2}B(T, p)\, I_0\{e^{-pt_0}(p-i\omega)^{-1}\}. \end{aligned}\right\} \tag{5.7}$$

We will call $A(T, p)$ and $B(T, p)$ defined by (5.4) and (5.6) respectively the generalized reflection coefficient operator and transmission coefficient operator for the constant current source.

For the constant voltage source, we can also define the generalized reflection coefficient operator and transmission coefficient operator which are represented by $A'(T, p)$ and $B'(T, p)$ respectively, related with $A(T, p)$ and $B(T, p)$ such that:

$$\left.\begin{aligned} A'(T, p) &= Z_0^{(1)}(p)\, A(T, p)\, Z_0^{(1)}(p)^{-1}, \\ B'(T, p) &= Z_0^{(2)}(p)\, B(T, p)\, Z_0^{(2)}(p)^{-1}. \end{aligned}\right\} \tag{5.8}$$

When $A'(T, p)$ and $B'(T, p)$ are used, the expressions of the current and voltage in the frequency domain for the constant voltage source are given by the following:

On the side of the terminals $(1, 1')$;

$$\left.\begin{aligned} I_1(x_1, p) &= Z_0^{(1)}(p)^{-1}\{e^{-\gamma_1(p)x_1} - e^{\gamma_1(p)x_1}A'(T, p)\}E_0\{e^{-pt_0}(p - i\omega)^{-1}\}, \\ E_1(x_1, p) &= \{e^{-\gamma_1(p)x_1} - e^{\gamma_1(p)x_1}A'(T, p)\}E_0\{e^{-pt_0}(p-i\omega)^{-1}\}, \end{aligned}\right\} \tag{5.9}$$

and on the side of the terminals $(2, 2')$;

$$\left.\begin{aligned} I_2(x_2, p) &= Z_0^{(2)}(p)^{-1}\, e^{-\gamma_2(p)x_2}B'(T, p)\, E_0\{e^{-pt_0}(p-i\omega)^{-1}\}, \\ E_2(x_2, p) &= e^{-\gamma_2(p)x_2}B'(T, p)\, E_0\{e^{-pt_0}(p-i\omega)^{-1}\}. \end{aligned}\right\} \tag{5.10}$$

As seen from (5.8), when the transmission lines (I) and (II) are non-dispersive i.e. $Z^{(1)}(p)$ and $Z^{(2)}(p)$ do not include p, $A'(T, p)$ and $B'(T, p)$ coincide with $A(T, p)$ and $B(T, p)$ respectively.

The author is sure that such a problem as has been described in this section, cannot be easily treated by other methods.

6. Some examples

(i) As an example of the linear varying network described in §4, we will consider the circuit shown in Fig. 3, which acts as a varying low pass filter.

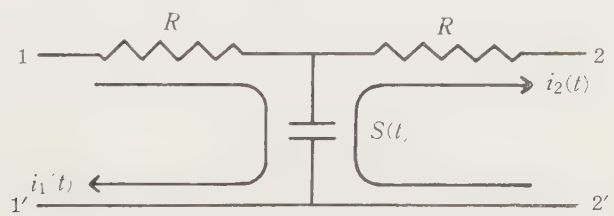

Fig. 3

The circuit equations are given as follows:

$$\begin{bmatrix} E_1(p) \\ E_2(p) \end{bmatrix} = \begin{bmatrix} Z_{11} & Z_{12} \\ Z_{21} & Z_{22} \end{bmatrix} \begin{bmatrix} I_1(p) \\ I_2(p) \end{bmatrix}, \tag{6.1}$$

where

$$q_1(0) = q_2(0) = 0,$$

and

$$\left.\begin{aligned} Z_{11}(T, p) = Z_{22}(T, p) &= R + \{\sigma^{(0)} + \sigma^{(1)}(T(\omega_0) + T^{-1}(\omega_0))\}\frac{1}{p}, \\ Z_{12}(T, p) = Z_{21}(T, p) &= -\{\sigma^{(0)} + \sigma^{(1)}(T(\omega_0) + T^{-1}(\omega_0))\}\frac{1}{p}. \end{aligned}\right\} \tag{6.2}$$

From (6.1) we obtain:

$$\frac{1}{2}(E_1(p)+E_2(p)) = R\frac{1}{2}(I_1(p)+I_2(p)),$$

$$\frac{1}{2}(E_1(p)-E_2(p)) = \left\{R+2\{\sigma^{(0)}+\sigma^{(1)}(T(\omega_0)+T^{-1}(\omega_0))\}\frac{1}{p}\right\}\frac{1}{2}(I_1(p)-I_2(p)),$$

and further by these equations,

$$\left.\begin{aligned}\frac{1}{2}(I_1(p)+I_2(p)) &= \frac{1}{R}\frac{1}{2}(E_1(p)+E_2(p)),\\ \frac{1}{2}(I_1(p)-I_2(p)) &= \frac{1}{R}p\,e^{-\beta(T(\omega_0)-T^{-1}(\omega_0))}\\ &\quad\times\frac{1}{p+\tau^{-1}}e^{\beta(T(\omega_0)-T^{-1}(\omega_0))}\frac{1}{2}(E_1(p)-E_2(p)),\end{aligned}\right\} \tag{6.3}$$

where $\beta=\dfrac{2\sigma^{(1)}}{iR\omega_0}$ and $\tau=\dfrac{R}{2\sigma^{(0)}}$.

Solving (6.3) for $I_1(p)$ and $I_2(p)$, we obtain:

$$\begin{bmatrix}I_1(p)\\ I_2(p)\end{bmatrix} = \begin{bmatrix}Y_{11} & Y_{12}\\ Y_{21} & Y_{22}\end{bmatrix}\begin{bmatrix}E_1(p)\\ E_2(p)\end{bmatrix}, \tag{6.4}$$

where

$$\left.\begin{aligned}Y_{11}(T,p) &= Y_{22}(T,p) = \frac{1}{2R}\left\{1+pU^{-1}(T(\omega_0))\frac{1}{p+\tau^{-1}}U(T(\omega_0))\right\},\\ Y_{12}(T,p) &= Y_{21}(T,p) = \frac{1}{2R}\left\{1-pU^{-1}(T(\omega_0))\frac{1}{p+\tau^{-1}}U(T(\omega_0))\right\},\end{aligned}\right\} \tag{6.5}$$

and

$$U(T(\omega_0)) = \exp\left\{\frac{2\sigma^{(1)}}{i\omega_0 R}(T(\omega_0)-T^{-1}(\omega_0))\right\}.$$

Now, assuming that

$$e_1(t) = A_1 e^{i\omega t},$$
$$e_2(t) = A_2 e^{i\omega t},$$

and taking into account the considerations in §4, part I, we obtain $i_1(t)$ and $i_2(t)$ by converting (6.4) to the representation in the time domain as follows:

$$\begin{bmatrix}i_1(t)\\ i_2(t)\end{bmatrix} = \begin{bmatrix}y_{11}(t) & y_{12}(t)\\ y_{21}(t) & y_{22}(t)\end{bmatrix}\begin{bmatrix}e_1(t)\\ e_2(t)\end{bmatrix}, \tag{6.6}$$

where

$$\left.\begin{aligned}y_{11}(t) &= y_{22}(t) = \frac{1}{2R}(1+\eta(t)),\\ y_{12}(t) &= y_{21}(t) = \frac{1}{2R}(1-\eta(t)),\end{aligned}\right\} \tag{6.7}$$

and

$$\eta(t) = e^{-i\omega t}\frac{d}{dt}\left\{U^{-1}(e^{i\omega_0 t})\,e^{-\frac{t}{\tau}}\int_0^t e^{\left(\frac{1}{\tau}+i\omega\right)t'}U(e^{i\omega_0 t'})\,dt'\right\}.$$

It seems worth noticing that the steady state solution can be obtained if, for the

lower limit of integration in $\eta(t)$, zero is replaced by $-\infty$ corresponding to $\tau>0$, while $+\infty$ is taken when $\tau<0$.

(ii) As an example of § 5, we consider the non-dispersive transmission lines in which the varying condenser is inserted.

The elastive coefficient of the condenser is assumed to vary sinusoidally with angular frequency ω_0, so that it can be expressed as follows:

$$S(t) = S_0 + 2\Delta S \cos(\omega_0 t + \varphi),$$

or

$$S(t) = \sigma^{(0)} + \sigma^{(1)} e^{i\omega_0 t} + \sigma^{(-1)} e^{-i\omega_0 t},$$

where

$$S_0 = \sigma^{(0)}, \quad \Delta S e^{i\varphi} = \sigma^{(1)}, \quad \Delta S e^{-i\varphi} = \sigma^{(-1)}.$$

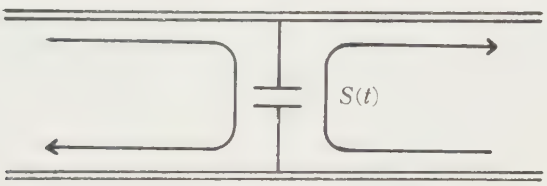

Fig. 4

Now, the x-axis is taken along the transmission lines and the origin set at the position of the inserting terminals, the right-hand side of the terminals being positive and the left-hand side negative.

Next the surge impedance and the propagation constant in the frequency domain are represented by Z_0 and $\gamma(p)$ respectively.

We assume that for the constant voltage source the waves are incident from the negative side and they are given by the following expressions:

$$\left.\begin{aligned} E^{(i)}(x, p) &= E_0 e^{-\gamma(p)x}\{e^{-pt_0}(p-i\omega)^{-1}\}, \\ I^{(i)}(x, p) &= Z_0^{-1} E_0 e^{-\gamma(p)x}\{e^{-pt_0}(p-i\omega)^{-1}\}. \end{aligned}\right\}$$

Then the currents and the voltages for $x<0$ and $x>0$ are given as follows:

for $x<0$,

$$\left.\begin{aligned} E(x, p) &= E_0\{e^{-\gamma(p)x} - e^{\gamma(p)x}A'(T, p)\}\{e^{-pt_0}(p-i\omega)^{-1}\}, \\ I(x, p) &= Z_0^{-1}E_0\{e^{-\gamma(p)x} + e^{\gamma(p)x}A'(T, p)\}\{e^{-pt_0}(p-i\omega)^{-1}\}, \end{aligned}\right\} \tag{6.8}$$

and for $x>0$,

$$\left.\begin{aligned} E(x, p) &= E_0 e^{-\gamma(p)x}B'(T, p)\{e^{-pt_0}(p-i\omega)^{-1}\}, \\ I(x, p) &= Z_0^{-1}E_0 e^{-\gamma(p)x}B'(T, p)\{e^{-pt_0}(p-i\omega)^{-1}\}, \end{aligned}\right\} \tag{6.9}$$

where $A'(T, p)$ and $B'(T, p)$ are given by the following expressions:

$$\left.\begin{aligned} A'(T, p) &= \{2Z(T, p)\, Z_0^{-1} + 1\}^{-1}, \\ B'(T, p) &= 1 - A'(T, p) = \{1 + 2Z(T, p)\, Z_0^{-1}\}^{-1}\{2Z(T, p)\, Z_0^{-1}\}, \\ Z(T, p) &= \left\{\sigma^{(0)} + (\sigma^{(1)}T(\omega_0) + \sigma^{(-1)}T^{-1}(\omega_0))\right\}\frac{1}{p}. \end{aligned}\right\} \tag{6.10}$$

Now, if we assume that these transmission lines are lossless Lecher lines or coaxial cables with induction coefficient per unit length l and capacity per unit length c, the expressions for $A'(T, p)$ and $B'(T, p)$ become as follows:

$$\left.\begin{aligned} A'(T, p) &= pU^{-1}(T(\omega_0))\,\frac{1}{p+\tau^{-1}}\,U(T(\omega_0))\,, \\ B'(T, p) &= 1-pU^{-1}(T(\omega_0))\,\frac{1}{p+\tau^{-1}}\,U(T(\omega_0))\,, \end{aligned}\right\} \tag{6.11}$$

where

$$U(T(\omega_0)) = \exp\left\{\frac{2}{iZ_0\omega_0}\,(\sigma^{(1)}T(\omega_0)-\sigma^{(-1)}T^{-1}(\omega_0))\right\},$$

$$\tau = \frac{2Z_0}{\sigma^{(0)}}.$$

Substituting (6.11) in (6.8) and taking the inverse Laplace transforms of the resulting expressions, we obtain the following expressions for $i(x, t)$ and $e(x, t)$ which denote the inverse Laplace transforms of $I(x, p)$ and $E(x, p)$ respectively.

Putting $v^{-1}=\sqrt{lc}$, we get, for $x<0$,

$$\left.\begin{aligned} e(x, t) &= E_0\{P(x, t)-R(x, t)\}\,, \\ i(x, t) &= Z_0^{-1}E_0\{P(x, t)+R(x, t)\}\,, \end{aligned}\right\} \tag{6.12}$$

where

$$\left.\begin{aligned} P(x, t) &= 0 \qquad \left(t-t_0-\frac{x}{v}<0\right), \\ P(x, t) &= e^{i\omega\{(t-t_0)-\frac{x}{v}\}} \qquad \left(t-t_0-\frac{x}{v}>0\right), \\ R(x, t) &= 0 \qquad \left(t-t_0+\frac{x}{v}<0\right), \\ R(x, t) &= \frac{d}{dt}\left\{U^{-1}(e^{i\omega_0(t*+t_0)})\,e^{-\frac{t^*}{\tau}}\int_0^{t^*} e^{(\frac{1}{\tau}+i\omega)t'}U(e^{i\omega_0(t'+t_0)})\,dt'\right\} \\ &\qquad \left(t-t_0+\frac{x}{v}>0\right) \end{aligned}\right\}$$

with $t^*=t-t_0+\frac{x}{v}$, and for $x>0$,

$$\left.\begin{aligned} e(x, t) &= 0 \qquad \left(t-t_0-\frac{x}{v}<0\right), \\ i(x, t) &= 0 \qquad \left(t-t_0-\frac{x}{v}<0\right), \\ \left.\begin{aligned} e(x, t) &= E_0 \\ i(x, t) &= Z_0^{-1}E_0 \end{aligned}\right\} &\times\left[e^{i\omega t'^*}-\frac{d}{dt}\left\{U^{-1}(e^{i\omega_0(t'^*+t_0)})\right.\right. \\ &\qquad \left.\left.\times e^{-\frac{t'^*}{\tau}}\int_0^{t'^*} e^{(\frac{1}{\tau}+i\omega)t'}U(e^{i\omega_0(t'+t_0)})\,dt'\right\}\right] \\ &\left(t-t_0-\frac{x}{v}>0\right), \end{aligned}\right\} \tag{6.13}$$

where $t'^* = t - t_0 - \frac{x}{v}$.

The steady state solution can be obtained by the same procedure as stated in (i).

7. Conclusion

By introducing the translational operator, the circuit equations of the linear fixed network can be more naturally extended to the cases of the linear varying network than by other authors' theories.

Further, the ideas such as impedance, admittance, reflection coefficient and transmission coefficient can also be generalized by the present author's method. The present theory can explicitly give the impedance and the admittance in terms of the circuit elements. Particularly, as described in § 5, we can easily perform the treatment of the cases when the linear varying network is inserted in the transmission lines. Such cases have never been treated by other authors.

As described in part I, in order to obtain the solution of the circuit equations, we must generally rely on the method of series expansion.

However, according to this method, the transient parts of the solutions sometimes take complex forms and so it seems necessary to obtain the transient parts in tractable forms by means of a more ingeneous method. Since it is important to consider in detail the transient parts which are associated with the stability, we should make researches on this aspect of the subject. The author hopes to carry out the researches in future.

Finally the author wishes to thank Professor S. Tomotika and Professor I. Takahashi for their powerful guidance and persistent encouragement.

REFERENCES

1. J. R. Carson, Theory and calculation of variable electrical systems. Phys. Rev. **17** (1921), 116.
2. J. Neufeld, Extension of the methods of Heaviside's calculus in calculation of circuits containing parameters varying with time. Phil. Mag. [7] **15** (1933), 170.
3. L. A. Pipes, Operational and matrix methods in linear variable networks. Phil. Mag. [7] **25** (1938), 585.
4. M. Akiyama, The fundamental theory of the linearly modulating network. J. Inst. Electr. Comm. Japan **119** (1939), 524 (in Japanese).
5. M. Akiyama, The theoretical considerations of the linearly modulating four-terminals network. J. Inst. Electr. Comm. Japan **120** (1939), 591 (in Japanese).
6. M. Akiyama, The theoretical considerations of the linearly modulating four-terminals network. J. Inst. Electr. Comm. Japan **121** (1939), 699 (in Japanese).
7. L. A. Zadeh, Frequency analysis of variable networks. Proc. Inst. Radio Eng. **38** (1950), 291.
8. L. A. Zadeh, The determination of the impulsive response of variable networks. J. Appl. Phys. **21** (1950), 642.
9. L. A. Zadeh, Circuit analysis of linear varying-parameter networks. J. Appl. Phys. **21** (1950), 1171.

10. L. A. ZADEH, Initial conditions in linear varying-parameter system. J. Appl. Phys. **22** (1950), 782.

11. Z. KIYASU, The theory of the ring modulator. Report Res. Electr. Comm. Lab. No. 1, March (1951) (in Japanese).

12. I. TAKAHASHI and T. WATANABE, On the linear network containing circuit elements periodically varying with time (I). Preparing draft at the joint meeting of Kansai branches of three Electrical Societies, Oct. 18, 1951 (in Japanese).

13. I. TAKAHASHI and T. WATANABE, On the linear network containing circuit elements periodically varying with time (II). Preparing draft at the joint meeting of Kansai branches of three Electrical Societies, Oct. 17, 1953 (in Japanese).

14. I. TAKAHASHI and T. WATANABE, On the linear network containing circuit elements periodically varying with time (III). Preparing draft at the joint meeting of Kansai branches of three Electrical Societies, Oct. 17, 1954 (in Japanese).

Memoirs of the College of Science, University of Kyoto, Series A,
Vol. XXVIII, No. 4, Article 4, 1958.

THE COMPLEX DIELECTRIC CONSTANT AND PERMEABILITY OF Ni-Cd FERRITE SYSTEM AT MICROWAVE FREQUENCIES*

BY

Susumu TAKEMOTO**

(*Received December 17, 1957*)

ABSTRACT

The complex dielectric constant $\varepsilon=\varepsilon'-j\varepsilon''$ and permeability $\mu=\mu'-j\mu''$ of many ferrites have already been studied in low and radio frequency regions, and excellent ferrites have successfully been utilized for many electrical devices. The present author measured the dielectric constant and permeability of the polycrystalline sintered ferrite system $Ni_{1-x}Cd_xFe_2O_4$ at 9300 MC and 24000 MC at room temperature. Such experiments as those by the present author have been made only seldom, and especially for the Ni-Cd ferrite system, no experiment seems to have been carried out yet so far as the author is aware of. In this paper, the mechanisms of conductivity and of dispersion of permeability at microwave frequencies will be discussed, and the relationship between conductivity and dielectric constant will also be discussed.

1. Introduction

The dielectric and magnetic properties of ferrites are greatly improved by making the solid solution of normal spinel ferrite in inverse spinel ferrite. This fact is very interesting from both theoretical and practical points of view, and recently a great number of studies (**1**) on such mixed ferrites have been carried out in low and radio frequency regions, but the studies (**2**) in the microwave range have been rather inactive. While zinc ferrite has usually been employed as a normal spinel, cadmium ferrite has been used seldom due to some reasons.

Both cadmium ferrite and zinc ferrite have the normal spinel structure, and it is known that the radii of Cd ion and Zn ion are 1.03 Å and 0.83 Å respectively, while the radius of oxygen ion is 1.32 Å. So, it is expected that the electric and magnetic properties will be influenced by this and other differences between Cd ion and Zn ion. The author measured the complex dielectric constant and permeability of Ni-Cd ferrite system in the microwave region simulaneously by the so-called short-circuit and open-circuit method. According to the experimental data obtained, the conductivity σ and the dielectric constant ε have a close relation with each other and especially a

* Communicated by Professor Isao TAKAHASHI.

** Department of Physics, Faculty of Literature and Science, Shimane University.

remarkable reduction appears on both at the 70% Cd concentration. The results of measurement shows that the values of μ' are all less than unity owing to the dispersion phenomenon in the microwave region, and the orders of ε' and μ' are 15 and 0.6 at 9300 MC and those of ε' and μ' are 10 and 0.4 at 24000 MC.

2. Preparation of ferrite samples

The Ni-Cd ferrite system, $Ni_{1-X}\ Cd_XFe_2O_4$ was prepared by the following process. The values of X were varied from 0 to 1.0 successively. The raw materials NiO, CdO, and Fe_2O_3 of high purity were milled in steel ballmills for about 24 hours, and the mixture of these very fine particles obtained was dried and prefired in order to obtain a homogeneous sample. After prefiring, the material is milled. Then, the powder was pressed in steel dies at the pressure of 1 ton/cm^2 into a final shape. The final sintering was performed at about 1300°C in the air atmosphere, and the end-product was annealed slowly in the air.

3. Theory of measurement

The dielectric constant and permeability of ferrite are complex quantities, having the resonance absorption in the microwave region by the spin relaxation phenomena. We denote them by $\varepsilon = \varepsilon' - j\varepsilon''$ and $\mu = \mu' - j\mu''$ respectively. Hitherto the following two methods have mainly been adopted for the simultaneous measurements of ε and μ in the microwave range. One is the resonant cavity method, in which we can determine separately the imaginary and real parts of ε and μ by measuring the change of quality factor and the shift of resonance frequency of the cavity resonator, respectively. Healy (**3**), Birnbaum (**4**), Okamura (**5**), Ogasawara (**6**) and other researchers discussed the resonant cavity method and attained valuable results in practice. The other is the so-called short-circuit and open-circuit method, and by using it we can obtain the complex ε and μ from the measurement of the standing wave ratio and the change of the position of the voltage minimum. Since no special considerations are needed in the theory of the second method, it is a reliable and orthodox method so far as the precise measurement of the standing wave ratio is possible. Birks (**7**), Nishioka (**8**), Mori (**9**) and others studied ε and μ of various ferromagnetic substances by this method. Since there are some practical difficulties which limit the first method when applied at the frequencies above 9000 MC,

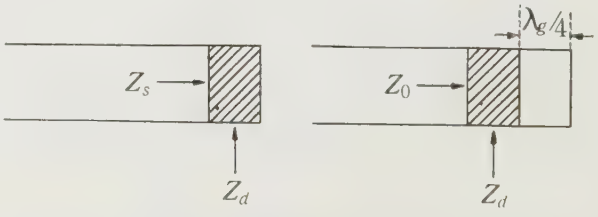

Fig. 1. Schematic representation of the sample at the wave guide termination.

the author adopted the second method. The outline of the theory of this measurement is as follows.

As shown in Fig. 1 the sample is inserted tightly into the wave guide with the free surfaces perpendicular to the guide axis while only the H_{10} wave is excited. The normalized short-circuit and open-circuit impedances are denoted by Z_s and Z_0 respectively in Fig. 1. Then the normalized impedance Z_d and the propagation constant γ in the sample become

$$Z_d = \sqrt{\frac{1-(\lambda/\lambda_c)^2}{(\varepsilon'-j\varepsilon'')(\mu'-j\mu'')-(\lambda/\lambda_c)^2}}\,(\mu'-j\mu''), \tag{1}$$

and

$$\gamma = \frac{2\pi}{\lambda}\sqrt{(\lambda/\lambda_c)^2-(\varepsilon'-j\varepsilon'')(\mu'-j\mu'')} \equiv \alpha+j\beta, \tag{2}$$

where λ is the wave length in free space and λ_c is cutoff wave length in the empty guide.

It is well known that

$$Z_s = Z_d \tanh \gamma l, \tag{3}$$

and

$$Z_0 = Z_d \coth \gamma l, \tag{4}$$

where l is the thickness of the sample.

From equations (3) and (4), the following equations are obtained:

$$(Z_s/Z_0)^{1/2} = \tanh \gamma l = \tanh (\alpha+j\beta)l \equiv re^{j\theta}, \tag{5}$$

where r and θ are the absolute value and the phase angle respectively.

From equation (5), we obtain:

$$\alpha = \frac{1}{2l}\tanh^{-1}\frac{2r\cos\theta}{1+r^2}, \tag{6}$$

and

$$\beta = \frac{1}{2l}\tan^{-1}\frac{2r\sin\theta}{1-r^2}+\frac{n\pi}{2}. \tag{7}$$

The integer n is determined from the data obtained on two samples of the same material but of different thickness.

Now we put

$$(\varepsilon'-j\varepsilon'')(\mu'-j\mu'') = \varepsilon_1-j\varepsilon_2, \tag{8}$$

and

$$(\mu'-j\mu'')^2 = \mu_1-j\mu_2. \tag{9}$$

Then from equations (8), (2), (6) and (7), ε_1 and ε_2 can be calculated, and from (3) and (4) the following formula is obtained:

$$Z_s Z_0 = Z_a^2 \equiv a + jb\,. \tag{10}$$

When the left-hand side of the above equation is known, we can calculate a and b, and then from equations (1) and (10), μ_1 and μ_2 are obtaind. Therefore from equation (9) μ' and μ'' are determined and by substituting these values into equation (8), ε' and ε'' are obtained.

4. Description of equipment

A block diagram of the equipment is shown in Fig. 2. Similar equipments were used at both 9300 MC and 24000 MC.

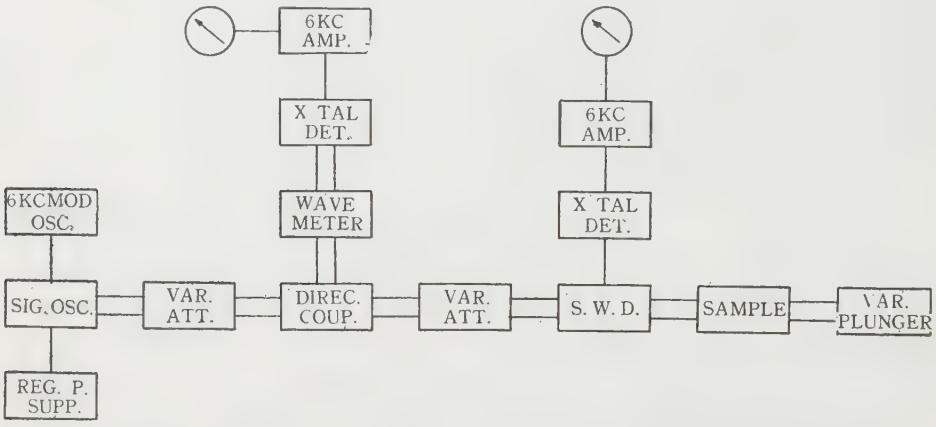

Fig. 2. Block diagram of the equipment used for measuring the complex dielectric constant and permeability of Ni-Cd ferrite system at 9300 MC and 24000 MC.

For the oscillators, Raytheon klystron 2K33 and Sylvania klystron 2K25 were used. The oscillator was modulated by a 6 kc square wave and the output from the detector was amplified by a linear narrow band amplifier. Since the precision of the reading of V. S. W. R. has a serious influence on the final result, the author used the standing wave detector manufactured by Shimada Rika-Kogyo Co. for both frequency ranges. The probe of the detector is movable by a screw micrometer along the main wave guide in such a way that it moves 1/100 mm per revolution with the 24000 MC detector and 1/10 mm with the 9300 MC detector. 1/10 mm was not precise enough for our purpose. From each ferrite, samples were formed to be square-shaped and to have two different thicknesses of 2 mm and 4 mm. Under the present conditions, the skin depth seems to be greater than 10 mm and so the EHF magnetic field is uniform throughout the sample. The output from the oscillator should always be monitored, in order to keep constant the output and frequency. It must be done with care to measure the voltage standing wave ratio, since it has a large effect on the precision of the whole measurement.

5. Result and discussion

A) *Dielectric constant and conductivity*

The ferrites are naturally semiconductors, and therefore the conductivities of ferrites are greatly affected by the presence of impurities. According to Verwey and de Boer (**10**) and others (**11**), the electronic conduction mechanism in oxide semiconductors can be associated with the simultaneous occurrence of metal ions of different valencies of a certain element on the identical lattice sites. Ferrous ions are substituted by other divalent metal ions in ferrites other than magnetite, and therefore these ferrites are practically insulators. But they show a small conductivity owing to the presence of a few ferrous ions which inevitably enter them in the course of heat treatment. The conductivity of ferrites are partly explained by the simultaneous presence of ferrous and ferric ions on the same sublattice in the spinel structure. The dielectric constant ε (real) and the resistivity ρ follow the same relaxation formulas (**12**) as a function of frequency:

$$\left.\begin{aligned} \varepsilon &= \varepsilon_\infty + \frac{\varepsilon_0 - \varepsilon_\infty}{1+\omega^2 T_\varepsilon^2}, \\ \rho &= \rho_\infty + \frac{\rho_0 - \rho_\infty}{1+\omega^2 T_\rho^2}, \end{aligned}\right\} \quad (11)$$

where ε_0 and ρ_0 are the values obtained by statical measurement and ε_∞ and ρ_∞ are those at EHF; T_ε and T_ρ denote the respective relaxation times. From these expressions ε and ρ at extremely high frequencies should tend to the limiting values ε_∞ and ρ_∞ respectively. As shown in Fig. 3 the high frequency limit of ε' seems to approach 10. As to the value of σ, it is known that the high frequency limit (**13**) becomes several times greater than its DC value. The result of measurement of DC resistivity ρ of the Ni–Cd ferrite system is given in Fig. 4, and this curve shows that one can obtain the ferrite of increased resistivity by properly mixing Ni–ferrite and Cd–ferrite.

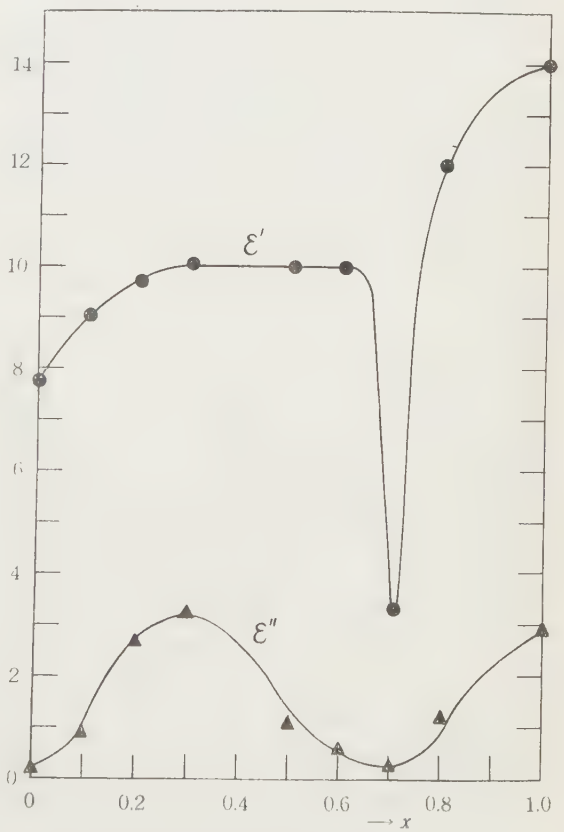

Fig. 3. ε' and ε'' measured respectively for various contents of Cd ion at 24000 MC.

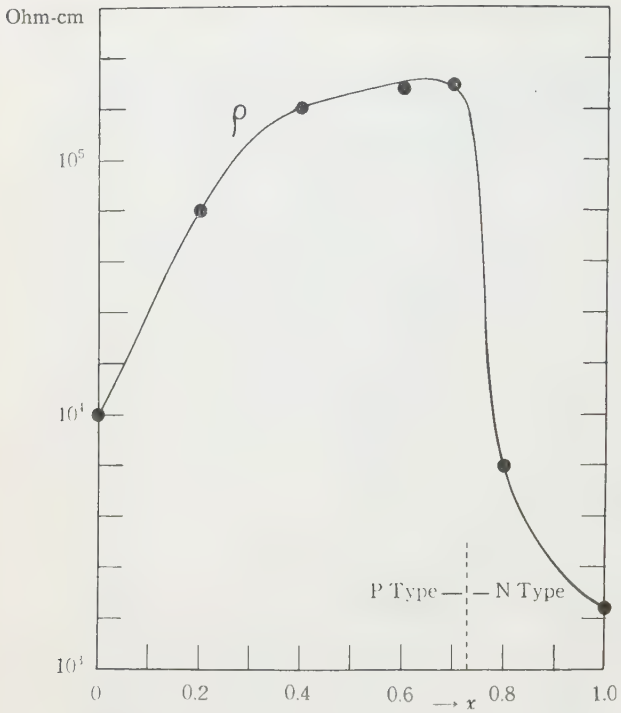

Fig. 4. The resistivity ρ of Ni-Cd ferrite system before surface grinding.

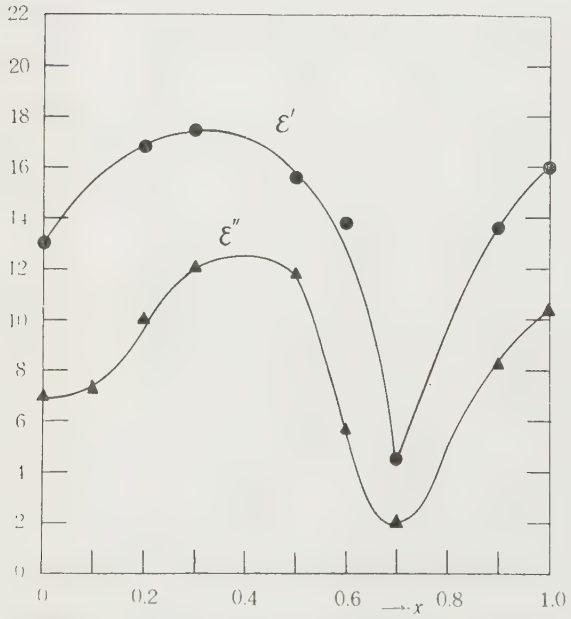

Fig. 5. ε' and ε'' measured respectively for various contents of Cd ion at 9300 MC.

It is remarkable that as seen in Figs. 3, 4 and 5, both ρ and ε' show a sharp reduction at the 70% Cd content. As seen in Figs. 3, 4 and 5 ε' increases together with ρ at the compositions between $X=0$ and $X=0.7$ and decreases above $X=0.7$. The break of the ρ curve at $X=0.7$ may be considered partly due to the cancelling effect of possible P-type (**14**) and N-type conduction mechanisms since Cd-ferrite is an N-type conductor. From these results it can be said that dielectric constant ε' has a close relation with conduction electrons, but the precise explanation of these phenomena should be postponed to future studies.

B) *The complex initial permeability and magnetic loss*

The magnetic structure of ferrite was first explained by Néel (**15**) in 1948 and the name 'ferrimagnetism' was proposed.

Fig. 6 shows that the saturation magnetization increases with the concentration of Cd-ferrite in Ni-ferrite up to $X=0.4$ contrary to the opposite expectation since it is non-magnetic, and then it decreases. This tendency was already observed on Ni-Zn ferrite which has the maximum saturation at $X=0.5$. As the interionic distances among the magnetic ions of Ni-Cd ferrite are somewhat

larger than those of Ni–Zn ferrite, it seems reasonable that the maximum saturation of Ni–Cd ferrite occurs at the smaller value of X. Further, in Fig. 6 the sharp reduction of magnetization is seen at the Cd content of $X = 0.7$. As is well known, these phenomena can be explained by the theory of ferrimagnetism. It is conspicuous that ρ, ε' and saturation magnetization M_s have all a break at $X = 0.7$. Notwithstanding the high resistivity, ferrites generally show pronounced ferromagnetic absorptions and large magnetic losses at high frequencies. This resonance absorption was first found in 1947 by Snoek (**16**) in the experiments on some mixed ferrites and named 'natural ferromagnetic resonance' or rotational resonance. The width of this resonance curve is very large owing to its origin and $(\mu' - 1)$ becomes negative due to the dispersion phenomena in the microwave region. The curves of μ' and μ'' *versus* Cd content are shown in Figs. 7 and 8. The mean values of μ' and μ'' are about 0.4 and 0.35 respectively at 24000 MC. These values are smaller than those at 9300 MC. When we discuss the initial permeability

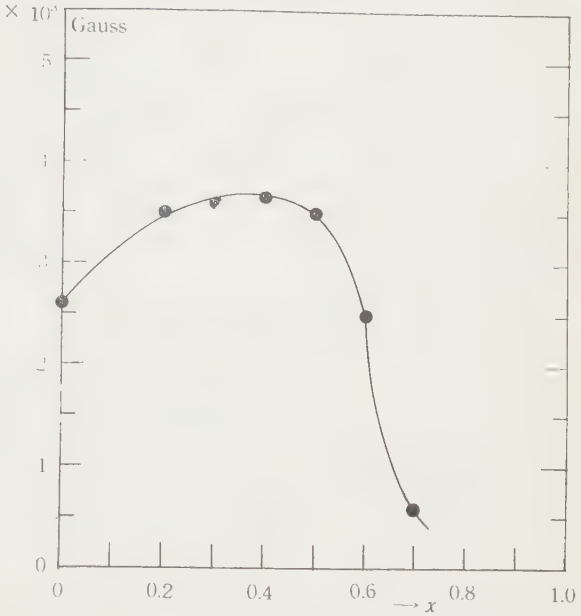

Fig. 6. Dependence of saturation magnetization $4\pi M_s$ for Ni-Cd ferrite on concentration of Cd ion.

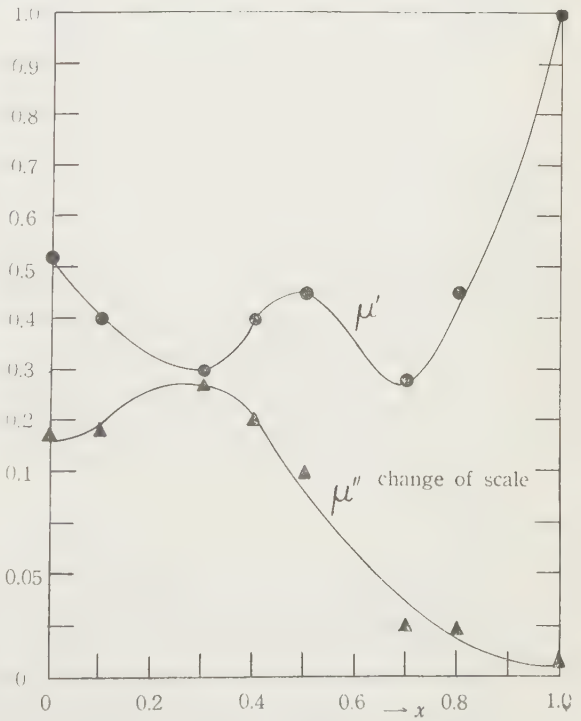

Fig. 7. μ' and μ'' of ferrite at 24000 MC.

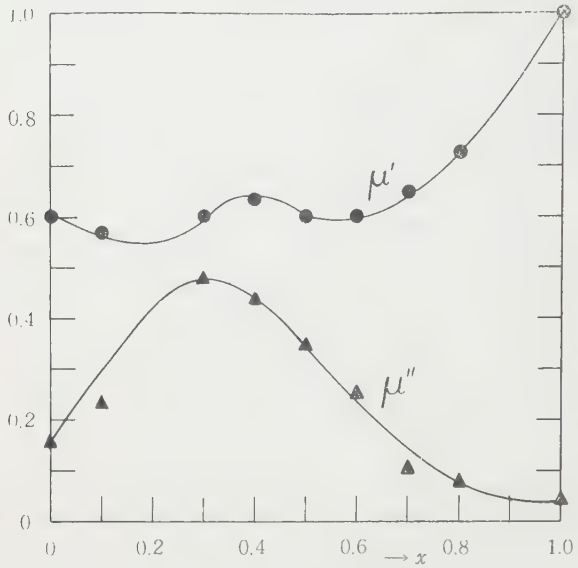

Fig. 8. μ' and μ'' of Ni-Cd ferrite at 9300 MC.

μ of ferrites at microwave frequencies, the hysteresis loss and eddy current loss can be neglected, but the residual loss cannot be neglected. The residual loss at the frequencies higher than 1 MC is composed of the losses corresponding to rotational, Bloch wall, and dimensional resonances in general, but in the present experiment, only the rotational resonance might be considered. The rotational resonance loss is ascribed to the absorption of energy due to the spin rotation in the internal anisotropy field. When there are the demagnetization fields in addition to the internal effective field, the condition of the resonance and the value of permeability are naturally affected. In such cases the maximum resonant frequency (**17**) is

$$\omega_r = \gamma(H_A + 4\pi M_s) , \tag{12}$$

where γ is the gyromagnetic ratio and H_A denotes the anisotropy field. For a free electron the numerical value of γ is 1.76×10^7 sec^{-1}. oersted^{-1} and usually H_A can be neglected as compared with $4\pi M_s$. In the present case the maximum resonant frequency exists in about 10,000 MC region which is the important frequency range in practice, and therefore the energy loss (μ'') shows a decrease with higher frequencies, which explains the experimental results shown in Figs. 7 and 8. Because of the dispersion due to the broad rotational resonance absorption, the ferrite of high μ' value will be difficult to obtain at microwave frequencies, but the mixed ferrites such as those used in this experiment may be utilized as low loss attenuator for microwave devices.

Acknowledgment

The author wishes to express his sincere thanks to Professor I. Takahashi of Kyoto University for his valuable advice and discussion. He is also indebted to Assistant Professor H. Mori of Shimane University for his help in the experiment and Tokyo Denki Kagaku-Kogyo Co. for preparing the excellent ferrite samples used for the present experiment. The present investigation has been partly supported by a grant-in-aid for scientific researches of the Ministry of Education.

REFERENCES

1, 2. Solid-state Electronics, Proc. I. R. E. **43** (1955), 245;
Advances in Electronics and Electron Physics, Vol. 2, p. 251 & Vol. 4, p. 70 (Academic Press, 1954);
J. L. Snoek, *New Developments in Ferromagnetic Materials* (Elsevier, 1949);
Rev. Mod. Phys. **25**, No. 1 (1953).
Ferrites Issue, Proc. I. R. E. **44**, No. 10 (1956).

3. D. W. Healy, Phys. Rev. **86** (1952), 1009.

4. G. Birnbaum, J. Appl. Phys. **20** (1951), 817.

5. T. Okamura, T. Fujimura and M. Date, Scientific Reports of the Research Institute, Tohoku Univ., **73** (1952), 191.

6. N. Ogasawara, Rev. E. E. Japan, **74** (1954), 795.

7. J. B. Birks, Proc. Phys. Soc. **60** (1949), 282.

8. A. Nishioka, Reports Res. Inst. Comm., No. 277 (1952), 5.

9. H. Mori, Bulletin Shimane Univ. (Natural Science), No. 6 (1956), 34.

10. E. J. W. Verwey and J. H. de Boer, Recueil des travaux chimiques des Pays-Bas, **55** (1936), 531.

11. E. J. W. Verwey and P. W. Haayman, Physica **8** (1941), 979.
E. J. W. Verwey and P. W. Haayman, Philips Research Report, **5** (1950), 173.

12. C. G. Koop, Phys. Rev. **83** (1951), 121.

13. J. Smit and H. P. J. Wijn, *Advances in Electronics and Electron Physics*, Vol. 4 (1955), 119.

14. L. G. Van Uitert, J. Chem. Phys. **23** (1955), 1183.

15. L. Néel, Ann. de Phys., **3** (1948), 137.

16. J. L. Snoek, Nature **160** (1947), 90; Physica **14** (1947), 207.

17. D. Polder and J. Smit, Rev. Mod. Phys., **25** (1953), 89.

MEMOIRS OF THE COLLEGE OF SCIENCE, University of Kyoto, Series A,
Vol. XXVIII, No. 4, Article 5, 1958

AN ELECTROMAGNETIC ISOTOPE SEPARATOR

BY

Jiro MUTO and Kotoyuki OKANO

(*Received February 6, 1958*)

ABSTRACT

In Kyoto University an electromagnetic isotope separator was constructed and has been in operation since September 1956. This article contains the description of main features of this machine and the discussions of experiments made on ion source efficiency as well as on the resolving power, together with some description of the separation of isotopes of neon, magnesium and silicon.

1. Introduction

Before the Second World War, it was very rare that the separated stable isotopes were applied in scientific researches. After the War, however, the isotopically pure or enriched samples have been employed in many scientific researches, because of the technical development of isotope separation acquired in the uranium separation project in U. S. A.

Nowadays, large isotope separating machines of production type which have the ion current of the order of 100 mA are in operation at the Oak Ridge National Laboratory in U. S. A. and at the Harwell Atomic Energy Research Establishment in England. In other European countries, i. e., France, Denmark, Sweden and others, comparatively small machines are constructed and in operation aiming at scientific researches.

In Japan, a model testing machine of a large isotope separator of Smythe type magnet was constructed in Osaka University (**1**) and has been in operation since 1953, and a machine of beam radius of 80 cm was constructed in 1955 at the Institute of Scientific Research in Tokyo (**2**), and now in the Institute for Nuclear Study of Tokyo University a comparatively large machine is under construction.

At Kyoto University, the construction of a medium size isotope separator began in 1955 and was finished in autumn, 1956 (**3**). Later, the test operation of the apparatus was done and some separated isotopes have been obtained in appreciable amount by this apparatus. In the following sections, the outlines of the isotope separator in Kyoto University are described, and some detailed data obtained in its operation are discussed.

2. Outlines of isotope separator

The main specifications of European isotope separators as compared with Kyoto-Separator are listed in Table 1. This apparatus is composed of a main magnet, an ion deflection chamber, a low voltage arc type ion source, and an ion collector. These

Table 1.

Situation	Year of completion	Type of magnet (deflection angle)	Magnetic gap (cm)	Radius of the magnet (cm)	Weight of magnet (ton)	Maximum magnetic field (gauss)	Maximum acceleration voltage (KV)	Literature
Copenhagen	1941	90°	6.0	80	4.5	8,000	70	4
Stockholm	1948	90	10.3	160	6.5	3,500	60	5
Amsterdam	1952	180	17.0	100	40	3,150	25	6
Saclay	1952	60°	6.6	50	5	12,000	35	7, 8
Kyoto	1956	60	8.0	60	7	8,000	50	3

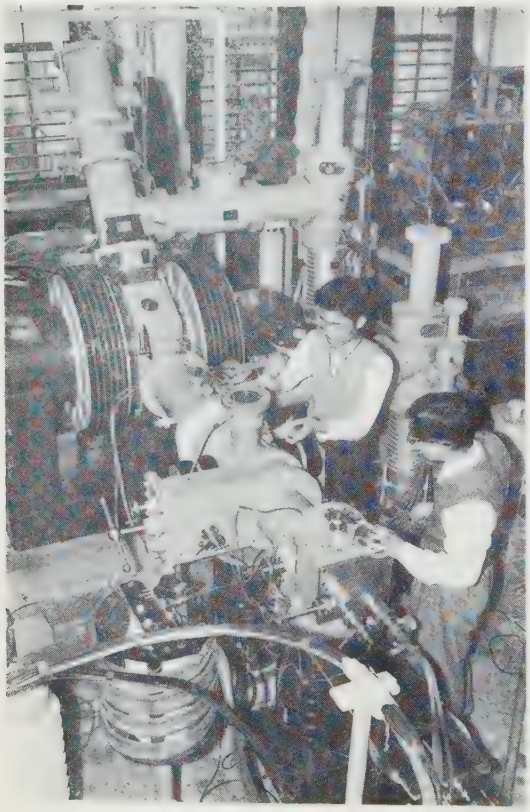

Fig. 1. Photographic view of isotope separator in Kyoto University.

main parts of the apparatus, as well as vacuum system and driving electric circuits, are described in the following sections. The main features of this apparatus are illustrated in photographic view of Fig. 1, and the vertical sectional view of the main body is shown in Fig. 2.

The magnet

The shape of the magnet pole face is pentagonal, the distance between the pole pieces being 8.0 cm, and their maximum usable width is 22 cm (edge length=40 cm). This usable width can be varied by the movable wing shutter, so that the half diverging angle of the ion beam entering the magnetic region from the ion source is varied from zero to the maximum of 6° (~0.1 radian). The ion optical relations of ion beams

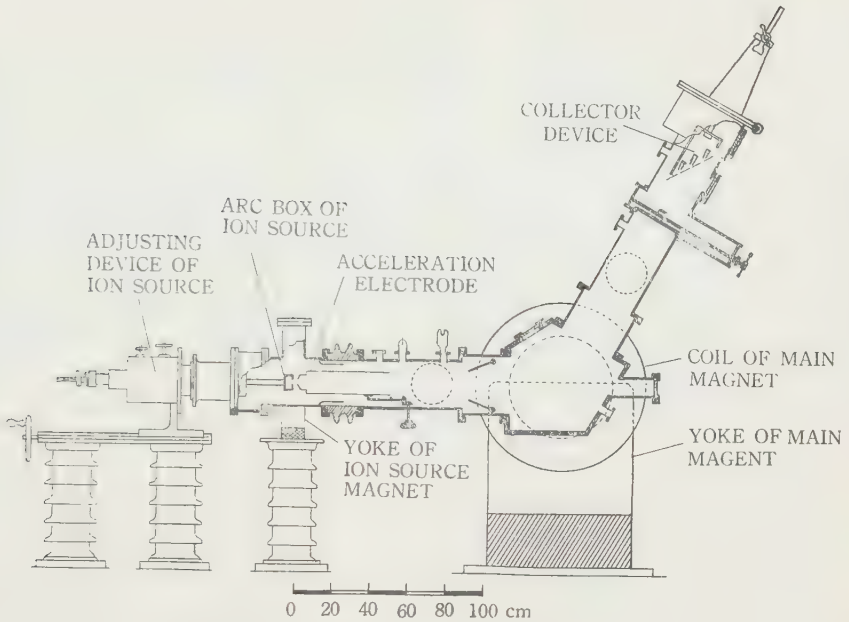
COLLECTOR DEVICE
ARC BOX OF ION SOURCE
ADJUSTING DEVICE OF ION SOURCE
ACCELERATION ELECTRODE
COIL OF MAIN MAGNET
YOKE OF MAIN MAGENT
YOKE OF ION SOURCE MAGNET
0 20 40 60 80 100 cm

Fig. 2. The vertical sectional view of the main body of the separator.

are illustrated in Fig. 3. As is well known, the mass dispersion D and the second order aberration B in the symmetric arrangement of 60° wedge type magnet are represented as follows:

$$D = r_0,$$

$$B = \alpha^2 r_0,$$

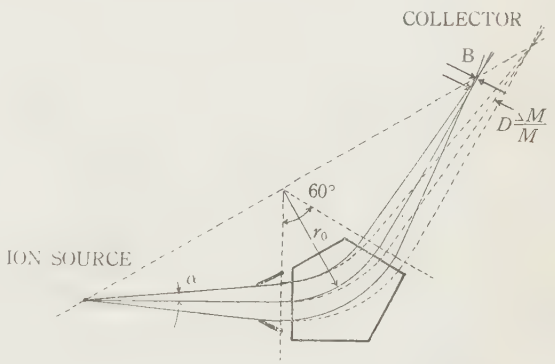

Fig. 3. Ion optical relation in the separator.

where r_0 is the radius of curvature of ion beam and α is the half diverging angle of primary ions. In this apparatus $r_0 = 60$ cm, and so the distance between the ion beams of atomic mass number A and $A+1$ at the focal point is represented by

$$D\frac{1}{A} = \frac{r_0}{A} = \frac{60}{A}\text{ cm}.$$

Therefore the image displacement for one atomic mass number difference at $A=200$ (mercury ions) is 3 mm. On the other hand, the width of the image is represented by

$B+$(width of the slit of ion source).

Thus if the slit width is 2 mm, α is permitted to be 0.04 radian ($\sim$2.3°), for the separation of neighbouring isotopes of mercury. These values show that the machine is capable of separating the isotopes of almost all elements. However, these values are for ideal cases, and in practice they are considerably affected by many factors; namely (1) stability of ion acceleration voltage, (2) homogeneity and stability of magnetic field strength, (3) scattering of ion beams by residual gases, and (4) broadening effect of space charge on the path of ion beams.

Because of the so-called fringing effect of the magnetic field boundaries, the actual magnetic pole boundaries were retired by 9 cm from the ion optical boundaries.

The configuration of magnet yoke (Figs. 1 and 2) is of *C* type, and its gap is vertical. The iron of the magnet is a low carbon steel (carbon content being less than 0.06%). Two exciting coils are provided and each coil consists of 6 layers of 150 turns of copper ribbons and of the cooling copper sheets soldered to the cooling pipes at the round edges (Fig. 1). Total electric resistance of two coils in series is about 3.2 ohm, and the temperature rise of the coils is 25°C after loading the current of 37.5A for 5 hours at room temperature of 16°C and with the circulating rate of cooling water of 32 litre/min. The magnetic field strength at the centre of the magnetic gap is measured and the excitation curve is illustrated in Fig. 4.

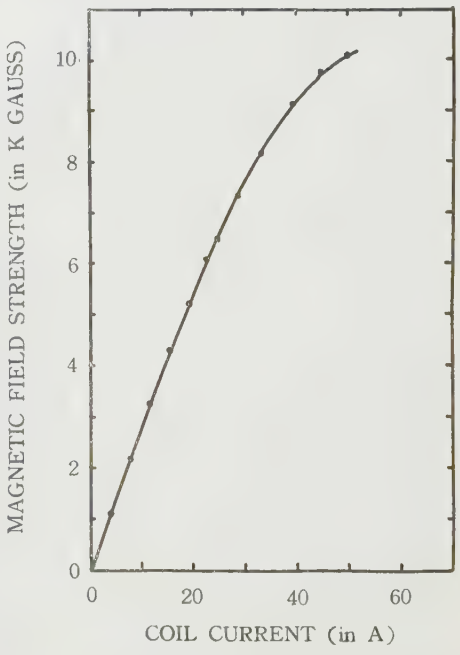

Fig. 4. Excitation curve of the magnet.

Deflecting vacuum chamber

The vacuum chamber is a pentagonal rigid box constructed with two parallel iron walls of 8 cm thickness, and five side walls of brass. The iron walls serve as the magnetic pole pieces by fixing the chamber between the magnetic yokes. The mechanical accuracy and strength of the chamber is maintained by the five spacers at the corners as well as the five side walls fixed to the iron walls. On the other hand, the vacuum seal is achieved by soldering the edges of thin copper sheets which are also soldered to the boundary edges of each iron walls and brass side walls by hard solder. The mechanical error of the magnetic gap distance is $\pm$3.5/100 mm over the

whole pole face, so that the homogeneity of the magnetic gap distance is within the error of 0.05%. On the inner surface of the chamber, thin exchangeable linings of copper sheets are provided for the protection from the erosive effect of various material ions.

Vacuum system

Two sets of evacuating pumps are employed. Each set of pumps consists of an 8 inch oil diffusion pump with the pumping speed of 1250 litre/sec at 2×10^{-6} mmHg and a Kinney type rotary pump with pumping speed of 680 litre/min at 1 mmHg. Arrangement of the vacuum pumps and many valves are schematically illustrated in Fig. 5. Some of these valves are operated by the compressed air supplied through the electromagnetic valves from a 4 atm. air compressor, and these valves can automatically shut down the pumping system for the protection of the apparatus under various accidents, namely the stopping of the cooling water and electrical power supply, or the sudden leakage in the vacuum system.

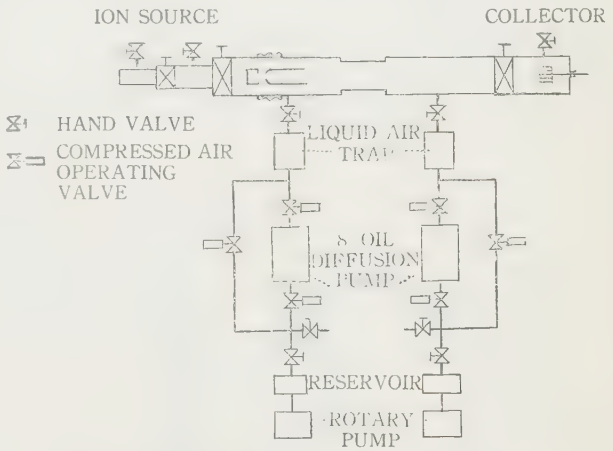

Fig. 5. Vacuum system of the isotope separator.

The exchanges of the filament of ion source, the whole assembly of ion source and the ion collecting devices may be done, keeping the vacuum of the main parts of the apparatus. The adjustments in all directions and slight rotations of ion source position are possible without affecting the vacuum.

Ion source

Structure of the ion source used for gaseous samples are illustrated in Fig. 6. A carbon box placed between the magnetic pole tip is the arc chamber. Electrons emitted from the wolfram filament

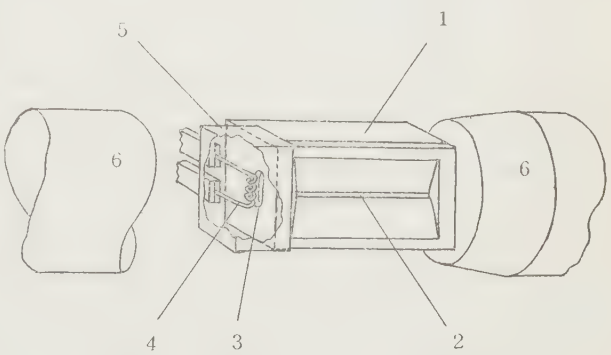

Fig. 6. Ion source for gaseous samples
1. arc box (carbon) 2. slit 3. discharge slot
4. filament 5. filament cover
6. pole of magnet

enter through the discharge slot (4 mm×8 mm) of the side wall of the box along the magnetic field direction, and the plasma column of arc is produced behind the narrow slit (1~2 mm×50 mm) of the front wall of the arc box. The sample in gaseous state is introduced into the arc box through a pipe with a gas leak adjuster outside the apparatus.

For solid state samples, the crucible of alumina heated by the molybdenum wire is furnished under the arc box (Fig. 7). The sample in the crucible is evaporated at an appropriate temperature maintained by the automatic controller with thermocouple temperature guage. Evaporated gas of the sample is led to the position of arc column by the defining chimney of stainless steel.

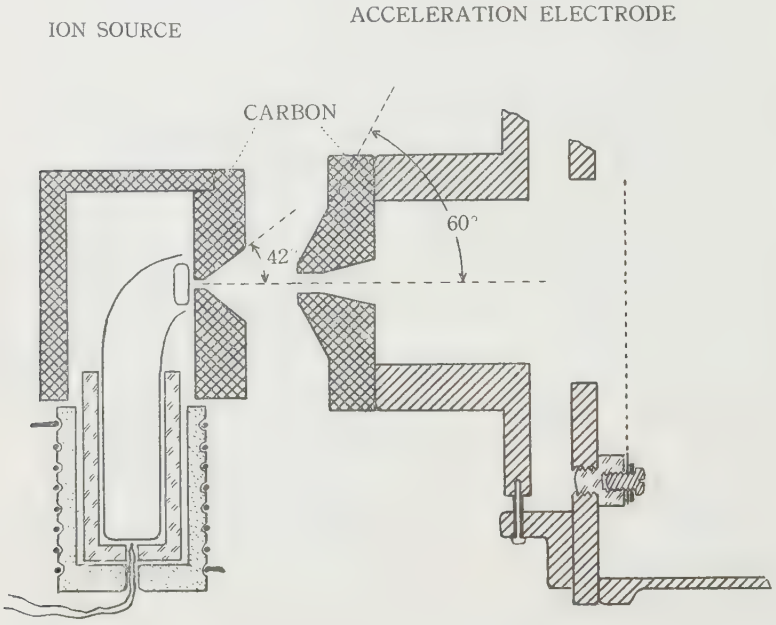

Fig. 7. Ion source for solid state samples and acceleration electrode.

The wolfram filament (1 mm dia.) of 6 turn spiral (outer diameter=4 mm) is heated by direct current of maximum 50A and is maintained at the negative potential of maximum 300 volts with respect to the potential of the arc box. The repeller electrode plate of stainless steel placed at the position opposite to the electron introducing slot is insulated from the arc box, so that the potential of this electrode is negative as the result of the accumulation of electron charges, and thus it serves to increase the ionization efficiency by the electron reflection.

The whole system of the ion source is in the positive potential (maximum 60 KV), and the extraction of ions as well as the acceleration of them are carried out by an acceleration electrode in the ground potential. This cylindrical electrode of stainless

steel has a bill of carbon at the end faced to the ion source slit, and the length of acceleration gap (Fig. 7) is finely adjustable by a screw outside the apparatus. In the cylinder of acceleration electrode, a grid of molybdenum fine mesh is spread near the carbon bill, and is electrically insulated from the electrode so as to supply negative potential of several hundred volts for the use of space charge compensation.

Stabilization of magnetic field

The magnet coil current is delivered by a 10 KW motor generator and is stabilized by a high current regulator (**9**). The schematic circuit of this regulating system is illustrated in Fig. 8. Total magnet current gives a voltage drop over the 40 mΩ manganin resistance series to the main coil circuit. The difference between this voltage

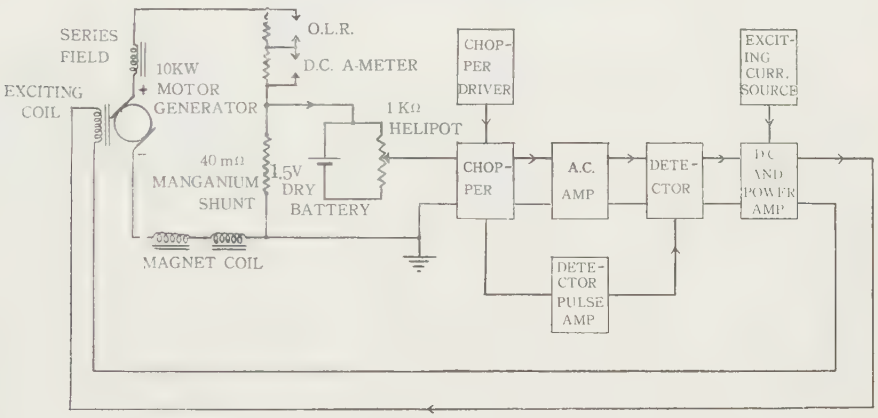

Fig. 8. Magnet current stabilizer.

and the voltage of a standard battery is amplified by the system of a 400 cycle chopper-converter, an a. c. amplifier, a phase detector, and a d. c. amplifier, whose output voltage controls the grid of valve 807 output power stage. The output current from the cathode of the valve 807 is fed back to the field coil of main d. c. current generator.

The stability of this current supplying system was measured to be within the deviation of 1/4000 at the current of 10A during 3 hours continuous operation.

Stabilization of acceleration voltage

Acceleration voltage is supplied by a d. c. high voltage source of rectifier-condenser system, and is regulated (**10**) by the valve 5T31 (Fig. 9). Divided voltage derived from a carbon resistor is referred to the voltage of standard dry cells (67.5 V, 135 V, or 202.5 V), and the difference of these voltages is amplified and this modulates the 4 MC high frequency oscillation. By a well-insulated high frequency transformer, the modulated high frequency oscillation supplies the control voltage through a rectifier

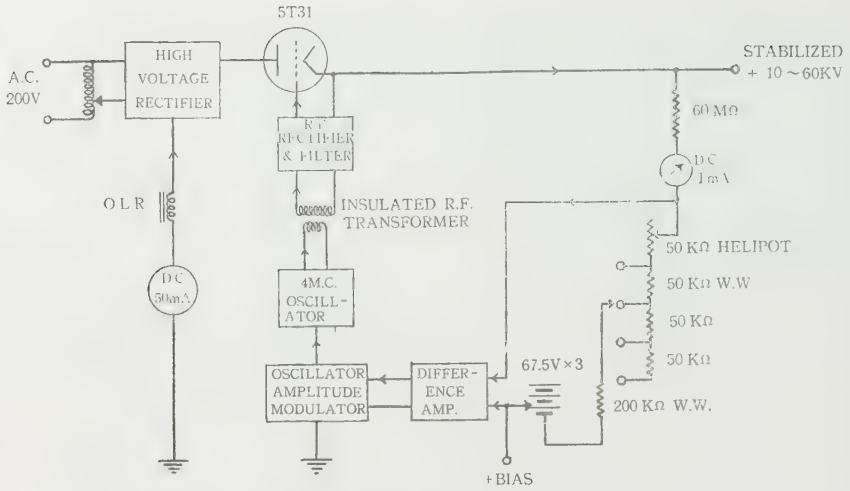

Fig. 9. Acceleration voltage stabilizer.

unit to the grid of valve 5T31. The acceleration voltage can be adjusted precisely to any desired value by the switching of 50 KΩ resistors and by the continuous rotation of helical potentiometer at the lowest stage of dividing resistors.

The stability of this voltage supplier was measured after 30 minutes warm up period to be about 1/2000 at the voltage of 25 KV.

Collector device

The collector device consists of a framework or a plate cooled by water and the attachments of various type collecting pockets. These collecting pockets are to be made of the materials suitable for the properties of ions collected. Some materials were tested in various forms. For the magnesium ions stainless steel boxes, copper or graphite pockets were tried, and for the neon ions silver plates were used.

The whole assembly of collector devices is movable along the beam direction and may be set easily at the desired position (Fig. 10).

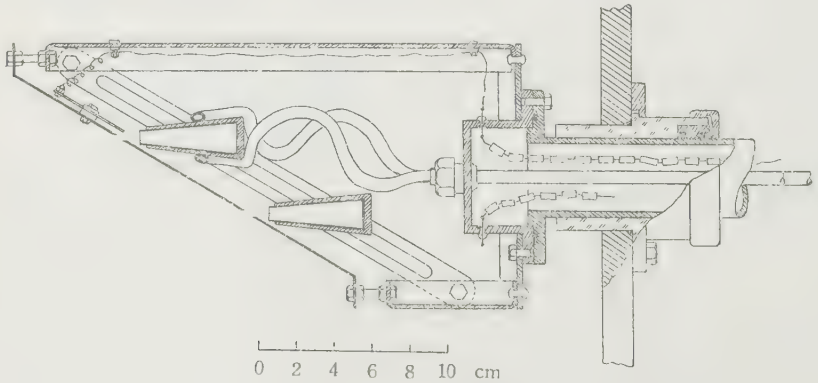

Fig. 10. Collector device.

3. Performance of the separator and discussion

The following three properties are essentially required for the isotope separator, that is

(1) collected ion current is as high as possible ;
(2) the resolving power is as large as possible ;
(3) the operation of the apparatus is as stable as possible during a long period.

In a primary test operation with argon, neon, or magnesium ions, we could not obtain satisfactory results in these respects, so various improvements and adjustments have been done. The knowledges obtained in this procedure will be discussed in the following.

Increasing of ion source efficiency

In order to obtain high collector current, it is important to have as high ionization efficiency as possible. Efficiency of the ion source is indicated by the minimum pressure of gas necessary to ignite the arc, so the factors deciding the minimum operating pressure in the ion source were considered.

In igniting the arc, it is considered that the surface of the electron emitting filament is surrounded by the double layer of ions and electrons (**11**). From this idea follows the relation :

$$J_e \leqq \gamma \sqrt{\frac{m_+}{m_e}} J_+ ,$$

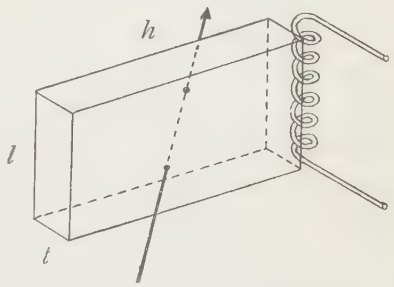

Fig. 11. Arc column.

where J_e and J_+ are the currents of electron and ion, m_e and m_+ the masses of electron and ion respectively, and γ is a correction factor of $\frac{1}{3}\sim\frac{2}{3}$.

On the other hand, the following relations hold independently, for an arc column of flat type (Fig. 11) :

$$J_+ = \frac{N_0 V_n A'}{2} f_k P(j_e) ,$$

$$J_e = A j_e ,$$

where N_0 : density of neutral molecule,
V_n : velocity of neutral molecule,
j_e : current density of electron,
$A = lt$: cross sectional area of arc column (area of electron entrance slot),
$A' = lh$: area of side surface of arc column,

$P(j_e)$: mean probability that a neutral molecule is ionized in its passage through the arc column,

f_k: ratio of the number of ions reaching the filament to the total number of ions produced by ionization.

The function $P(j_e)$ depends on V_n as well as on the shape of arc column, and for small values of j_e it is nearly proportional to j_e.

From the above three relations it is derived that

$$N_0 \geq \frac{2}{\gamma V_n}\sqrt{\frac{m_e}{m_+}}\,\frac{1}{P_0(j_e)}\,\frac{1}{hf_k},$$

where $P(j_e)=tj_eP_0(j_e)$.

According to this relation it is evident that $P_0(j_e)$ and f_k must be increased to decrease the minimum value of N_0. To increase f_k, we made some improvements over the area, form, and depth of electron entrance discharge slot, and adjusted the filament position to the discharge slot. To increase $P_0(j_e)$ we furnished the floating type repeller electrode for electron reflection (8), and made some adjustment of the chamber position relative to the source magnet. Moreover we increased the number of turns of the filament spiral, and covered the filament part outside the arc box to increase the density of neutral molecule near the filament. In the case of solid sample, e. g. magnesium, we also employed a vapour confining chimney of stainless steel (8) in the graphite arc box as a reflector of neutral atoms and radiation. After these reformations the efficiency of the ion source appeared to be remarkably improved.

In Table 2, the achieved performances under normal operation of the ion source are listed and compared with those obtained before.

In the case of magnesium, a remarkable improvement was readily seen by the fact that the glass of the peep window of the ion source parts which had been silvered by the vapour of neutral metallic magnesium in a minute after igniting the arc, remained almost un-silvered during several hours' operation.

Table 2.

Operating conditions of ion source	Argon		Magnesium	
	before	now	before	now
Gas supply (cc N.T.P./hour)	250	50		
Arc discharge current (A)	0.5	0.5~1	0.2	0.2~0.8
Applicable voltage of acceleration without spark down (KV)	10	30	15	30
Collector current (mA) (no correction for secondary electron emission at the collector, $2\alpha=12^\circ$)	0.2	3	0.2	5

The relation between the acceleration voltage and the collector current is shown in Fig. 12, for various values of acceleration current. The acceleration current is a total load current of the high tension set, which includes total ion current extracted from the ion source, and the small contribution of electron current to the ion source. The value of this acceleration current is nearly constant with the increase of extraction voltage, because the current value is determined mainly by the ion density of the ion emitting plasma surface and its area. It is readily seen in Fig. 12 that at the lower acceleration voltage the collector current is poor. This is due to the space charge divergence of the beam at the accelerating gap at lower voltage, and will be improved by the more refined focusing property of the accelerating electrode system. With the electrode system of this apparatus 30 KV is needed for mA-order operation, and this voltage value is somewhat higher than the theoretically (Pierce's geometry (**12**)) expected one.

In conclusion, the improvement of ion source efficiency lead to the reduction of

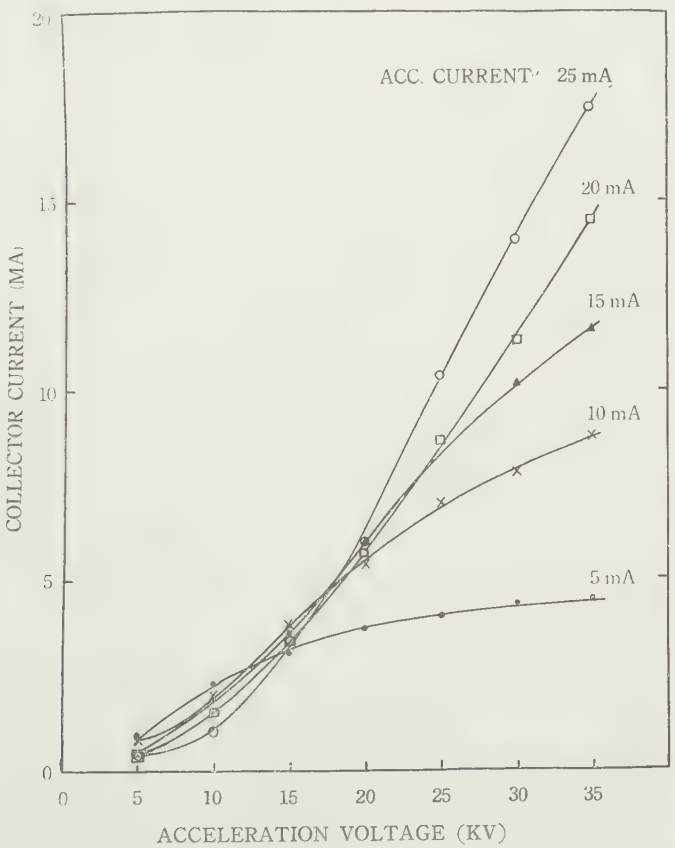

Fig. 12. Relation between the acceleration voltage and the collector current.

gas supply, and accordingly permitted the application of high accelerating voltage without spark down, and decreased the loss of ions scattered by the residual gas, and then resulted the increases of ion current reaching the collector.

The resolving power and the affecting factors on it

The breadth of the ion beam at the collector is largely affected by the deviation of focal point, and the minimum beam width obtainable at the focal point is determined by many factors; namely, the space charge broadening effect, scattering of the ion beam by the residual gas, ion optical second order aberration and object width, fringing fields effect, inhomogeneity of the initial velocity of ions, and the local inhomogeneity of magnetic field strength. Of these, the last two are estimated to be very small. Because the measured ripple voltage of the acceleration at 30 KV is about 10 V peak to peak, and considering that in the low vlotage arc type ion source no appreciable voltage gradient exists, initial velocity inhomogeneity is less than 1/1000. The local magnetic field inhomogeneity has not been measured but must be

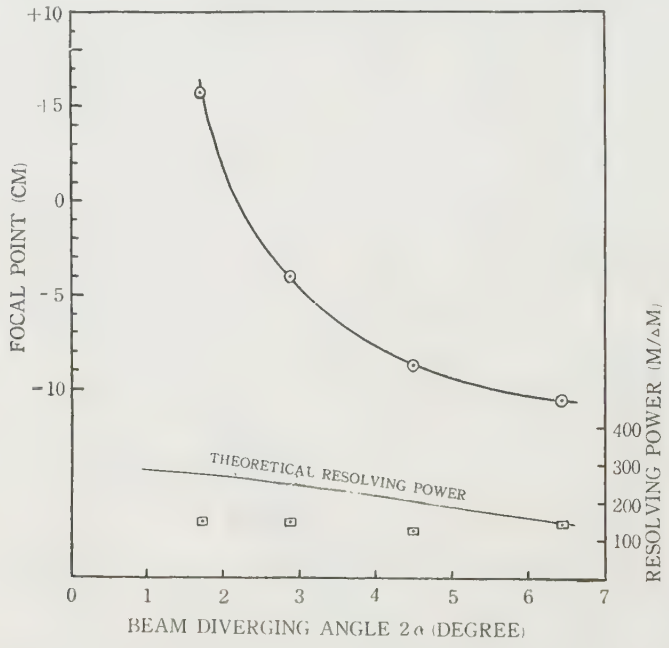

Fig. 13. Variation of focal point (⊙) as a function of beam diverging angle 2α. The origin of the ordinate is the expected focal point (Fig. 16), and positive sign means the direction opposite to the deflection magnet. Limit of error in focal point determination is about ± 2 cm. Beam resolving power obtained at each angle is also shown (⊡). Theorteical resolving power was calculated considering the object width to be that of ion source slit, 2 mm. These data were obtained by the use of the Mg^{24} ion beam accelerated to 26 KV, and the collector current was 4.5 mA at $2\alpha = 6.4°$.

small considering the mechanical accuracy of the length of magnetic pole gap $\left(\pm\frac{3.5}{100}\text{ mm}\right)$. So, in the following, we will discuss the other factors.

To determine the true focal point, a Faraday cage with a slit of 1.5 mm width and 40 mm length was mounted on a movable collector plate, and the ion beams were scanned electrically by a motor driven helipot. The output current from the Faraday cage was recorded on an electronic recorder chart. The spectrum of the images was thus measured at the various positions along the central axis of the collector side arm, and the base width of the beam as well as the variation of spectrum shape were taken as a measure for determining the focal point.

The focal point thus determined was found to vary considerably with the beam diverging angle, ion current intensity, or ion source conditions. Fig. 13 shows the observed variation of focal point with the diverging angle 2α. Fig. 14 shows the variation of it with ion current intensity. Beam resolving power observed (calculated from the width at $\frac{1}{10}$ of the maximum) is also shown in each case. Other parameters such as vacuum condition and acceleration voltage were noticed to affect the focusing

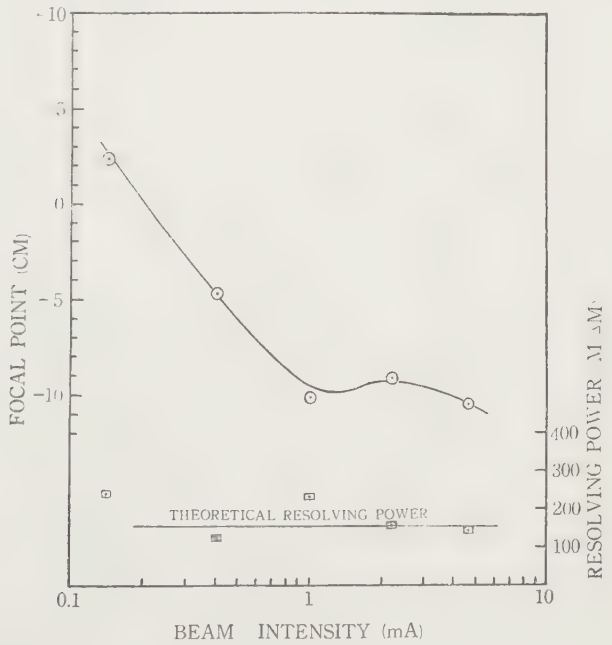

Fig. 14. Variation of focal point as a function of beam intensity. Coordinate of focal point is taken as in Fig. 13. Limit of error in focal point determination is ± 2 cm. Beam resolving power obtained is also shown. Mg^{24} ion beam was used and beam diverging angle 2α was 6.4°, acceleration voltage being 25 KV.

property in smaller extent, but the exact relations were not examined.

Theoretically, if the ion beam of the intensity of 1 mA/cm or more were not neutralized at all, it would diverge outside at the exit boundary of the magnetic field by its own space charge, and would have electric field of about 100 volts/cm at the surface (Fig. 15). In practice, however, beam absorbs electrons created by the ionization of the residual gas, making itself a kind of plasma. An imperfectly neutralized part of the beam, however, produces electric field in the beam. This field makes the trajectory of the charged particle parabolic, and leads to the focal point displacement (Fig. 16). By the two-dimensional calculation of the path of ion beam, postulating the beam intensity to be equal to any direction, focal point displacement Δf is obtained to be

$$\Delta f = \frac{5E_s}{2V\alpha} r_0^2,$$

where E_s is the electric field at the beam surface and V is the acceleration voltage. E_s indicates the degree of neutralization and is determined by the rate of production and loss of slow electrons. E_s is not considered to depend on α markedly, and so the above relation explains the $1/\alpha$ dependence of Δf as observed in Fig. 13.

Beam intensity modulation due to plasma oscillation with a frequency of about 15~50 KC was observed, which makes the space charge neutralization incomplete, and results in the increase of E_s. The ratio of the amplitude of this high frequency current to the time averaged total current changed with the ion source conditions as is shown in Fig. 17. This will explain the focal point variation as shown in Fig. 14.

The focal point displacement caused by the variation of virtual object point was estimated to be maximum +2 cm~−5 cm. This may also account for a part of the observed one.

From the above expression of Δf and Fig. 13, we can conclude that if no space charge effect existed, the ion optical focal point is deviated by (-16 ± 2)cm from the expected one. This means 2 cm over correction of the magnet boundary (9 cm correction was made for 8 cm gap length), although focal point displacement Δf, due to space charge, partly compensates this circumstance. These relations are presented in Fig. 16.

Beam scattering due to residual gas was found to be appreciable at the pressure above $\sim5\times10^{-5}$mmHg, especially in the case of rare gas ions or heavy ions. On the other hand, below $\sim2\times10^{-6}$mmHg, space charge compensation became insufficient, and considerable broadening was observed with the Mg^+ beam of a few mA intensity. But around 1×10^{-5}mmHg, beam width *versus* pressure relation was rather flat, although these absolute pressure values would vary somewhat with the nature of the ions and the residual gases.

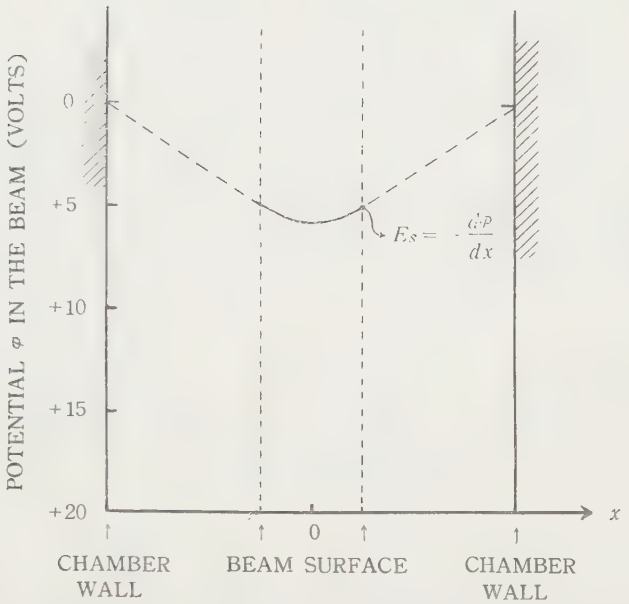

Fig. 15. Potential distribution inside and outside the beam. Potential value at the valley varies according to the degree of neutralization.

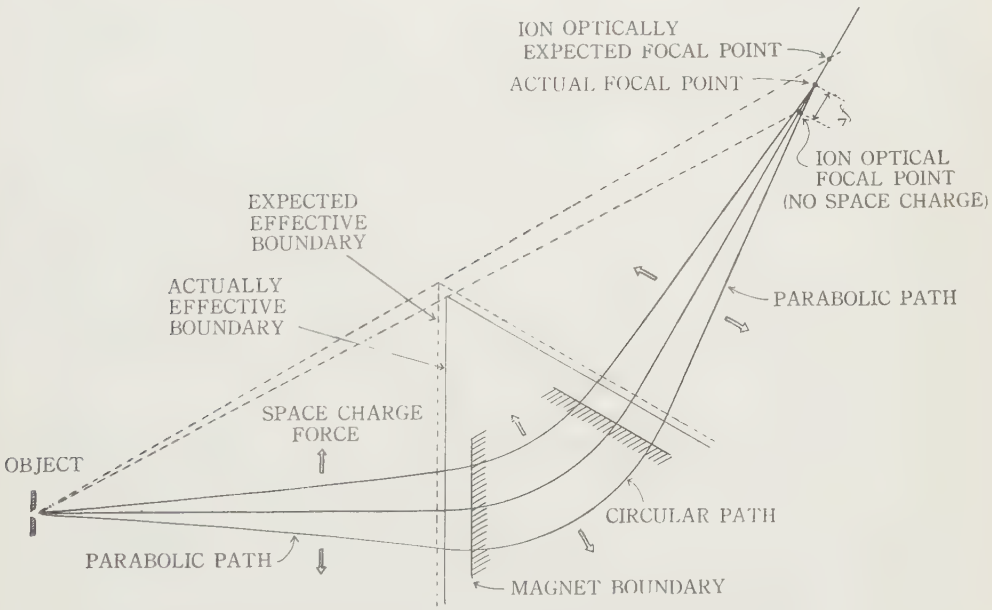

Fig. 16. Focal point displacement due to space charge effect.

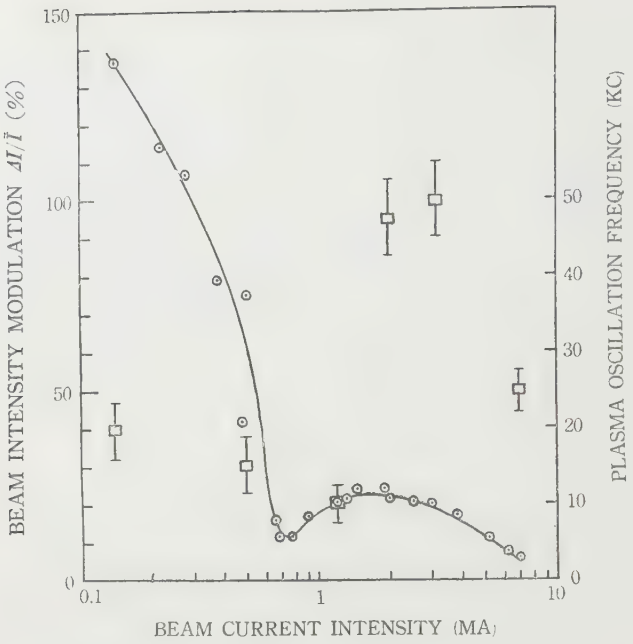

Fig. 17. Observed relation of beam intensity modulation to beam current intensity. The points ⊙ show the modulation ratio $\Delta I/\bar{I}$, and the points □ show the oscillation frequency. ΔI is a peak amplitude of modulation and $\bar{I}$ is a time average value of beam current.

Stray magnetic field of a few hundred gauss due to ion source magnet exists behind the accelerating electrode as well as between the accelerating gap. It is troublesome because the ion beam receives slight deflection in passing through this region, resulting the deflection of beam centre axis of several degrees in light element ions. This deflection can be corrected to some extent by adjusting the position of ion source chamber relative to the accelerating electrode, though this procedure sometimes results in broadening the object width. In view of space charge compensation, however, this stray field may play as stopping action for the flow of slow electrons, which in case of no magnetic field flow back to the ion source along the potential gradient in the beam, and makes space charge compensation insufficient.

In order to stop the flow of slow electrons to the ion source, a grid of fine molybdenum mesh with a potential of maximum −350 volts was mounted behind the acceleration electrode according to Bernas (**8**), but it showed no improvement upon the minimum beam width at the focal point. So the electron flow is considered to be already prevented from escaping by other effects such as stray magnetic field mentioned above, and we dismounted the grid.

Curving of beam image at the collector plate mounted normal to the beam direc-

tion was observed, which is mainly due to fringing fields effect. Radius of curvature of the image was (80±5)cm compared to the theoretical value (**13**) of (250±100)cm calculated with the geometry of this apparatus. This discrepancy suggests other effects than purely two-dimensional fringing fields effect. Anyway, image curvature is almost negligible for practical purpose.

In conclusion, we may say that in spite of the complexity of beam focusing property owing to the space charge and other effects, appropriate adjustment of the collector position makes $M/\Delta M \sim 150$ attainable in normal operation, and $M/\Delta M \sim 250$ in favourable conditions as can be seen in Figs. 13 and 14.

4. Actual performance of the isotope separation of several elements

In general, charged materials in the arc box of the ion source must be in gas phase. In this point, almost all the elements are classified into three groups in preparing for the ion source. The elements of the first group have the sufficient vapour pressure to introduce into the arc box at room temperature; for example, neon, nitrogen, argon, etc. The second is the group of the elements which can have the necessary vapour pressure (10^{-2}mmHg) at the temperature of several hundred degrees centigrade; for example, magnesium, potassium, calcium, zinc, mercury and so on. The third group contains the elements the vapour pressure of which does not reach the sufficient value at the above-mentioned temperature. In many cases the elements of the last group are charged in the forms of suitable chemical compounds, such as chloride, bromide or iodide (**14**).

We tried to separate three elements; neon, magnesium and silicon, each of which is considered to belong to one of the three groups.

Separation of magnesium isotopes

A piece of metallic magnesium was charged in the crucible of alumina which was hung under the arc box of ion source and heated by the molybdenum wire. The temperature of the crucible can be regulated by the temperature regulator with a mercury switch operated by the output voltage of a thermocouple and maintained at a constant temperature of ~300°C. On account of temperature gradient which exists between the sample and the thermocouple junction this temperature is lower than the true temperature of magnesium sample itself.

An example of the operating conditions of the separator is shown in Table 3, and an example of mass spectrum of magnesium, obtained by the separator using a Faraday cage with a slit of 5 mm width (electric scanning) is illustrated in Fig. 18.

As the collector, stainless steel boxes, copper and graphite pockets were tried. In the case of stainless steel boxes, the films of metallic magnesium accumulated on

Table 3. Operating conditions of separator in the cases of three elements.

	Magnesium	Neon	Silicon ($SiCl_4$)
Acceleration voltage (KV)	30	30.7	31
Acceleration current (mA)	8	2.5	8
Total collector current* (mA)	5	1.3	0.75
Arc voltage (V)	40	300	120
Arc current (A)	0.2	0.3	1.6
Filament current (A)	42	48.5	47
Gas supply (cc N.T.P. hour)		210	10
Ion source efficiency** (%)	5.1	1	18†
Mean pressure*** (mmHg)	5×10^{-6}	3×10^{-5}	1.1×10^{-4}
Collection hour (hour)	3	4	$3\frac{1}{4}$

* At $2\alpha = 6.4$.
** Ion source efficiency is the ratio of the number of ions extracted from the ion source to the number of neutral atoms consumed in the ion source.
† Percentage of Si^+ is assumed to be 27%.
*** Reading of ionization gauge calibrated for air.

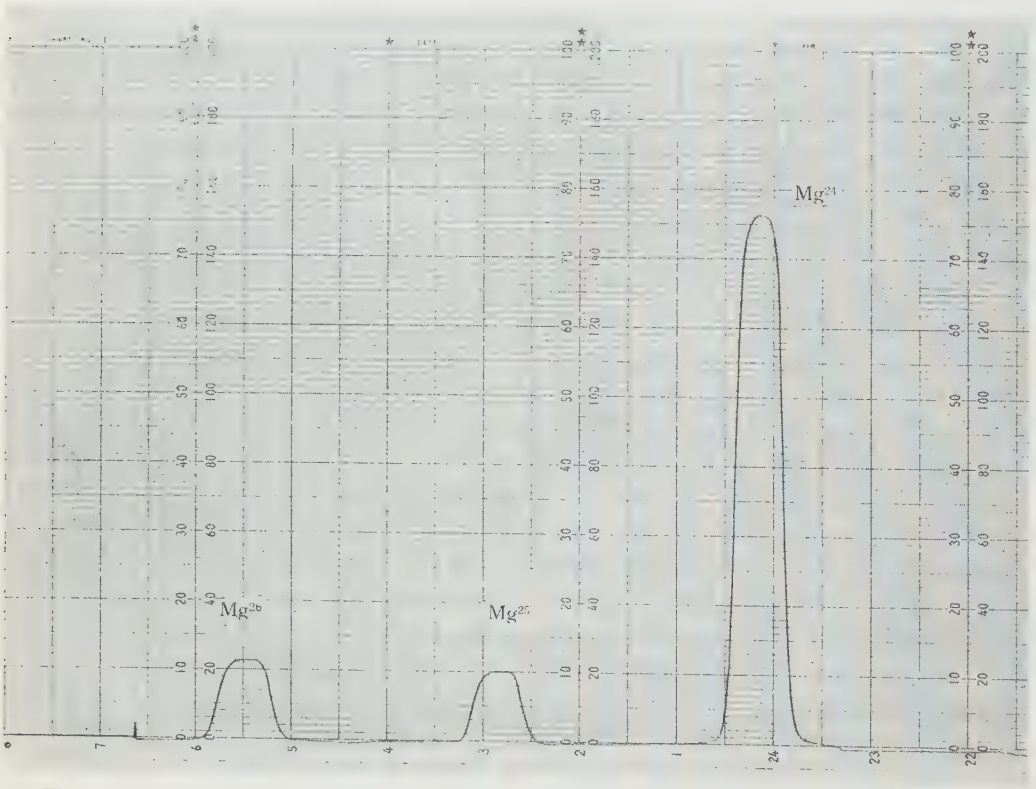

Fig. 18. Mass spectrum of natural magnesium. 5 mm slit Faraday cage was used as an ion collector.

the backward surface of the box unexposed to the direct ion beam easily exfoliated from the surface. On the surface directly exposed to the ion beam no accumulation was recognized. In the case of copper pockets, however, the metal films on it tightly held like the electroplating, and the accumulated amount of magnesium at the positions of direct bombardments was about 150μg/cm^2 per hour.

For the ion current over $\sim$200μA/cm^2, re-sputtering to the neighbouring walls increases appreciably, and almost no accumulation is recognized at the directly bombarded positions. In the case of graphite collector the re-supttering phenomenon is weaker so that the efficiency of direct deposition is better than in the case of copper collector.

Separation of neon isotopes

The collection of ions of gas samples, especially chemically inactive noble gases, is achieved by the method of ion bombarding. This method was tried by Koch (**4**, **15**) and by other authors (**16**, **17**), and the calculations about the range of 50 kev ions in metal are presented by Nielsen (**18**).

We have applied this method to the collection of neon isotopes. The apparatus of gas supply is shown in Fig. 19, and an example of the operating conditions of the separator is listed in Table 3.

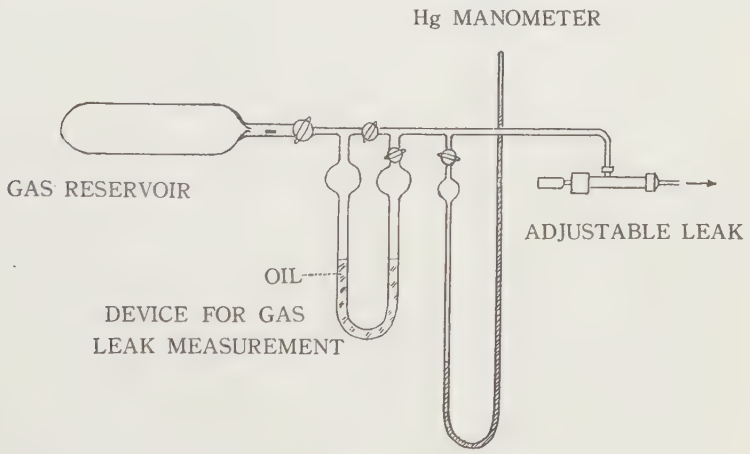

Fig. 19. Apparatus for gas supply.

As the collector material, the silver plates were used. The thin silver plates of 1.3 cm$\times$10 cm$\times$0.02 cm were polished and heated red hot in the induction vacuum furnace for about two hours and the absorbed gas in silver was driven out. Then these degassed silver plates were mounted tightly on the collector plate of the isotope separator and bombarded by the 30 kev ion beams of separated neon isotopes 20, 21 and 22 for 1.5$\sim$4 hours with 3$\sim$10μA/cm^2 intensity. Irradiated plates were removed

and again heated in the quartz tube induction vacuum furnace to the temperature slightly lower than before for a few minutes, and the gas evolved from the silver was collected in a vessel of the volume of 108 cc. The apparatus used in these gas processings is shown in Fig. 20. The mass analysis of these collected gas samples were performed by the C.E.C. Model 21-401 mass spectrometer*. An example of these mass-spectroscopic patterns (after correction for the background and for time variation of the pressure in sample gas container) is illustrated in Fig. 21. From these mass pattern the relative quantities of three neon isotopes in each isotopically separated sample were calculated with the correction of A^{++} and CO_2^{++} contributions and are listed in Table 4 together with their collection conditions. The quantities of impurity gases mainly caused by the absorption of air were relatively so large that the values of the isotopic purities of the separated neon were not very accurate. The quantities of separated neon which was held in the collector silver plates were calculated from the sensitivity of the spectrometer and the spectrum peak height. The quantities of neon caught and held in the thin layer of metal surface cannot be increased proportionally to the increase of integrated current of bombardment,

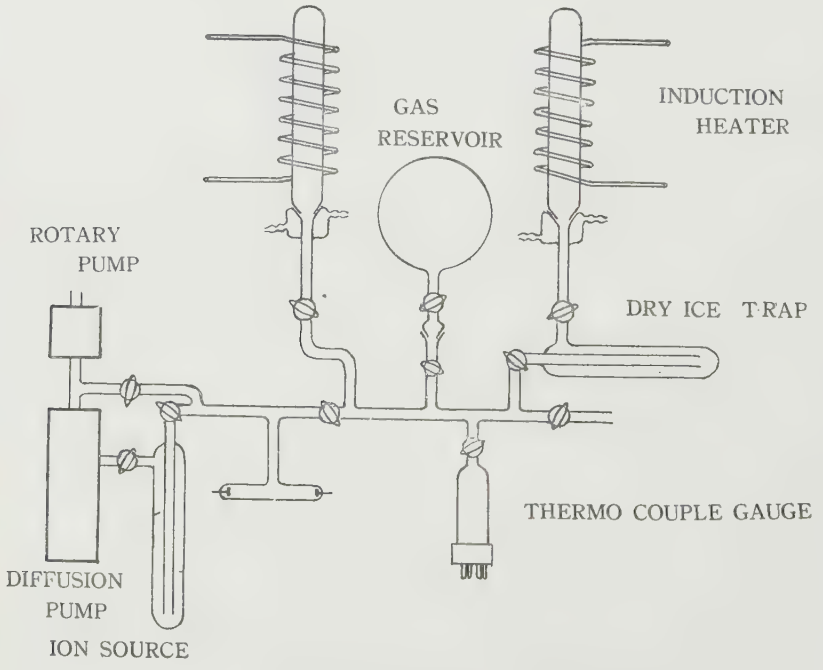

Fig. 20. Apparatus for gas preparation.

* This mass spectroscopic analysis was carried out by Mr. T. Makita in Sasaki Laboratory in the Department of Chemistry in Kyoto University.

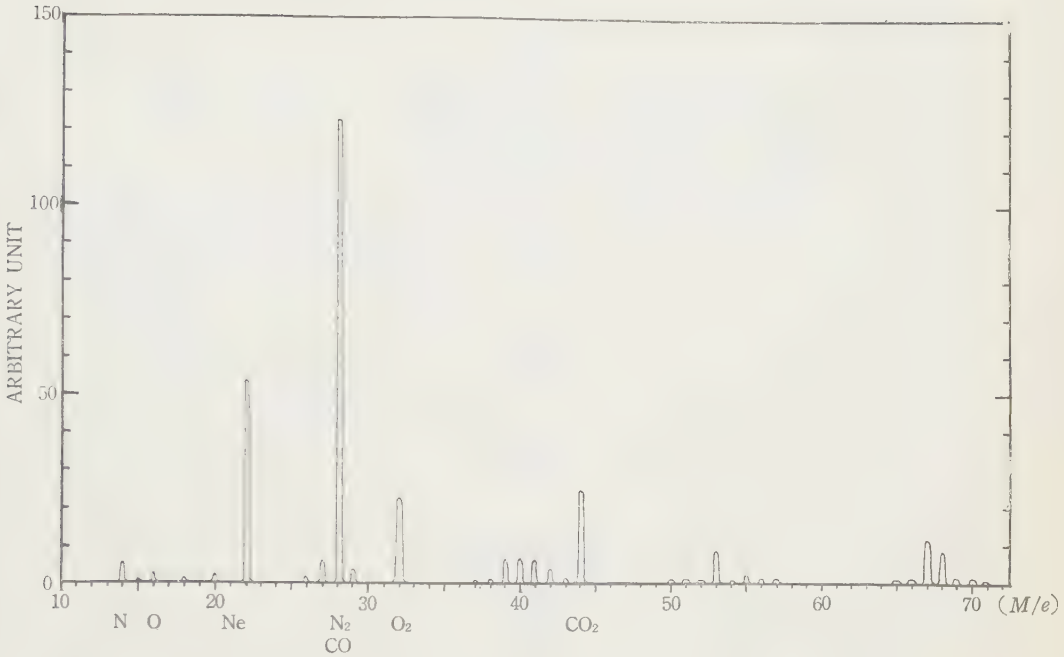

Fig. 21. Mass spectrum of sample No. 5. (enriched in Ne^{22}). Each peak value is corrected for time variation of sample gas pressure and background of the spectrometer.

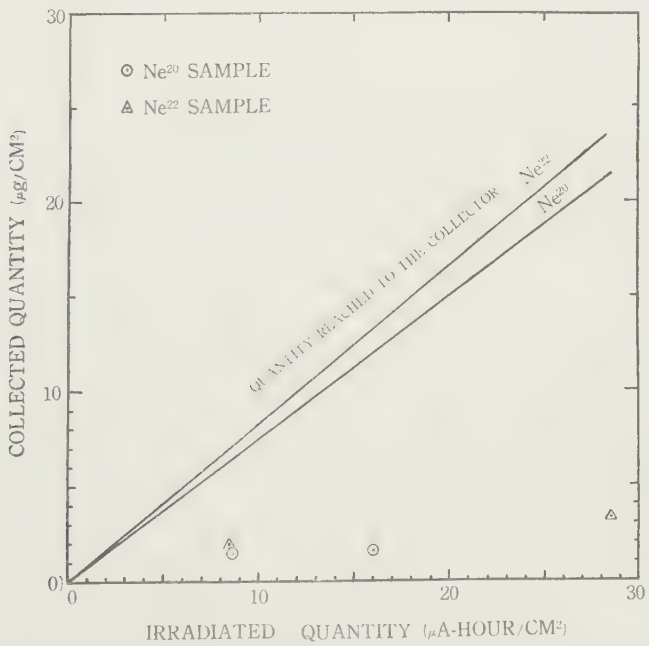

Fig. 22. Collected quantity is shown as a function of irradiated quantity. Saturation phenomenon is clear.

Table 4.

Sample number	Collected isotope	Current density (μA/cm^2)	Collection time (hour)	Irradiated area (cm^2)	Collected quantity (μg/cm^2)	Collection efficiency (%)	Isotopic purity (%)**		
							Ne^{20}	Ne^{21}	Ne^{22}
1	Ne^{20}	10.7	1.5	1.9	1.6	14	100 ± 3.5	0.0 ± 0.4	0.0 ± 2.0
2	Ne^{20}	3.4	2.5	5.5	1.6	25	$99.2\ ^{+0.9}_{-1.8}$	$0.0\ ^{+0.1}_{-0.1}$	$0.8\ ^{+0.6}_{-0.7}$
3	Ne^{21}	0.88/S	4.1	S*	0.69/S	25	66.0 ± 9.8	15.1 ± 3.2	$18.9\ ^{+5.4}_{-7.6}$
4	Ne^{22}	3.4	2.5	0.57	2.0	28	2.3 ± 5.6	0.0 ± 1.2	97.7 ± 6.8
5	Ne^{22}	7.0	4.1	4.3	3.3	14	$2.6\ ^{+1.1}_{-1.0}$	0.0 ± 1.0	$97.4\ ^{+1.8}_{-1.5}$
natural neon***							90.92	0.257	8.82

* Irradiated area could not be measured accurately in this case, so it is designated by S.
** $\pm$ indicates the limit of error in linear scale.
*** These isotopic abundances of natural neon are the values obtained by A.O. Nier (Phys. Rev. **79** (1950), 450)

but saturate at an amount of content (as clearly seen in Fig. 22 and Table 4). In our experiment at the acceleration voltage of 30 KV, the saturated value was about 3μg/cm^2 which is consistent with the value obtained by Koch (**4**) and Thulin (**17**).

Separation of silicon isotopes

Silicon is a solid state element which has the melting point of high temperature, namely 1414°C. But the silicon tetrachloride $SiCl_4$ is a liquid state compound that has the vapour pressure of 22 cmHg at 20°C. We used the vapour of silicon tetrachloride as sample, and introduced into the arc box through a leak valve as in the case of neon separation. Silicon tetrachloride and its dissociated product chlorine are both chemically very active materials, so that the special precaution is needed for the protection of pump oil, especially of the rotary pumps. For this purpose liquid air traps were used between the diffusion pumps and evacuated main body. In the preliminary tests of this chemical effect using another small rotary pump, we have experienced that if the liquid air trap was not used the oil in the rotary pump became violet coloured after about 14 hours pumping of the total of 160 cmHg–l of silicon tetrachloride vapour.

We observed the cracking pattern that indicated the mode of dissociation of the molecules in the arc box of ion source. An example (corresponding to the case II in Table 5) of the mass spectrum obtained by the magnetic field scanning with a deep and wide slit (5 mm$\times$40 mm silt) Faraday cage is illustrated in Fig. 23. In this spectrum

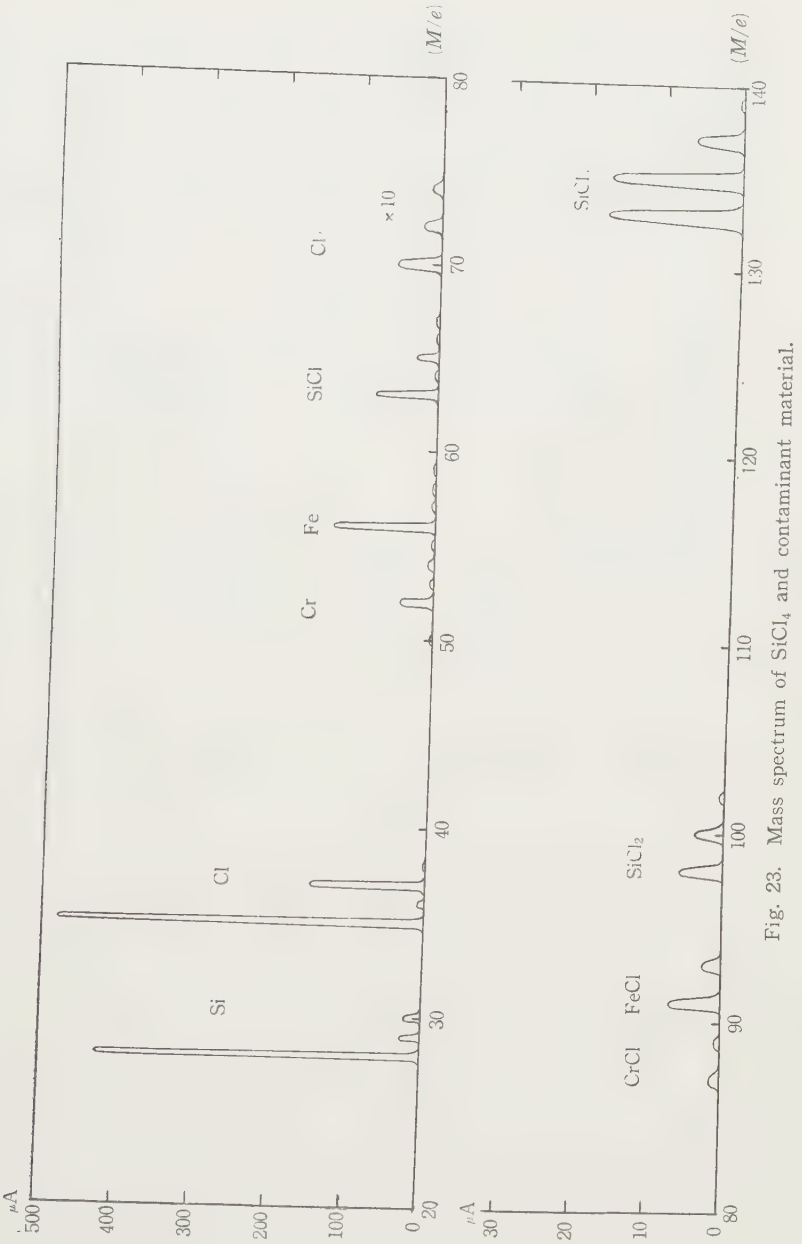

Fig. 23. Mass spectrum of $SiCl_4$ and contaminant material.

some peaks are assigned to the iron and chromium that should be originated from the stainless steel sheet in the graphite arc box. The cracking patterns of tetrachloride are influenced by the conditions in the ion source. But this dependence is very complicated and difficult to examine because the conditioning factors of the ion source cannot be stabilized in this apparatus. Also, mass discriminating effect of the ion source magnet

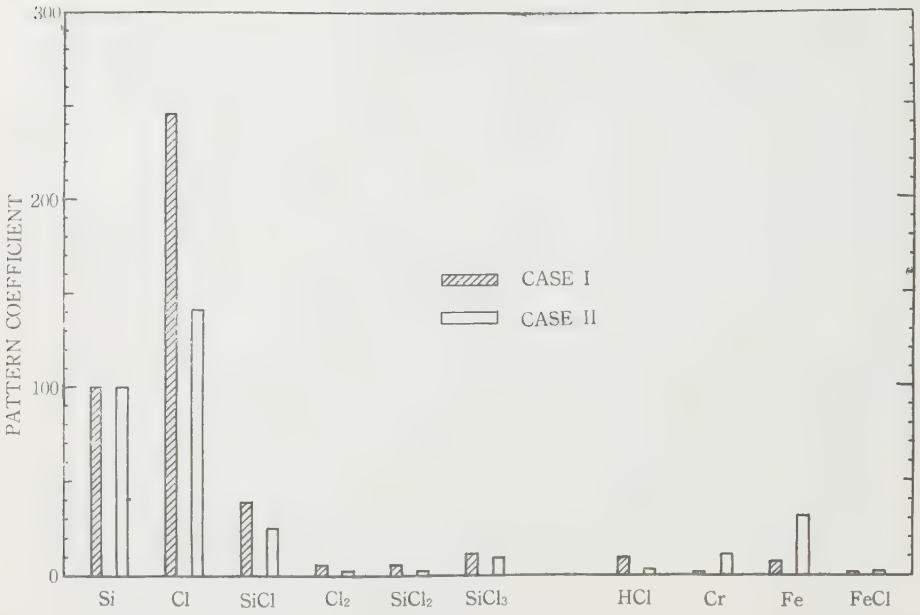

Fig 24. Cracking pattern of $SiCl_4$ and contaminant compounds. Ion source operating conditions in each case are shown in Table 5.

Table 5. Operating conditions in two cases of Si separation

		Case I	Case II
Gas supply	(cc N.T.P./hour)	6.5	13
Arc voltage	(V)	150	150
Arc current	(A)	0.9	3.0
Filament current	(A)	48	45
Acceleration voltage	(KV)	31.5	31.5
Acceleration current	(mA)	3.3	15.9
Collector current*	(mA)	0.3	1.6
Percentage of Si^+**	(%)	23.4	30.4
Ion source efficiency***	(%)	9.9	31.2
Mean pressure	(mmHg)	6×10^{-5}	1.6×10^{-4}

* At $2\alpha=6.4°$
** Percentage of Si ions in the all ions extracted from the ion source.
*** Ratio of the number of ions Si^+ extracted from the ion source to the number of neutral $SiCl_4$ molecules supplied to the ion source.

was noticeable, and wide beam collection must be employed. Pattern coefficients in two different conditions of gas supply are shown in Fig. 24, and operating conditions in these cases are listed in Table 5.

A comparison of these two indicates that the high pressure (strong arc) operation is preferable with respect to the mono-atomic ratio of cracking pattern.

The collector box is made of copper plates of 1 mm thick. The operating conditions in actual collection are described in Table 3. After these operations the separated silicon isotope Si^{28} of a few mg and Si^{29}, Si^{30} of $\sim 30 \mu g/cm^2$ (calculated from the integrated current) were obtained in metallic state on the copper surface. As in the collection of magnesium, abundant isotope Si^{28} accumulated mainly on the side wing wall of the collector box rather than on the portion of direct bombarding.

5. Summary

As is mentioned in foregoing sections, the isotope separator of Kyoto University has the sufficient resolving power (150～250) for the separation of almost all elements, the good stability for long time operation, and has sufficient ion current intensity (several mA continuously) for making the isotopically pure samples for the experimental use in physical researches.

About the focusing point variation due to the space charge force acting on the ion beam, several new remarks and experimental results are presented.

Now, the several experimental researches in nuclear physics are planned by use of the separated isotopes obtained by this separator.

Acknowledgements

The writers express their thanks to Prof. K. Kimura and Prof. N. Sasaki for their kind guidance throughout the construction of this apparatus and the studies of its characters. They wish to thank to Prof. K. Ogata and Mr. J. Okano in Osaka University, Assist. Prof. M. Sakai in the Institute for Nuclear Study of Tokyo University, Dr. K. Okamoto in the Institute of Scientific Research in Tokyo, and to Assist. Prof. Y. Uemura and Mr. K. Miyake in the Chemical Institute of Kyoto University for many useful advices in making the plan of this machine. They also express their thanks to Mr. I. Kumabe, Mr. H. Takekoshi* and other laboratory members in the Department of Physics in Kyoto University for their valuable advices and assistances in constructing and testing of this machine. They wish also to thank to Mr. S. Fukunaga and Mr. K. Takamatsu of this laboratory for their helpful assistance, and to thank to Dr. T. Kambara*, Dr. S. Shima, Dr. S. Saito, Mr. Y. Ohno*, Mr. T. Tsuchimoto, Mr. M. Soneda, Mr. Y. Kondō and Mr. S. Takahashi in the Hitachi Manuf. Co. for the manufacturing of this machine.

The construction of this machine was financially supported by a grant-in-aid for scientific researches of the Ministry of Education.

* Now at the Atomic Energy Research Establishment of Japan.

REFERENCES

1. K. Ogata and J. Okano, Read before the meetings of the Physical Society of Japan (1953).
2. A. Sugimoto and K. Okamoto et al., Read before the meetings of the Physical Society of Japan (1955).
3. K. Kimura, J. Muto, I. Kumabe, H. Takekoshi, K. Okano, H. Tsuchimoto, M. Soneda and Y. Kondo, Mass Spectroscopy No. 8 (Mar. 1957), 12 (in Japanese).
4. J. Koch, *Mass Spectroscopy in Physics Research*, N. B. S. Washington (1953).
5. I. Bergström, S. Thulin, N. Svartholm and K. Siegbahn, Arkiv f. Fysik, **1** (1949), 281.
6. J. Kistemaker and C. J. Zilverschoon, *Mass Spectroscopy in Physics Research*, N. B. S. Washington (1953).
7. R. Bernas, J. Phys. Rad., **14** (1953), 34.
8. R. Bernas, Thèses, Faculté des Sciences de l'Université de Paris, Paris (1954).
9. J. R. Wolff and Freedman, R. S. I., **22** (1951), 736.
10. R. Pepinsky and P. Jarmotz, R. S. I., **19** (1948), 247.
11. A. Guthrie and R. K. Wakerling, *The Characteristics of Electrical Discharges in Magnetic Fields*, National Nuclear Energy Series I-5, (McGraw-Hill, 1949).
12. J. R. Pierce, J. Appl. Phys., **11** (1940), 548.
13. C. E. Berry, R. S. I., **27** (1956), 849.
14. C. P. Keim, Nature, **175** (1955), 98.
15. J. Koch, Nature, **161** (1948), 566.
16. J. Bergström, Arkiv f. Fysik, **5** (1952), 191.
17. S. Thulin, Arkiv f. Fysik, **9** (1955), 107.
18. K. O. Nielsen, *Electromagnetically Enriched Isotopes and Mass Spectrometry*, (Edited by M. L. Smith, Butterworths Scientific Publications, London, 1956).

MEMOIRS OF THE COLLEGE OF SCIENCE, University of Kyoto, Series A,
Vol. XXVIII, No. 4, Article 6, 1958.

A CONSIDERATION ABOUT THE MECHANISM OF OCCURRENCE OF LARGE-SCALE EARTHQUAKES, I.

BY

Saburô KOMURA

(Received December 26, 1957)

ABSTRACT

It is pointed out that the period of the first maximum ground-motion of p-waves due to a large-scale earthquake as observed at various seismological stations shows a systematic pattern of distribution concerning the azimuthal angles of the stations as seen from the origin of the earthquake. This regularity may be explained by assuming that the seismic crack composing of a series of small cracks and generating seismic waves, develops with a certain definite velocity from one end to the other along either of the nodal lines of initial motions and that the period of waves originating from the crack and propagating into various directions is modified by Doppler effect.

Further, the writer has applied the above-mentioned idea with satisfactory results to observational data for Kita-Tango (March 7, 1927), Kita-Izu (November 26, 1930), Tottori (September 10, 1943), Tônankaidô (December 7, 1944), Nankaidô (December 21, 1946), Tokachi-Oki (March 4, 1952) Earthquakes. Finally, the writer gives the result of a model experiment carried out for the purpose of testing the assumptions of his idea by glass plate.

1. Introduction

If we examine the period of the first maximum ground-motion of p-waves observed at seismological stations due to a large-scale earthquake, we may throw light on the physical meaning as regards the regularity of distribution of this period, by assuming that a great crack runs in a given direction along one of the so-called nodal lines of initial motions of p-waves and that the seismic source moves along the crack which generates the elastic waves. And if the wave source moves in an elastic medium, we might recognize the evidence of Doppler effect in the propagation of seismic waves. Based on this idea, it is possible to account for the regularity of symmetrical pattern regarding the above-mentioned time distribution in a large-scale earthquake.

It is found that the azimuthal distribution of the calculated periods of the first maximum ground-motion of p-waves coincides well with that of the observed periods. Thus, the writer is able to make somewhat clear the mechanism of occurrence of some remarkable earthquakes concerning the geographical or azimuthal distribution of the period of the first maximum ground-motion of p-waves observed at seismological stations.

2. On the Fukui Earthquake of June 28, 1948

To begin with, the writer deals with the Fukui Earthquake which occurred on June 28, 1948. The collective report on this earthquake has been already published by the authorities of the Central Meteorological Observatory and the Earthquake Research Institute (**1**). The distribution pattern showing the so-called four-quadrants type with respect to the push and pull of initial impulsive motions of p-waves was given by Dr. T. Hirono, as reproduced in Fig. 1 (**2**).

Fig. 1. The directions of initial ground-motions in the Fukui Earthquake of June 28, 1948.

Assuming that, in this Fukui Earthquake, a great crack runs horizontally from north to south along the nodal line in the direction of N 20° W at the seismic centre and considering that the seismic waves are modified by Doppler effect as the seismic source accompanied by the crack moves, the writer calculated the period of the first maximum ground-motion of p-waves observable at various stations, and compared it with that of actual ground-motion of p-waves obtained from the recorded seismogram by integration. This result will be described later.

(i) The propagation speed and length of crack

Selecting some comparatively clear seismograms from those recorded in the Fukui Earthquake at various seismological stations located within the distance of 320 km from the epicentre, the writer has calculated the period T of the first ground-motion of p-waves by integration from clear horizontal seismograms included in the above report.

In the first place, taking the focal depth of the concerned earthquake as 33 km (**3**), we have discussed the correlation between the focal distance S to each seismological station and the period T, as given in Table I, obtaining sampling correlation

coefficient r as 0.0073. Since, however, this value is less than each value in the significance level of 5% and 1% respectively, with a degree of freedom $\phi=7$, it is not significant. Also, testing the linearity of regression between S and T by means of statistic F, we have obtained the value $F=3.067$, which, however, is not significant because this value is less than either of 6.59 and 16.69 corresponding to the significance level of 5% and 1% respectively, with degrees of freedom $\phi_1=4$, $\phi_2=3$. Thus, it is difficult to assert the existence of the correlation between the focal distance S and the initial period T.

Table I
(The Fukui Earthquake)

No.	Station	T (sec)	S (km)	$\pm\alpha$
1	Abuyama	2.3	139	−0.744
2	Ôsaka	2.7	184	−0.726
3	Owashi	2.1	223	−0.923
4	Kanazawa	3.4	76	+0.520
5	Gifu	1.8	98	−0.909
6	Tsuruga	3.0	62	−0.670
7	Toyama	3.6	113	+0.303
8	Niigata	3.3	326	+0.348
6	Wajima	3.5	159	+0.724

Next, we have calculated the propagating speed v and the length l of a crack. Assuming that a crack was formed horizontally at the focus of 33 km in depth, from north to south along the N 20° W nodal line, let V be the mean velocity of p-waves originating from the crack and α be the cosine of the acute angle between the direction towards the focus from each observation station and the direction of the formation of the crack. Also, let T_p be the initial period of the seismic source at the focus.

Then by virtue of Doppler effect, we have

$$T = T_p \frac{V \pm v\alpha}{V} .$$

Inserting the values of T and α as given in Table I into this formula and taking the mean velocity V of p-waves to be 7.5 km/sec, we have calculated the propagating speed v of the crack by the method of least squares, thus obtaining

$$v = 2.1 \pm 0.3 \text{ km/sec.}$$

Further, we assume that the time of crack formation is approximately equal to the seismic duration time t, which can be calculated by the empirical formula:

$$\log t = -0.7 + M/4 ,$$

where M is the magnitude of an earthquake. In the case of the Fukui Earthquake, this formula gives $t=13$ sec corresponding to $M=7.2$.

Thus, the length l of the crack in the case of the Fukui Earthquake is finally estimated to be

$$l = vt = 27 \pm 4 \text{ km.}$$

(ii) The result compared with observed values

If we assume that the crack generating the seismic waves is horizontally formed at the focus along the N 20° W nodal line from north to south, with the propagating speed $v=2.1$ km/sec; that is to say, if we assume that the seismic source moves accompanying the crack, the period T' of the first maximum ground-motion of p-waves to be observed at seismological stations can be obtained according to Doppler effect as shown in Table II. This calculated value T' agrees well with the actually observed value T.

Table II
(The Fukui Earthquake)

No.	Station	T'_{cal} (sec)	T_{obs} (sec)	$\lvert \Delta T \rvert$
1	Abuyama	2.5	2.3	0.2
2	Ôsaka	2.5	2.7	0.2
3	Owashi	2.4	2.1	0.3
4	Kanazawa	3.3	3.4	0.1
5	Gifu	2.3	1.8	0.5
6	Tsuruga	2.4	3.0	0.6
7	Toyama	3.8	3.6	0.2
8	Niigata	3.3	3.3	0.0
9	Wajima	3.7	3.5	0.2

Moreover, as the limit of errors regarding the period T is estimated as 0.4 sec, the difference $|\Delta T|$ between the values T' and T seems to be unavoidable, considering the fluctuation of assumptions, for instance, the nonlinearity of the direction of crack-formation and the speciality of the crustal structure, etc.

3. Analysis of the ground-motion of the Fukui Earthquake observed at Abuyama

Fig. 2 shows the wave-form of the actual ground-motion of p-waves before the advent of the S-waves, obtained by integrating the seismograms of the Fukui Earthquake which were recorded by two Sassa-type seismographs installed at Abuyama. These are designed to record each motion of N-S and E-W; their proper periods are both 22.4 sec, and their statical magnifications are both 1, while their damping ratios are 2.6 and 1.6 respectively.

Besides, Fig. 3 shows the wave-form projected to the vertical plane containing the direction which combines the Abuyama seismological station with the focus of the Fukui Earthquake. Here, the writer comprehends that wave-form is composed of three small cracks. Generally speaking, when the n sine waves of the same periods and amplitudes pass through a certain station with the phase difference φ, the resultant amplitude S of superposed waves, at any time t between $(n-1)\varphi$ and $n\varphi$, can be represented by

$$S = \sum_{i=1}^{n} \sin \omega(t-\overline{i-1}\varphi) ,$$

where the maximum amplitude of each wave has been taken as unity.

Therefore,

$$S = \frac{\sin(\omega t-\omega\varphi\overline{n-1}/2)\sin(n\omega\varphi/2)}{\sin(\omega\varphi/2)} .$$

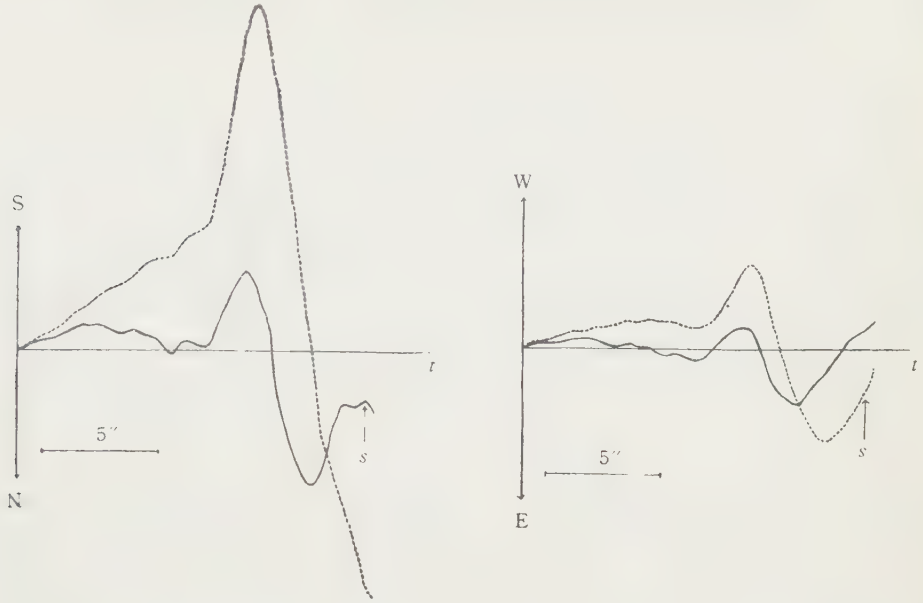

Fig. 2. The unbroken curves represent the horizontal seismograms of p-waves observed at Abuyama, and the dotted curves represent the horizontal ground-motions (determined by integration) connected with them.
(The Fukui Earthquake)

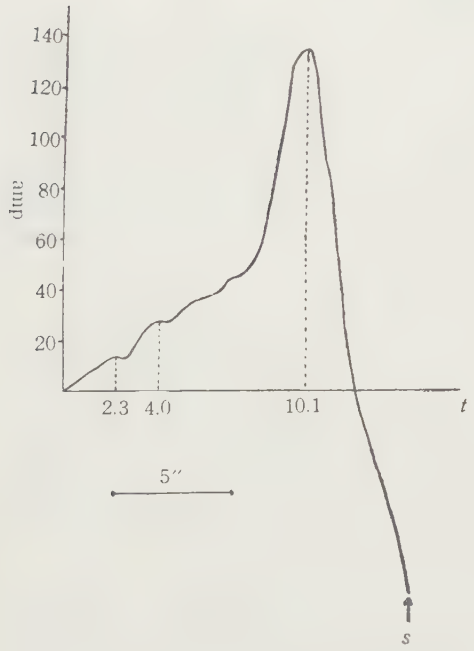

Fig. 3. The horizontal component of the ground-motion projected to the vertical plane containing the direction which combines Abuyama station with the epicentre of the Fukui Earthquake.

When n cracks generate successively at equal time-intervals of t_0 sec and equal distance-intervals of x_0 km, the phase difference φ_i among n waves arriving successively at the observational station is given by

$$\varphi_i = t_0 - \frac{x_0}{V}\cos\theta_i ,$$

where V is the velocity of p-waves, v is propagating speed of each crack and θ_i is the acute angle between the direction of propagation of the crack and the line connecting the observation point and the starting point of each crack.

In the present case, we have $\theta_i \fallingdotseq \theta$, $\varphi_i \fallingdotseq \varphi$, so that the following formula for the angular velocity ω is obtained:

$$\omega = 2\pi \Big/ T_0\left(1-\frac{v}{V}\cos\theta\right) \qquad \text{rad./sec.}$$

Each time t_i which determines the maximum value of the resultant amplitude of the observed ground-motion of p-waves during the time between $(n-1)\varphi$ and $n\varphi$ is induced as below: Now, we measure the time t from the arrival instant of the first motion of p-waves and we consider the resultant amplitude S as the one-valued continously differentiable function of t. Thus, each time t_i above-mentioned is obtained by differentiating S once or twice associated with t, i. e., from

$$\frac{dS}{dt} = 0, \quad \frac{d^2S}{dt^2} < 0,$$

we have

$$t_i = \frac{mT_0}{4}\left(1-\frac{v}{V}\cos\theta\right)+\frac{n-1}{2}\left(t_0-\frac{x_0}{V}\cos\theta\right),$$

$$\text{for } m = 1,\ 3,\ 5, \cdots\cdots .$$

In the Fukui Earthquake, by analyzing the wave-form of the actual ground-motion of p-waves observed at Abuyama, we shall find it composed of three sine waves. Thus, we may consider that three horizontal cracks were generated successively at the intervals of the distance $x_0=9$ km and of the time $t_0=3.5$ sec in the focal region from north to south very closely along the N 20° W nodal line.

In the present circumstances, we have $\cos\theta=0.744$, $V=7.5$ km/sec, $v=2.1$ km/sec, $T_0=4T_p=12.2$ sec, so each t_i which fixes the first, second and third maximum parts of the superposed wave-form can be calculated as 2.4 sec, 4.0 sec and 10.4 sec, respectively. Although these times approximately correspond to the actual ones given in Fig. 3, we find that the ratios of resultant amplitudes corresponding to each maximum part of ground-motion are quite different from those of the actual ground-motion given in Fig. 3, as will be easily understood by a simple calculation.

But, if only we assume that each crack is made at different intervals of time t_0 and distance x_0 and we determine their suitable values, the ratios of the resultant amplitude among the maximum parts considerably resemble the actually observed ones as in the following explanation. In other words, we suppose that the first, second and third cracks occurred in the focal region from north to south very closely along the N 20° W nodal line with such intervals of distance x_0 and time t_0 as given by

$$x_{(12)},\ x_{(23)};\ t_{0(12)},\ t_{0(23)},$$

wherein suffix (ij) shows the notation of the number of cracks formed in these turns. When the maximum amplitudes of the three fundamental sine waves composing the wave-form of the actual ground-motion observed at Abuyama are denoted by a_1, a_2, a_3, respectively, the resultant amplitudes S obtained by superposing the three sine waves are represented by

$$S = a_1 \sin \omega t + a_2 \sin(\omega t - \omega\varphi_1) + a_3 \sin(\omega t - \omega\varphi_1 - \omega\varphi_2) .$$

Now, when we have

$$x_{(12)} = 4 \text{ km}, \qquad x_{(23)} = 6 \text{ km};$$
$$t_{0(12)} = 3.0 \text{ sec}, \qquad t_{0(23)} = 4.0 \text{ sec};$$
$$a_1 : a_2 : a_3 = 1 : 2 : 12;$$
$$\omega\varphi_1 = 1.684 \text{ rad.}, \qquad \omega\varphi_2 = 2.202 \text{ rad.},$$

the ratios among resultant amplitudes S_1, S_2, S_3, corresponding to each time which determines the positions of the first, second and third maximum parts of the ground-motion are calculated as follows:

$$S_1 : S_2 : S_3 = 1 : 2.1 : 10.2 .$$

The times showing each maximum part of the ground-motion are given as 2.4 sec, 9.5 sec. These values as well as the ratios of resultant amplitudes approximate to those actually observed as shown in Fig. 3.

Judging from the accuracy of present seismograms and from the assumption that the fundamental waves are composed of the sine waves having the same periods, the discordance of such a degree may be unavoidable.

Moreover, if the times T_1, T_2, T_3 required for the formation of each crack are proportional to the square roots of maximum amplitudes a_1, a_2, a_3 of the fundamental sine waves corresponding to each crack, i. e., if we have

$$T_1 : T_2 : T_3 = \sqrt{a_1} : \sqrt{a_2} : \sqrt{a_3} ,$$

using the value $t = 13$ sec as given in the foregoing § 2 (i), the times T_1, T_2, T_3 are calculated as follows:

$$T_1 = 2 \text{ sec}, \qquad T_2 = 3 \text{ sec}, \qquad T_3 = 8 \text{ sec}.$$

By combining the above-stated values with the intervals of distance and time of each crack, the distance between the starting point of the first crack and the terminal point of the third crack, the time and the mean velocity necessary for crack-formation are calculated to be 26.8 km, 15 sec and 1.8 km/sec, respectively. This mean velocity of crack-formation coincides with the above-mentioned value of 2.1 km/sec within the limit of errors. Therefore, in the Fukui-Earthquake, it would be safe to say that one great crack was horizontally formed in the focal region with the velocity of 2.1 km/sec from north to south along the N 20° W nodal line. Taking for granted, however, that the mechanism of occurrence of a large-scale earthquake is understood in such a way as to be composed of a series of small cracks, we may just as well deal with them as one crack, if only we determine suitable intervals of distance and time. As a matter of fact, however, judging from the stand-point of the mechanism of elastic

wave occurrence accompanying the crack, we may arrive at a rational conclusion by regarding it as composed of three cracks.

4. Other large-scale earthquakes

The writer has applied the above-mentioned idea to the following remarkable earthquakes, i. e., Kita-Tango (March 7, 1927), Kita-Izu (November 26, 1930), Tottori (September 10, 1943), Tônankaidô (December 7, 1944), Nankaidô (December 21, 1946), Tokachi-Oki (March 4, 1952) earthquakes.

Picking up some comparatively clear seismograms, the writer has calculated the time T' which indicates the maximum part of initial ground-motion observed at seismological stations due to each earthquake, according to his idea already described. It is very interesting to notice that the above values of T' are in satisfactory agreement with the observed ones represented by T, as given in Tables III~VIII. The figures corresponding to these tables are shown in Figs. 4~9. In these figures, each short arrow shown by the dotted line along the unbroken nodal line represents the direction of crack-formation in the focal region.

Table III
(The Kita-Tango Earthquake)

No.	Station	T' (sec)	T (sec)	$\pm\alpha$
1	Kyôto	0.8	0.7	−0.982
2	Kôchi	1.4	1.6	−0.515
3	Kôbe	0.8	0.6	−0.921
4	Sumoto	1.0	0.9	−0.819
5	Sendai	2.1	2.0	+0.087
6	Tôkyo	1.5	1.7	−0.431
7	Numazu	1.3	1.6	−0.588
8	Hamada	2.2	2.1	+0.174

Further, each value of the crack-length relative to each earthquake taken up here is estimated as follows:

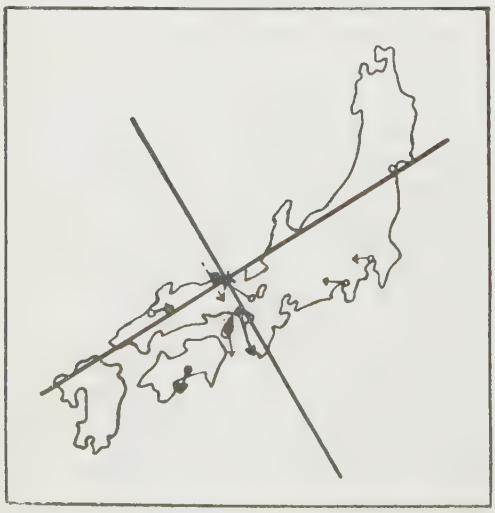

Fig. 4. The directions of initial ground-motions in the Kita-Tango Earthquake of March 7, 1927. The crossing unbroken lines show the so-called nodal lines, and arrow drawn with dotted line along one of them represents the direction of cracking.

Kita-Tango Earthquake	34 ± 5 km ($M = 7.6$)
Kita-Izu Earthquake	28 ± 4 km ($M = 7.3$)
Tottori Earthquake	29 ± 4 km ($M = 7.4$)
Tônankaidô Earthquake	42 ± 6 km ($M = 8.0$)
Nankaidô Earthquake	46 ± 7 km ($M = 8.2$)
Tokachi-Oki Earthquake	49 ± 7 km ($M = 8.2_5$) (4)

Table IV
(The Kita-Izu Earthquake)

No.	Station	T' (sec)	T (sec)	$\pm\alpha$
1	Akita	2.1	2.0	+0.998
2	Ôsaka	0.9	1.0	−0.292
3	Kumagaya	2.1	1.9	+0.982
4	Sionomisaki	0.6	0.5	−0.629
5	Hachijojima	0.4	0.4	−0.917
6	Hikone	1.1	0.9	−0.070
7	Maebashi	2.1	2.3	+0.997
8	Misima	0.6	0.6	−0.725
9	Mera	1.0	0.9	−0.276
10	Wajima	1.8	1.7	+0.713

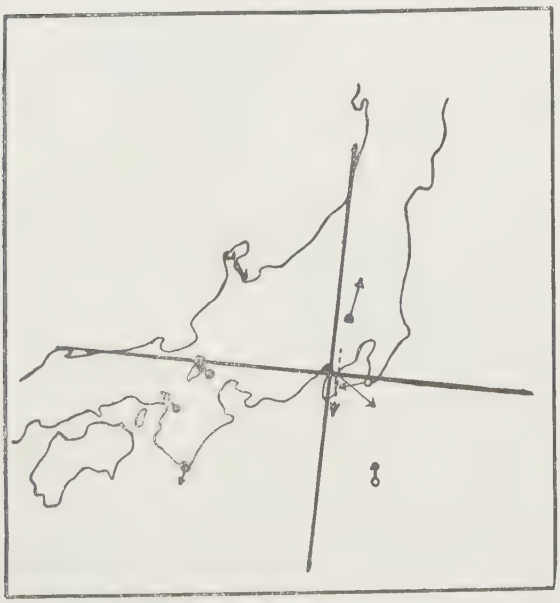

Fig. 5. The directions of initial ground-motions in the Kita-Izu Earthquake of November 26, 1930. The crossing unbroken lines and arrow are the same as those in Fig. 4.

Table V
(The Tottori Earthquake)

No.	Station	T' (sec)	T (sec)	$\pm\alpha$
1	Ôsaka	1.6	1.8	−0.515
2	Kôbe	1.7	1.9	−0.407
3	Sumoto	1.8	1.5	−0.105
4	Takamatsu	2.1	2.0	+0.454
5	Hikone	1.4	1.3	−0.887
6	Murotomisaki	2.1	2.0	+0.358
7	Yonago	2.4	2.6	+0.970

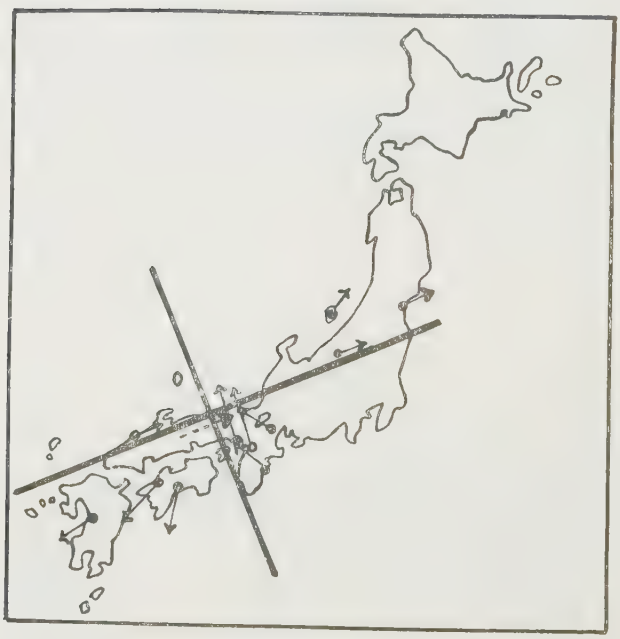

Fig. 6. The directions of initial ground-motions in the Tottori Earthquake of September 10, 1943. The crossing unbroken lines and arrow are the same as those in Fig. 4.

Table VI
(The Tônankaidô Earthquake)

No.	Station	T' (sec)	T (sec)	$\pm\alpha$
1	Owashi	1.6	1.3	−0.848
2	Kyôto	2.0	2.0	−0.682
3	Sionomisaki	1.6	1.7	+0.927
4	Nara	1.6	1.7	−0.656

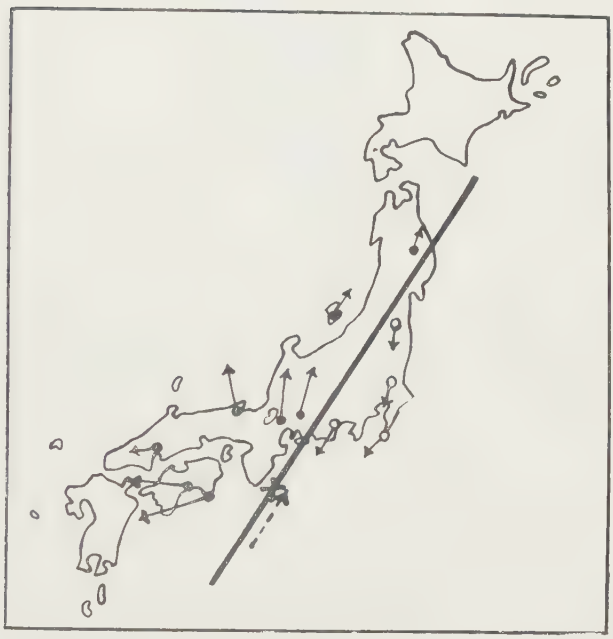

Fig. 7. The directions of initial ground-motions in the Tônankaidô Earthquake of December 7, 1944. The unbroken line and arrow are the same as those in Fig. 4.

Table VII
(The Nankaidô Earthquake)

No.	Station	T' (sec)	T (sec)	$\pm\alpha$
1	Ôsaka	2.5	2.4	−0.814
2	Kameyama	2.4	2.3	−0.980
3	Kôchi	3.5	3.8	+0.242
4	Kyôto	2.5	2.4	−0.871
5	Hikone	2.4	2.4	−0.943

Fig. 8. The directions of initial ground-motions in the Nankaidô Earthquake of December 21, 1946. The unbroken line and arrow are the same as those in Fig. 4.

Table VIII
(The Tokachi-Oki Earthquake)

No.	Station	T' (sec)	T (sec)	$\pm\alpha$
1	Aomori	0.9	1.0	−0.771
2	Obihiro	1.4	1.2	+0.528
3	Kushiro	1.5	1.7	+0.891
4	Sapporo	1.2	1.2	+0.086
5	Sendai	0.8	0.8	−0.990
6	Tsukubasan	0.8	0.8	−0.988
7	Hachinoe	0.9	0.9	−0.907
8	Miyako	0.9	0.8	−0.928
9	Wakkanai	1.4	1.4	+0.640

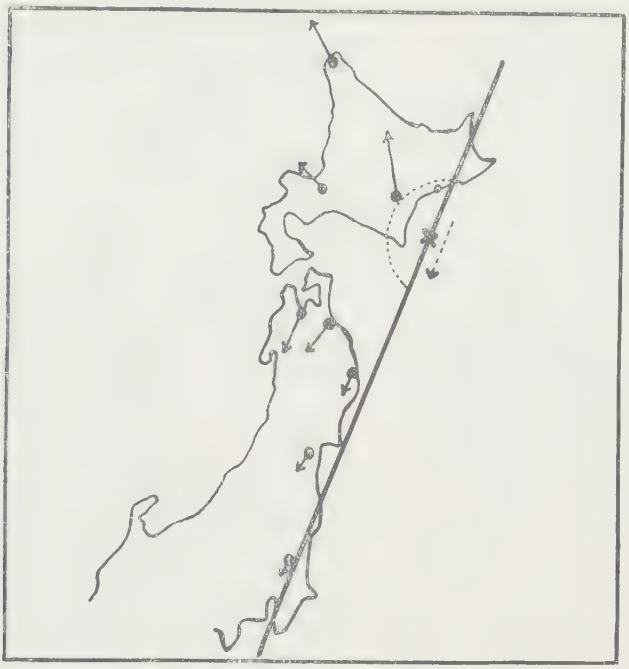

Fig. 9. The directions of initial ground-motions in the Tokachi-Oki Earthquake of March 4, 1952. The unbroken line and arrow are the same as those in Fig. 4.

When we consider the mechanism of occurrence of seven foregoing remarkable earthquakes which showed distinct nodal lines in connection with the regularity of the geographical or azimuthal distribution as regards the period of the first maximum ground-motion of each earthquake, it is of great interest to notice a satisfactory coincidence of the calculated period with the observed one, if only we apply Doppler effect to the generated waves, assuming that the crack is formed along the nodal line and the elastic waves accompany the crack. In other words, if we consider the physical meaning of the geographical or azimuthal distribution with regard to the above initial period from the stand-point of the movement of the seismic source accompanying the formation of the crack, we shall be able to give a new phenomenological explanation to the mechanism of occurrence of large-scale earthquakes.

5. A model experiment

In order to establish the validity of the writer's assumptions, the following simple experiment with glass plate was tried. First, let us describe an outline of this experiment. As shown in Fig. 10, the rectangular glass plate abcd (21 cm×31 cm ×0.2 cm) is stuck to the square glass plate ABCD (61 cm×61 cm×0.2 cm) with a binding agent, for instance, cellophane tape, and all the plates are supported on the

stay at its gravity-centre.

Thus, let us look at Fig. 10. (i) When we strike the glass plate at the point 0, and (ii) when the crack runs through the plate abcd, from e to g along the line ef, the moving coils which are set up at the positions marked with the signs ①, ②, ③ on the glass plate ABCD, catch tremors propagating through the glass plate in the cases of (i) and (ii), respectively.

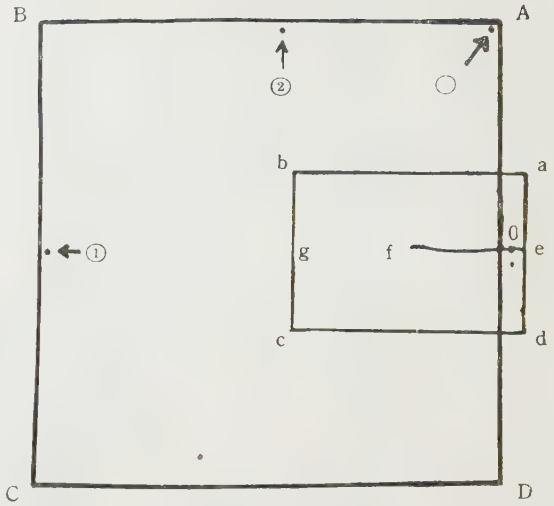

Fig. 10. The rectangular glass plate abcd is previously damaged by a diamond pencil for the purpose of inducing the crack along the line ef, and is stuck to the square glass plate ABCD as shown in this figure.

In this manner, the tremors caught by moving coils at the positions ①, ②, ③ are optically recorded on the roll paper set up in the oscillograph. In the case of (ii), however, the plate abcd is previously damaged by a diamond pencil for the purpose of inducing the crack along the line ef on the plate abcd.

When we heat the plate abcd near the point e with the flame of an alcohol lamp a crack will run through the plate abcd from e to g along the line ef on it.

Judging from the result of such an experiment as shown in Fig. 11, we may distinguish the period of the first maximum motion of tremors caught at the positions ①, ②, ③ in the case (ii) from that in (i).

Thus, applying the writer's idea to the result as described in Table IX concerning the case (ii), we shall have the propagating speed of the crack in the glass plate as follows:

$$1.5_2 \pm 0.0_4 \text{ km/sec},$$

wherein the velocity of p-waves propagating through the glass plate is taken as 4.0 km/sec.

In consequence of this simple model experiment using a glass plate, it seems valid and adequate to recognize the following two facts, i. e., the facts that elastic waves are always generated on the occasion of the crack formation and that azimuthal distribution concerning the period of their first maximum parts is regular.

Admitting of these facts derived from this very simple model experiment, we may grasp from the view-point of the movement of seismic source accompanying the

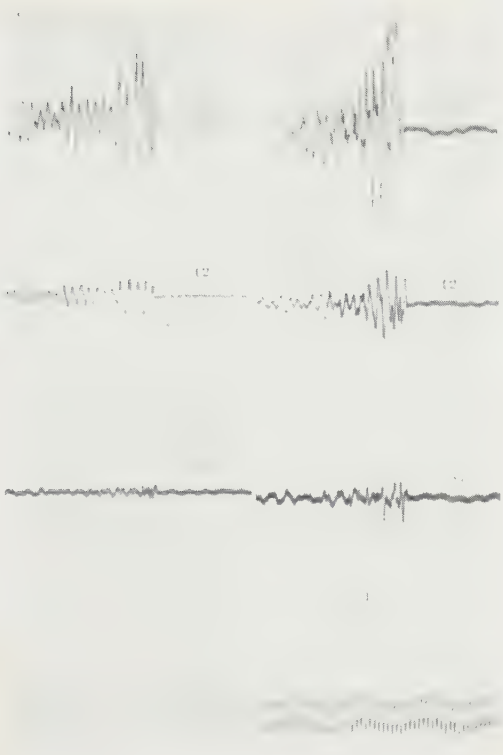

Fig. 11. A pair of records of tremors caught at the positions ①, ②, ③ on the plate ABCD shown in Fig. 10. Records marked with the sign (ii) show the tremors when we strike the plate at the point 0, and those shown in (ii) represent the tremors accompanying the crack which runs through the plate from e to g along the line ef (in Fig. 10). (Period of tuning fork is 1 100 sec.)

Table IX

Position	T' $\times 100^{-1}$sec.	T $\times 100^{-1}$sec.	α
(1)	0.36	0.34	−1.000
(2)	0.41	0.42	−0.731
(3)	0.55	0.54	−0.104

formation of the crack along the nodal line, the regularity of geographical or azimuthal distribution regarding the initial period of the maximum ground-motion of p-waves due to a remarkable earthquake.

Acknowledgements.

In conclusion, the writer expresses his hearty thanks to Professor K. Sassa for his kind encouragement and guidance in the course of this study. The writer's thanks are also due to Professor S. Tomotika for his kind inspection of the manuscript.

Moreover, the writer expresses his sincere appreciation to Dr. U. Inoue, the Director of Seismic Research Department and Dr. T. Hirono, the chief of the Seismological Section, both in the Meteorological Agency of Japan, who have shown him

special kindness in permitting him to use valuable data of the seismograms as regards the above remarkable earthquakes.

Sincere gratitude is also due to the headmaster of the Meteorological Observatory in Kyôto District, members in its seismological section, and seismic members of each meteorological station whom the writer asked for the valuable seismic data necessary for this investigation.

REFERENCES

1, 2, 3. The Special Committee of the Fukui Earthquake, Report of the Special Committee for the Study of the Fukui Earthquake, (1950), 1-197, 6, 29.

4. The Special Committee for the Investigation of the Tokachi-Oki Earthquake, (1954), 7.

Memoirs of the College of Science, University of Kyoto, Series A,
Vol. XXVIII, No. 4, Article 7, 1958.

A CONSIDERATION ABOUT THE MECHANISM OF OCCURRENCE OF LARGE-SCALE EARTHQUAKES, II.

BY

Saburô KÔMURA

(*Received December 26, 1957*)

ABSTRACT

In this paper, the writer intends to re-examine the results reported in the preceding paper from the view-point of both dislocation of the Earth's crust and the energy of the seismic waves produced by a large-scale earthquake.

Generally speaking, the direction of the crustal dislocation accompanying an earthquake does not always coincide with that of the initial ground-motion of *p*-waves. But in such earthquakes as Kita-Tango, Kita-Izu and Fukui, it has been said that the above-mentioned two directions agree with each other. Now, the result we obtained is that the horizontal dislocation of the crust computed according to Honda-Miura's or Whipple's idea agrees approximately with the actually surveyed one. And the writer pointed out that the mechanism of the occurrence of the Fukui Earthquake could be explained as composed of a series of three cracks which grew up from north to south along the N 20° W nodal line, as described in the preceding paper. Then, when computed according to Whipple's forces-model, the resultant dislocation at each surveying station shows a satisfactory agreement with the actual dislocation determined by geodesic survey; the similar satisfactory results may be obtained as regards Kita-Tango and Kita-Izu Earthquakes. Moreover, we may certify the validity of the estimated length of a great crack accompanying each earthquake, by recognizing that the seismic energy calculated from the length of the crack coincides fairly well in the order with the seismic energy computed by the newly corrected Gutenberg-Richter's formula.

1. Introduction

In the preceding paper, the writer pointed out that the periods of the first maximum ground-motions of *p*-waves due to a large-scale earthquake (as observed at various seismological stations) show a systematic pattern of distribution with respect to the azimuthal angles of the stations as seen from the origin of the earthquake. The seismic crack, which is composed of a series of small cracks—this is estimated by analyzing the actual ground-motion of *p*-waves observed, for instance, at Abuyama,—and from which the seismic waves are generated, is developed with a certain definite velocity from one of its ends to the other along either of the so-called nodal lines of initial motions of *p*-waves, and the writer also pointed out that the periods of waves originating from the crack during its formation and being propagated into various directions are modified according to Doppler effect in connection with the movement

of seismic source along the growing crack at the focus.

In the present paper, the writer intends to re-examine the above facts from the view-point of both the horizontal dislocation of the Earth's crust and the energy of the seismic waves produced by a large-scale earthquake.

2. Horizontal dislocation caused by a large-scale earthquake

Setting aside the question whether the deformation of the Earth's crust is the cause of a large-scale earthquake or not, we know well the fact that a remarkable dislocation of the crust is noticed near the epicentre before and after a large-scale earthquake. Furthermore, we often notice great faults when a shallow remarkable earthquake took place. Of course, we know the case in which the crustal dislocation reversely goes on before and after a large-scale earthquake. Generally speaking, we cannot always assert that the growing direction of the crustal displacement produced by an earthquake coincides with that of the initial ground-motion of p-waves accompanying it. As for such earthquakes as Kita-Tango (March 7, 1927), Kita-Izu (November 26, 1930), and Fukui (June 28, 1948), however, it has been recognized that the direction of the crustal dislocation agrees fairly well with that of the initial ground-motion of p-waves.

On the whole, many seismologists have already discussed the direction of deformation of displacement in a homogeneous, isotropic, semi-infinite elastic medium owing to forces-source applied to its boundary plane or its interior. They have theoretically calculated the special solutions of the problems in various cases. Recently N. Yamakawa (**1**) has summarily discussed the problem of this kind. Now, the writer intends to re-examine the horizontal dislocation of the Earth's crust accompanying a large-scale earthquake according to Honda-Miura's or Whipple's forces-model. According to Honda-Miura's model (**2**) about forces-source, the horizontal displacements U, V of the Earth's crust due to a shallow large-scale earthquake are given by

$$U = \frac{A \sin 2\varphi}{10\mu}\left[\frac{2}{3}\frac{1}{\tilde{\omega}^3} + \frac{5}{3}\frac{1}{b\tilde{\omega}(\tilde{\omega}^2+b^2)^{1/2}} - \frac{2}{3}\frac{b}{\tilde{\omega}^3(\tilde{\omega}^2+b^2)^{1/2}} - \frac{2b}{\tilde{\omega}(\tilde{\omega}^2+b^2)^{3/2}} - \frac{3}{2}\frac{b\tilde{\omega}}{(\tilde{\omega}^2+b^2)^{5/2}}\right],$$

$$V = -\frac{A\cos 2\varphi}{10\mu}\frac{1}{3}\left[\frac{2}{\tilde{\omega}^3} - \frac{2}{b\tilde{\omega}(\tilde{\omega}^2+b^2)^{1/2}} - \frac{2b}{\tilde{\omega}^3(\tilde{\omega}^2+b^2)^{1/2}} + \frac{b}{\tilde{\omega}(\tilde{\omega}^2+b^2)^{3/2}}\right],$$

assuming that Lamé's elastic parameters λ and μ are equal to each other.

Here, $\tilde{\omega}$, φ are the cylindrical coordinates, the origin of which is taken at a certain point on the boundary surface, the positive direction of the z-axis being taken downwards from the surface. U and V are the horizontal components of the crustal displacements parallel and perpendicular to $\tilde{\omega}$ respectively. The force at the focus is represented by

$$A\frac{\tilde{\omega}^3}{(\tilde{\omega}^2+b^2)^{7/2}}\sin 2\varphi$$

That is to say, when a force of the so-called four-quadrants type acts at the origin of coordinates along the boundary surface of a semi-infinite elastic medium, the horizontal components of displacement U and V on the surface are expressed by the above formulae, if we assume that Lamé's elastic parameters λ and μ are equal. In case when $b=10$, the calculated horizontal displacements at several points on the surface of a semi-infinite elastic solid become as shown in Fig. 1.

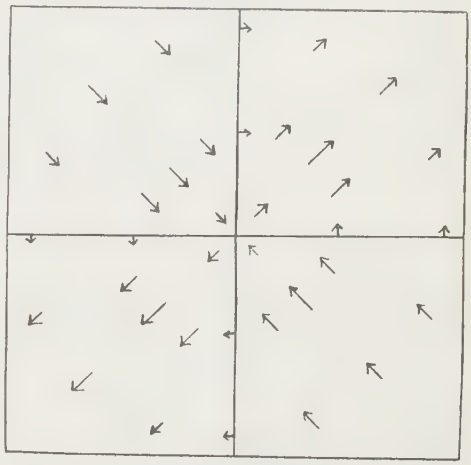

Fig. 1. Short arrows show the horizontal displacements of the crust according to Honda-Miura's model.
(After Drs. H. Honda and T. Miura)

On the other hand, F. J. W. Whipple (3) dealt with the crustal deformation produced by the so-called stress-nucleus situated in the interior of a semi-infinite elastic medium. He calculated the horizontal displacement-components U, V on the surface of the medium, as produced by the two "double forces with moment" (denoted by the symbol ⋕) acting on the plane situated at a depth b, parallel to the surface. His expressions for U, V are given by

$$U = A\,\frac{\tilde{\omega}\sin 2\varphi}{r^3}\left[\frac{\lambda+2\mu}{\mu}\frac{\tilde{\omega}^2}{r^2} - \frac{\lambda+2\mu}{3(\lambda+\mu)}\frac{\tilde{\omega}^2-2br}{(r+b)^2}\right],$$

$$V = A\,\frac{2}{3}\,\frac{\lambda+2\mu}{\lambda+\mu}\,\frac{\tilde{\omega}\cos 2\varphi}{r(r+b)^2},$$

with $r^2=\tilde{\omega}^2+b^2$, where, as before, $\tilde{\omega}$, φ, z are cylindrical coordinates with the origin on the surface and the z-axis is taken downwards. Assuming $\lambda=\mu$, the calculated displacements by the above formulae become as shown in Fig. 2.

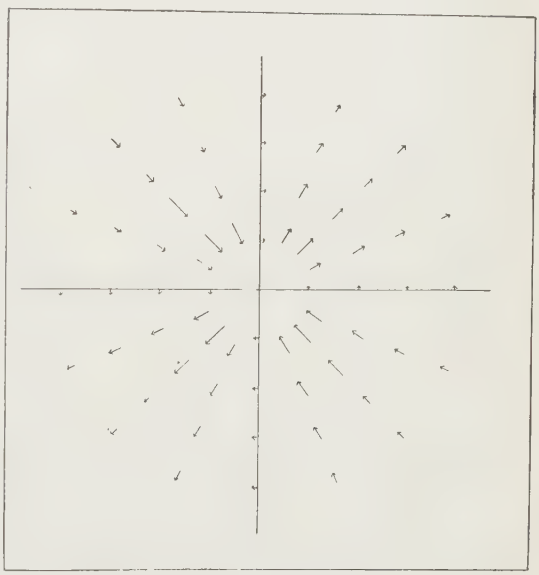

Fig. 2. Short arrows show the horizontal displacements of the crust calculated according to Whipple's model.
(After F.J.W. Whipple)

In case when the plane containing Whipple's forces is not horizontal, but has a certain inclination against the surface of a homogene-

ous, isotropic, semi-infinite medium, the expressions for the horizontal components U, V of the displacement at any point on the surface are given by (**4**):

$$U = \frac{2}{3} A\Big[\Big\{3\frac{\lambda+2\mu}{\mu}\frac{\tilde{\omega}^3}{r^5} - \frac{\lambda+2\mu}{\mu}\frac{\tilde{\omega}^2-2br}{r^3(r+b)^2}\tilde{\omega}\Big\}$$
$$\times(\cos\chi\cos\psi\cos\varphi+\sin\psi\sin\varphi)(\cos\psi\sin\varphi-\cos\chi\sin\psi\cos\varphi)$$
$$-\frac{2}{3}\frac{\lambda+2\mu}{\mu}\frac{\tilde{\omega}^2 b}{r^5}\Big(\frac{1}{2}\sin 2\chi\sin 2\psi\cos\varphi-\sin\chi\cos 2\psi\sin\varphi\Big)$$
$$-\Big\{3\frac{\lambda+2\mu}{\mu}\frac{\tilde{\omega}b^2}{r^5}+\frac{\lambda+2\mu}{\mu}\frac{(2r+b)b\tilde{\omega}}{r^3(r+b)^2}\Big\}\Big(\frac{1}{2}\sin^2\chi\sin 2\psi\Big)\Big],$$

$$V = \frac{2}{3} A\Big[\frac{\lambda+2\mu}{\lambda+\mu}\frac{\tilde{\omega}}{r(r+b)^2}\Big\{\cos\chi\cos 2\psi\cos 2\varphi+\frac{1}{2}\sin 2\psi(1+\cos^2\chi)\sin 2\varphi\Big\}\Big],$$

where χ and ψ are the Eulerian angles between the plane containing Whipple's forces and the boundary surface of the elastic medium.

However, we deal here with such a case in which the plane containing Whipple's forces is, as in his paper, parallel to the horizontal plane so that $\chi = 0$, $\psi = 0$. Of course, the components of the horizontal displacement U, V as obtained by setting $\chi = 0$, $\psi = 0$ in the above formulae are in complete agreement with those computed by Whipple himself.

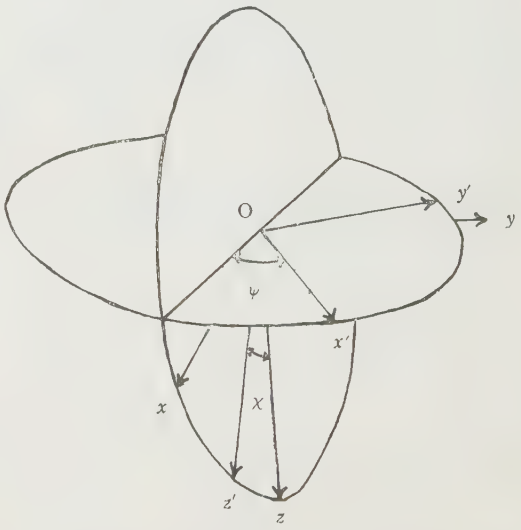

Fig. 3. The Eulerian angles χ, ψ representing the inclination between the plane parallel to the boundary surface (xy-plane) of a semi-infinite solid and the plane ($x'y'$-plane) containing Whipple's forces which act inside the solid.

If the above forces-source at the focus exists on the occasion of each crack-formation, it may be possible to compare the result of the actual survey with the resultant surface displacement of each station by organizing the vectors which show the distribution of our so-called four-quadrants type as regards the horizontal dislocation that each crack produces (Fig. 4). As already pointed out in the preceding paper, we may consider the mechanism of occurrence of the Fukui Earthquake as composed of three cracks. Namely, we suppose the first, second and third cracks C_1, C_2, C_3 were formed at the focus in such turns as indicated by suffixes 1, 2, 3 from north to south nearly along the N 20° W nodal line with such intervals of distance and time as already given. In this manner, the results obtained at each station by composing the vectors of the

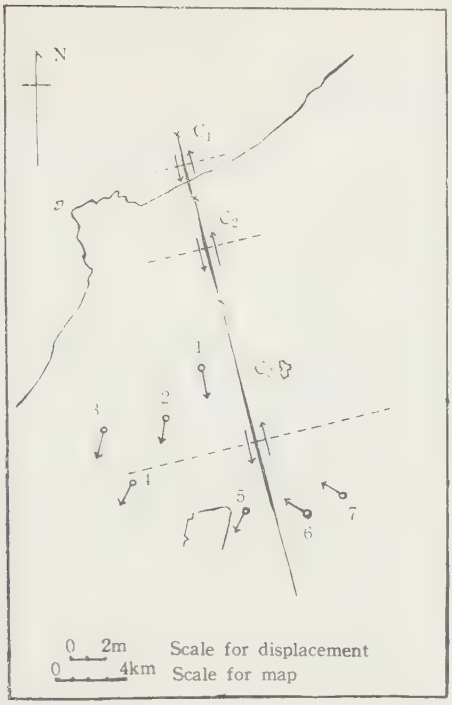

Fig. 5. Each short arrow shows the horizontal displacement calculated according to Honda-Miura's model near the focal region of the Fukui Earthquake of June 28, 1948. Each sign C_1, C_2, C_3 shows every crack formed in such turns as 1, 2, 3. The mark × shows its starting point, the unbroken line is drawn in order to correspond with its length, and the dotted line shows one of the nodal lines accompanying each crack.

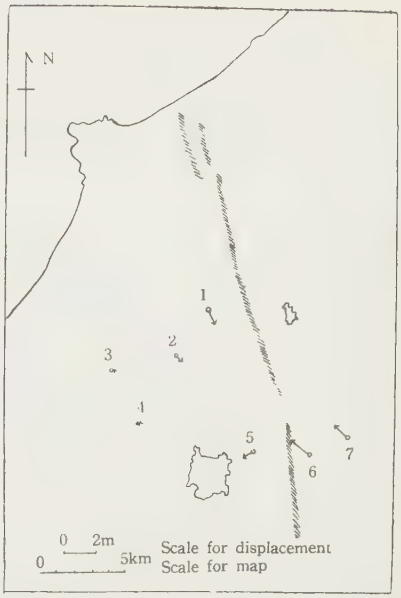

Fig. 4. Each short arrow shows the horizontal corrected dislocation of the crust, actually surveyed after the Fukui Earthquake of June 28, 1948, and shaded parts show the observed faults.

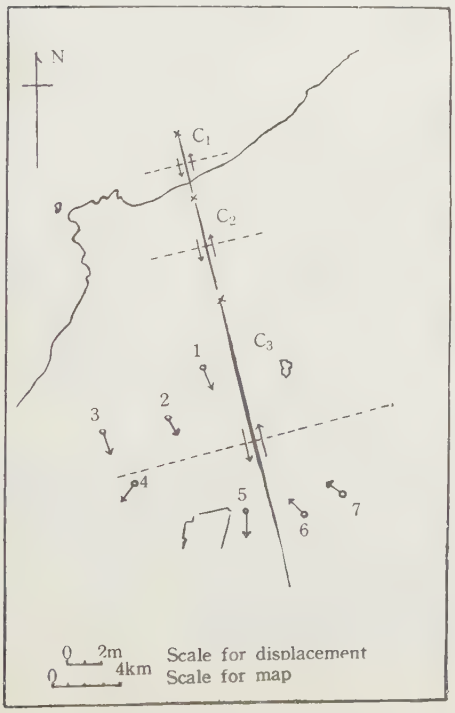

Fig. 6. The horizontal displacements of the crust calculated according to Whipple's model.

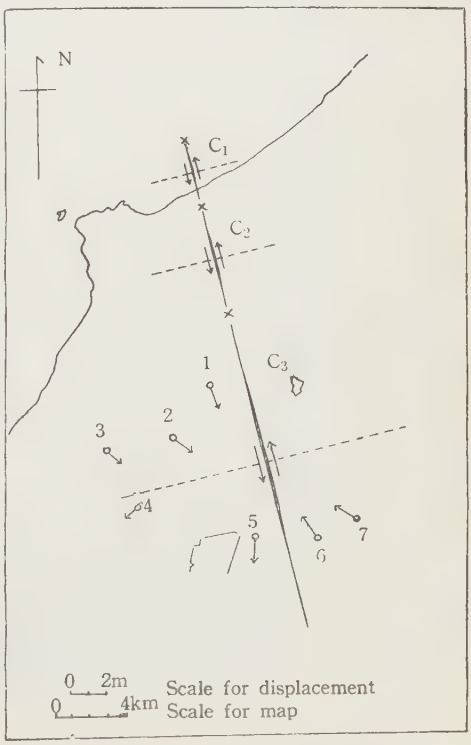

Fig. 7. The horizontal displacements of the crust are calculated just as they are proportional to the length of each crack, in accordance with Whipple's model.

horizontal displacement of the crust which show a distribution to be divided into four quadrants by two straight lines crossing at the centre of each crack are indicated in Figs. 5, 6 and 7.

In Figs. 5 and 6 are shown the above-mentioned results based on Honda-Miura's or Whipple's model, respectively. Furthermore, Fig. 7 shows the resultant displacement calculated according to Whipple's forces-model, assuming that each horizontal displacement is proportional to the length of each crack. So far, we cannot but say that it is of great interest to find that these calculated values of the horizontal dislocation of the crust are in satisfactory agreement with the actually surveyed ones. In these figures as well as in subsequent figures, each mark × represents the starting point of crack-formation. Now, when we compare these figures with the corrected one (**5**) (see Fig. 4) of the horizontal dislocation of the crust near the focus (as determined by geodesic survey after the Fukui Earthquake), we shall find a fairly good agreement between the trend of the horizontal dislocations as shown in Fig. 7 and that of actual dislocations shown in Fig. 4.

Considering that the standard points of survey are immovable, and various errors exist together with the inequality of geological structure, and that the horizontal dislocations are naturally added before and after the earthquake, it may be taken for granted that there exists such a disagreement as shown between Figs. 7 and 8.

Furthermore, let us apply the latter model (that is, Whipple's forces-model, horizontal displacement being proportional to the crack-length) to interpretations about the crustal dislocations after the Kita-Izu and Kita-Tango Earthquakes, respectively. Analyzing the ground-motion of p-waves due to the Kita-Izu Earthquake of November 26, 1930, such as observed at Kumagaya, we suppose the mechanism of its occurrence as composed of a series of three cracks C_1, C_2, C_3 which were horizontally formed in such turns as shown by suffixes 1, 2, 3 at the focal region with sizes (8, 15, 5 km), the directions, and the space intervals drawn in Fig. 8.

When we compose the displacement-vectors at each station which are estimated to be produced by each crack, we shall be able to obtain the result shown in the same figure. If we compare Fig. 8 with Fig. 9 (**6**) which represents the horizontal dislocations of the crust actually determined by a geodesic survey after the earthquake, we may be satisfied with good agreement in the trends of both the size and the direction of crustal dislocation.

Lastly, let us deal with the data of the Kita-Tango Earthquake of March 7, 1927. In the same way, analyzing the wave-form of the ground-motion of p-waves due to the earthquake, such as observed at Kôchi, we can grasp an outline of the horizontal dislocation of the crust near the focal region by dint of combining a series of three cracks C_1, C_2, C_3 along the N 29° W nodal line and a series of three cracks C_4, C_5,

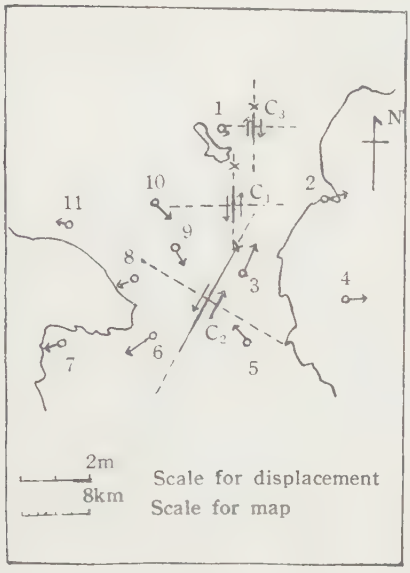

Fig. 8. The horizontal displacements of the crust calculated according to the same model as explained in Fig. 7. (The Kita-Izu Earthquake)

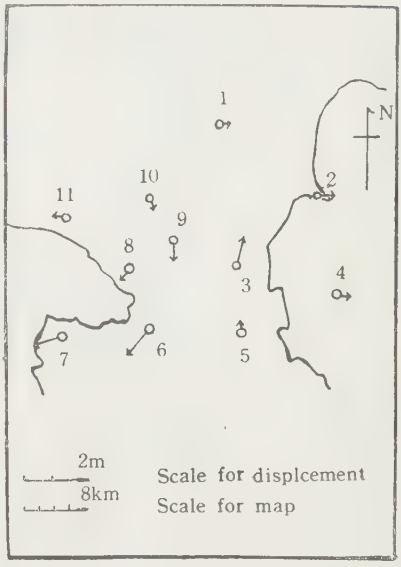

Fig. 9. The horizontal dislocations of the crust actually surveyed after the Kita-Izu Earthquake of November 26, 1930. (After Dr. C. Tsuboi)

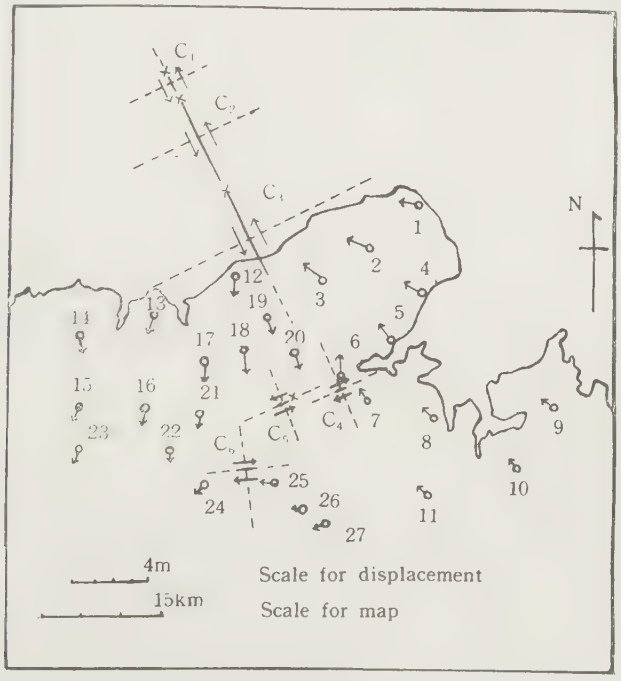

Fig. 10. The horizontal displacements of the crust calculated according to the same model as explained in Fig. 7. (The Kita-Tango Earthquake)

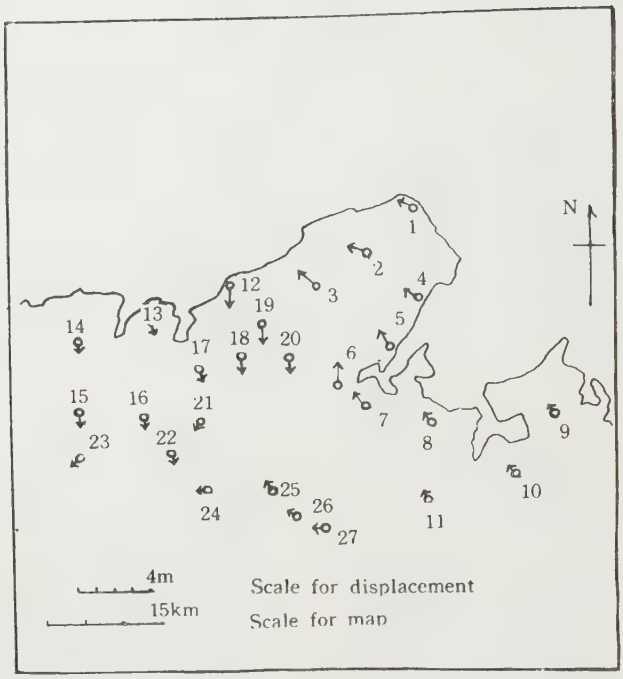

Fig. 11. This map shows the horizontal dislocations of the crust, actually surveyed after the Kita-Tango Earthquake of March 7, 1927. (After Dr. C. Tsuboi)

C_6, seemingly perpendicular to the former series; and all of them have such sizes, directions and intervals as mainly shown in Fig. 10. Thus, the result shown in Fig. 10 will be obtained by composing the horizontal displacement-vectors (by each crack) calculated according to the last forces-model.

If we compare this result with that (shown in Fig. 11) (**7**) of the actual dislocations determined by the geodesic method after the earthquake, we shall be unable to notice any remarkable difference between the computed result and the actual one.

3. Crack-length and seismic wave energy

Each crack-length estimated at the focal region of each large-scale earthquake reported in the preceding paper is described again in the third column of Table I.

Next, we shall calculate each order of seismic energy estimated from the crack-length. According to Jeffrey's or Bullen's consideration about the crack formed at the focus, the order of seismic energy released in the wave-form may be represented as Kl^2 ergs (**8**), when their so-called pseudotachylite is not formed along the shearing plane. Here l indicates the length of a crack in km, and K is taken as $K=4\times 10^{19}$. Of course, we must have a greater value for K than 4×10^{19} according to their

Table I.

Large-scale earthquake	Magnitude	Length of crack (horizontal)	Energy released in seismic waves in earthquake	
			Calculated from Kl^2	Calculated from formula (1)
Kita-Tango (Mar. 7, 1927)	7.6	34 km	4.6×10^{22} ergs	3.6×10^{22} ergs
Kita-Izu (Nov. 26, 1930)	7.3	28	3.1×10^{22}	1.3×10^{22}
Tottori (Sept. 10, 1943)	7.4	29	3.4×10^{22}	1.8×10^{22}
Tônankaidô (Dec. 7, 1944)	8.0	42	0.7×10^{23}	1.3×10^{23}
Nankaidô (Dec. 21, 1946)	8.2	46	0.9×10^{23}	2.2×10^{23}
Fukui (Jun. 28, 1948)	7.2	27	2.9×10^{22}	0.9×10^{22}
Tokachi-Oki (Mar. 4, 1952)	8.2_5	49	0.9×10^{23}	2.6×10^{23}

notes in case when the pseudotachylite is formed during the slipping. In other words, it means that the temperature during the slipping is more than 1000°C. The values of seismic energy of each large-scale earthquake calculated according to Kl^2 are given in the fourth column of the same table. On the other hand, the new relation (**9**) between the magnitude and the seismic wave-energy has been recently reported by Gutenberg and Richter as follows:

$$\log E = 9.1+1.75M+\log(9-M)\,. \qquad (1)$$

When a large-scale earthquake occurs, the energy released in the form of seismic waves is calculated by using this formula (1). Thus, the computed results are shown in the fifth column.

It is of great interest that we can find, on the whole, the agreement in the order between the seismic wave energy calculated according to its estimated crack-length and the energy calculated according to its magnitude M. Then, especially, in such cases (Tônankaidô, Nankaidô, and Tokachi-Oki Earthquakes) when the seismic energy calculated according to Kl^2 is less than the energy obtained from its magnitude, we may be able to understand that the pseudotachylite was possibly formed in the slipping and the temperature of the shearing plane was much more than 1000°C. But, considering that the crack-length denoted by l which is determined by Doppler effect is the horizontal component of the actual one which is suitably inclined to the boundary surface (namely, here, the horizontal plane), we shall be able to estimate from Kl^2 the more approximate value of the seismic energy than that shown in the same table. On the other hand, some unavoidable inequality among these values of the seismic energy may be considered to result from the fact that the crack-length occurring at the focus may differ from that of the fault which took place at the Earth's surface. Anyhow, these problems concerning the inclination of crack-line at the focus as well as the mechanism of the occurrence of the above three large earthquakes of Pacific origins will be discussed later on.

4. Summary

In the present paper, the writer re-examined the results reported in the preceding paper, from both sides of the horizontal dislocation of the Earth's crust actually produced by an earthquake and the seismic wave-energy calculated by using an estimated crack-length, and he obtained the approximately satisfactory results. Thus, it may safely be said that the writer has somewhat succeeded in the phenomenological explanation concerning the mechanism of occurrence in a large-scale earthquake. First of all, the azimuthal distribution of the period of the first maximum ground-motion of *p*-waves due to an earthquake should be noticed to be regular and its regularity may be accounted for by considering that the period of the initial ground-motion is modified according to Doppler effect in connection with the movement of seismic source along the growing crack at the focus.

Secondly, the resultant vector obtained by composing (at each triangular point) each crack displacement at the focal region coincides fairly well with what was actually determined by the geodesic survey. Thirdly, it seems to be of great interest that the order of the seismic wave-energy calculated according to the crack-length estimable in connection with the regularity of azimuthal distribution of the above-mentioned period coincides well, on the whole, with that of the seismic energy computed according to Gutenberg and Richter's recently reported relation between the magnitude and the energy of an earthquake.

Judging from the above interpretations on the observed or surveyed results regarding the ground-motion, the crustal dislocation, etc., produced by a large-scale earthquake, the writer cannot but consider the mechanism of occurrence of an earthquake as composed of a series of small cracks.

Acknowledgements

The writer expresses his hearty thanks to Professor K. Sassa for his kind encouragement and sincere guidance throughout the course of this study. The writer's thanks are also due to Professor S. Tomotika for his kind inspection of the manuscript.

Further, the writer expresses his deep gratitude to the director of the Meteorological Observatory of Kyôto District and to the members of its Seismic Section, who kindly offered him special permission to investigate the valuable seismic data preserved there.

REFERENCES

1. N. YAMAKAWA, On the strain produced in a semi-infinite elastic solid by an interior source of stress. Journ. Soc. Japan, **8** (1955), 84-98.
2. H. HONDA and T. MIURA, On the strain produced in a semi-infinite elastic solid by statical surface force, with some applications to seismology. Geophys. Mag. **9** (1935), 73.
3. F. J. W. WHIPPLE, On the theory of the strains in an elastic solid bounded by a plane when there is a nucleus of strain at an internal point, and on the relation of the theory to seismology. M. N. R. A. S. Geophys. Suppl. **3** (1936), 385.
4. S. NAKANO, On the displacement at the surface of a semi-infinite elastic solid in case when the plane containing the so-called Whipple's forces-source has any inclination to its boundary surface. Unpublished manuscript of Graduation Thesis for the Master's Degree in Faculty of Science, Kyôto Univ., (1957).
5. The Special Committee of the Fukui Earthquake, Report of the Special Committee for the Study of the Fukui Earthquake, (1950), 108.
6. C. TSUBOI, Investigation on the deformation of the Earth's crust in Idu Peninsula connected with the Idu Earthquake of Nov. 26, 1930. Bull. Earthq. Res. Inst., **10** (1932), 441.
7. C. TSUBOI, Investigation on the deformation of the Earth's crust in the Tango District connected with the Tango Earthquake of 1927 (Part I.). Bull. Earthq. Res. Inst. **8** (1930), 193.
8. K. E. BULLLEN, On the size of the strained region prior to an extreme earthquake. Bull. Seis. Soc. America, **45** (1955), 45-46.
   H. JEFFREYS, The *Earth*. (3rd ed., Cambridge, 1952), 341.
9. B. GUTENBERG and C. F. RICHTER, Earthquake, magnitude, intensity, energy, and acceleration (Second paper). Bull. Seis. Soc. America, **46** (1956), 134.

Memoirs of the College of Science, University of Kyoto, Series A,
Vol. XXVIII, No. 4, Article 8, 1958

SEISMOMETRIC INVESTIGATION OF THE EARTH'S INTERIOR PART IV. ON THE STRUCTURE OF THE EARTH'S MANTLE (II)

BY

Yoshimichi KISHIMOTO

(Received March 10, 1958)

1. Introduction

In our previous article (**1**), the earthquakes of shallow focus of Kamchatka-Kurile Islands and Formosa were investigated in order to clarify the structure and property of the upper mantle. The time-distance graphs of these earthquakes fitted fairly well to the Jeffreys-Bullen's 1939-Table in the range of from about 9° up to 26°. This result suggests that the structure of the upper mantle near Japan accords with that deduced from the J.-B. Table, except the uppermost part, probably down to about 100 km below the earth's surface.

In order to investigate the structure of this uppermost part, the time-distance graph of the shallow earthquake up to about 10° should necessarily be treated. And this problem, namely the time-distance graph of the shallow earthquake at short distances, has been investigated by many authors.

According to Gutenberg, *Pn*-branch extends up to about 5° with the velocity of 8.1~8.2 km/sec, and breaks off at that point, being followed by the diffracted wave of low apparent velocity (**2**). Jeffreys stated that *Pn* at short distances had the velocity of 8.0 km/sec in the case of the Burton-on-Trent Explosion in 1944 (**3**). On the other hand, Lehmann (**4**) investigated some North American earthquakes of shallow focus and obtained the result that *Pn*-branch extended up to about 14° with the velocity of 8.2 km/sec and thence ran parallel to the J.-B. surface focus curve, which probably suggests the constant velocity of *Pn*-wave down to some considerable depth. And the writer obtained previously 8.1 km/sec as the *Pn*-velocity at short distances in Japan (**5**).

Thus, recent investigations have almost consistently given 8 km/sec or more as the velocity of *Pn* at short distances. This suggests that the *P*-velocity at the mantle's surface is 8 km/sec or more. But we have not yet reached a coincident opinion as to the velocity-distribution thereafter, namely, there remain the problems whether or not the low-velocity layer exists, or how far that layer extends if existing, and etc. On this problem, Nishitake (**6**) has recently suggested a possibility of the existence of

the low-velocity layer by means of combining the rock experiments with the theoretical treatments.

In the present article, the time-distance graphs up to about 10° in the case of Japanese earthquakes of shallow focus were treated in some detail for the purpose of investigating the structure of the uppermost part of the mantle, and accordingly finding a connection between two data by us mentioned above, namely, the *Pn*-velocity of 8.1 km/sec at short distance and the good fit of the structure to the Jeffreys-Bullen's one in the considerable depths.

2. Data

The data used in the present analysis are seven normal earthquakes which are tabulated in Table 1. These earthquakes are favourable due to the followlng reasons; namely, they have considerably large observable distances and each of their foci is nearly in the same direction seen from the observatories in Japan, which minimize the variation of the gradient of time-distance graph by the small shift of epicenter. The epicenters and the time-readings of these earthquakes are after the Seismological Bulletin published by the Japan Meteorological Agency.

Table 1. List of the normal earthquakes used in the present investigation. All data are after the Japan Meteorological Agency, except the origin times and some of focal depths. * shows the earthquakes used in our previous article, Part II.

No.	Date	Origin time (G.M.T.)	Epicenter		Focal depth	Magnitude
		h m s	N	E	km	
1	1929 May 21*	16 35 32	31.°8	131.°8	<30	—
2	1939 March 20	03 22 26	32.°4	131.°8	<30	6.8
3	1948 June 28*	07 13 29	36°08′	136°17′	<20	7¼
4	1951 Oct. 15*	21 02 01	32.°8	134.°3	40~50	—
5	1951 Oct. 18	08 26 28	41.°4	142.°1	40	—
6	1955 July 27	01 20 50	33.°75	134.°3	<20	—
7	1957 June 12	08 28 37	41.°1	142.°9	40	6.1

3. Treatment and results

We shall consider the deviations of the travel-times of *P*-wave from the corresponding J.-B. Table, in order to determine the shape of the time-distance graph. As regards *S*-wave, the observations showed so large scattering of time-reading that the deduction of the reliable result was impossible. Consequently, the present analysis was obliged to analyse the *P*-wave only.

The earthquake of June 12, 1957 (No. 7 in Table 1), whose focal depth was about 40 km, gave us fairly good observations. As this focal depth corresponds to just below the Mohorovičić discontinuity, the J.-B. 0.00 Table was preferably applied. In Fig. 1,

the deviations (O–C) of the observed travel-times of *P*-wave (O) from the J.-B. 0.00 Table (C) are plotted, taking 08h28m37s as the origin time.

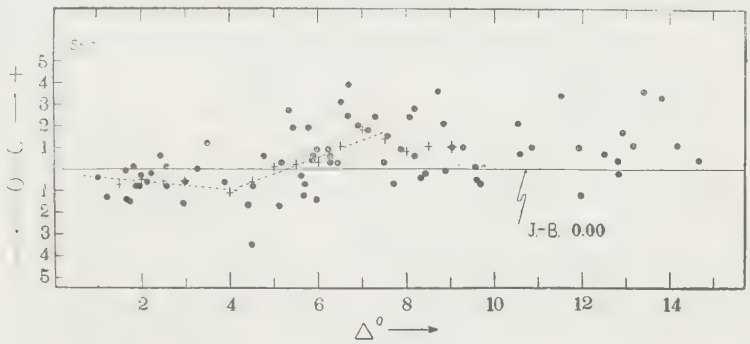

Fig. 1. The deviation graph of the earthquake of June 12, 1957.

The plotted points thus obtained are considerably scattered, because of uncertainty of time determination for small amplitude of refracted *Pn*-phase. But the large part of them, excepting anomalous ones, shows a tendency to cluster in a band of about 3 sec-breadth. Consequently, in the present treatment, the anomalous points which deviate more than 2 sec from the running mean in every 1°-distance were reasonably excluded. As seen in Fig. 1, which is thus corrected as above-remarked and in which the cross is the running mean in every 1°-distance after this correction, O–C decreases gradually up to epicentral distance of about 3.5° and reaching the minimum at this distance (this distance will tentatively be called the minimum-distance in the followings). O–C increases up to about 7.5° (this will be called the recovery-distance in like manner) and thence runs nearly parallel to the J. B. curve with the same value as at the recovery-distance or even slightly less.

The earthquake of October 18, 1951 (No. 5 in Table 1) occurred in the same epicentral region as one mentioned above and its focal depth was also estimated as

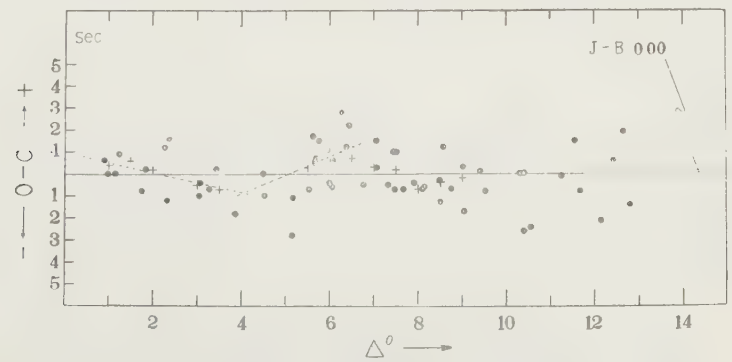

Fig. 2. The deviation graph of the earthquake of October 18, 1951.

about 40 km. Its deviation graph, which is samely corrected as in Fig. 1, is shown in Fig. 2, and moreover that correction will be made also in Figs. 3. 4 and 5. Fig. 2 shows nearly the same behaviours of deviation as in the case of the earthquake of June 12, 1957. In this case, the minimum- and recovery-distances were estimated as about 4° and 6.5° respectively.

The earthquake of July 27, 1955 (No. 6 in Table 1) was investigated by A. Kamitsuki (**7**). Its focus is considered to lie in the granodioritic layer (**5**). In Fig. 3, the deviation graph is shown, taking the J.-B. surface focus Table. The *Pn*-branch is observed from about 2.5° as the first arrival, which seems reasonable referring to such a shallow focal depth as in this case. In the range of from 2.5° up to 5.5°, the deviation decreases gradually followed by the slight increase from 5.5°.

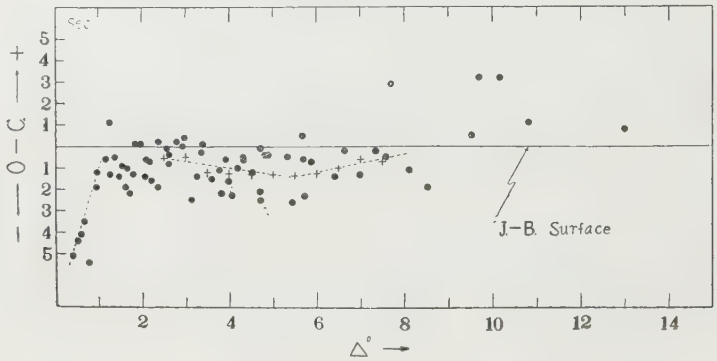

Fig. 3. The deviation graph of the earthquake of July 27, 1955.

Lastly, Figs. 4 and 5 show the corrected deviation graphs of two earthquakes of May 21, 1929 and March 20, 1939, the former of which was analysed in our previous article (**5**), in which the focus of the former was estimated to lie in the crust. As seen in both figures, the tendencies of deviation with distance show nearly the

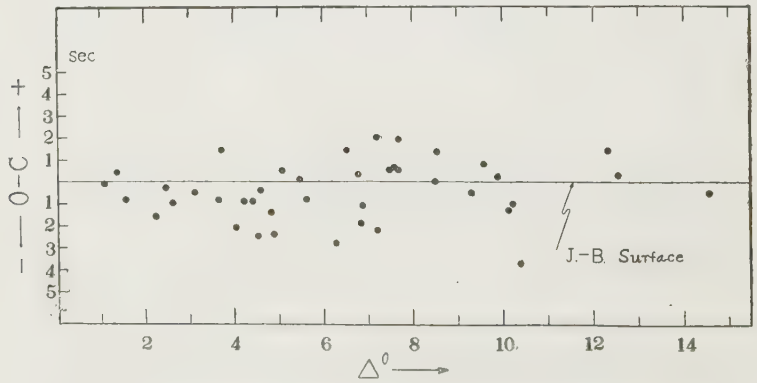

Fig. 4. The deviation graph of the earthquake of May 21, 1929.

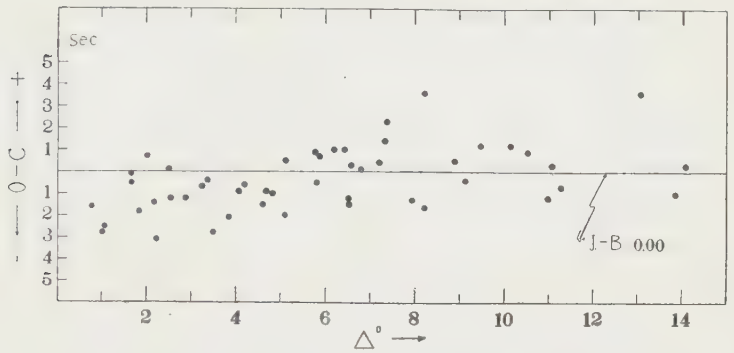

Fig. 5. The deviation graph of the earthquake of March 20, 1939.

same behaviours in both cases. The minimum- and recovery-distances are 4° and 7.5° for the former, and 3.5° and 7.5° for the latter respectively.

Thus, it was clarified that, if the focus lies in the crust or at not so great depth below the Mohorovičić discontinuity, the deviation of the travel-time of *Pn*-wave from the corresponding J.-B. Table shows a systematic distribution, namely, the slopes of the gradual decrease up to the minimum-distance and of the gradual increase from the minimum-distance up to the recovery-distance, and the interval between both distances, are nearly the same. Consequently, since this tendency is not likely to be the errors of observation, the time-distance graph at short distances (0°-10°) for the Japanese normal earthquake should be corrected for the J.-B. Table by the above-stated deviation graph.

Unfortunately, however, as each graph shows some fluctuations of observation and has not sufficient number of observation, we are obliged to use any statistical treatment. For this reason, the 'grouping method' was applied in like manner as used in our pervious article (8). Fig. 6 is the superposed deviation graph thus obtained of earthquakes in Table 1 except one of October 18, 1951, allowing for the differences in

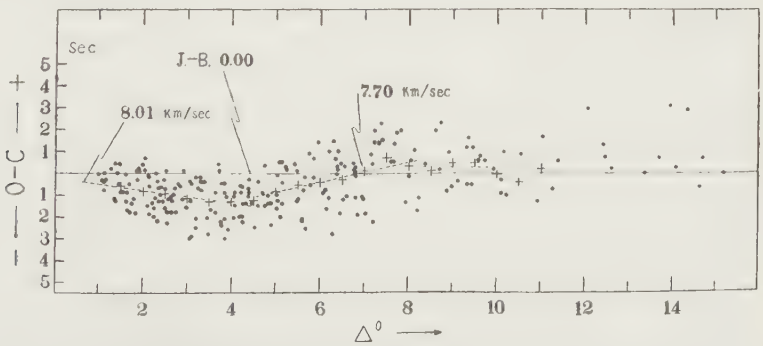

Fig. 6. The superposed deviation graph of six earthquakes listed in Table 1, except one of October 18, 1951.

the beginning distance of the *Pn*-branch due to the differences of focal depths of these earthquakes. In this process the earthquake of October 18, 1951 was omitted owing to its too fast arrival times beyond about 8°. In this figure, the crosses show the running means in every 1°-distance. The method of least squares was applied to two branches represented by the running means, namely, one is up to 4° and the other from 4.5° up to 7.5°. The results are as follows:

8.01 km/sec up to 4°,
7.70 km/sec from 4.5° up to 7.5°.

Consequently, the followings will be concluded as for the time-distance curve at short distances (0°–10°) of the Japanese normal earthquakes. The *Pn*-branch has the velocity of 8.0 km/sec up to about 4° with breaking off at that distance. The apparent velocity is very small, namely about 7.7 km/sec, at range between about 4° and 7.5°, and thenceforth the time-distance curve runs nearly parallel to the J.-B. 0.00 curve with no gap at 7.5°. Needless to say, the minimum- and recovery-distances will differ slightly from the values obtained just above, owing to the variations of the focal depth and the crustal structure. But the difference is within about 1°, and the slopes of the respective branches and the interval between both the minimum- and recovery-distances are kept unchangeable, as mentioned earlier.

4. Discussion

The writer examined previously (**1**) the Gutenberg's low-velocity layer in the mantle. And it was ascertained that at the epicentral distance from about 9° up to beyond 20° the time-distance graph of shallow earthquake fitted fairly well to the J.-B. Table for both *P*- and *S*-waves and the effect of the low-velocity layer was not observed. But at shorter distances the reliable conclusion was impossible owing to the lack of data.

As mentioned in § 3, 8.0 km/sec was obtained as the *Pn*-velocity at shorter distances, and this value coincides fairly well with our previous results (**5**) and with the values having been obtained by many authors. The *Pn*-branch breaks off at about 4°, and up to about 7.5° the apparent velocity is very small. At larger distances than about 7.5°, the time-distanc graph seems to run nearly parallel to the J.-B. curve, and this result coincides well with that in our previous article (**1**), namely, the fitness to the J.-B. curve beyond about 9°, as mentioned above.

The break of the *Pn*-branch at about 4° and the decrease of the apparent velocity thereafter seem to accord with Gutenberg's result (**2**) that the *Pn*-branch breaks off at about 5° and thence the diffracted wave-branch of low apparent velocity begins. But both cases differ in the point that our branch of low apparent velocity breaks at about 7.5°, although Gutenberg's diffracted wave extends up to about 12°. And the

apparent velocity of the so-called diffracted wave-branch was 7.7 km/sec in the present case, compared with 7.74 km/sec in Gutenberg's result.

These facts may suggest that the low-velocity layer exists also near Japan, but, if existing, it is of small scale as to the range of depths of existence compared with that in North America. In order to examine this problem, we treated time-distance graphs of some slightly deeper earthquakes, which are shown in Table 2. In Figs. 7 and 8, the deviation graphs of two earthquakes of July 17, 1952 and September 29, 1955

Table 2.

No.	Date	Origin time (G.M.T.)	Epicenter N	Epicenter E	Focal depth	Magnitude
		h m s			km	
1	1952 July 17	16 09 51	34°27′	135°49′	70	7 (Pasa.)
2	1953 Feb. 6	13 13 03	42.°0	144.°2	80	—
3	1955 Sept. 29	19 58 27	40.°1	141.°3	90–100	—

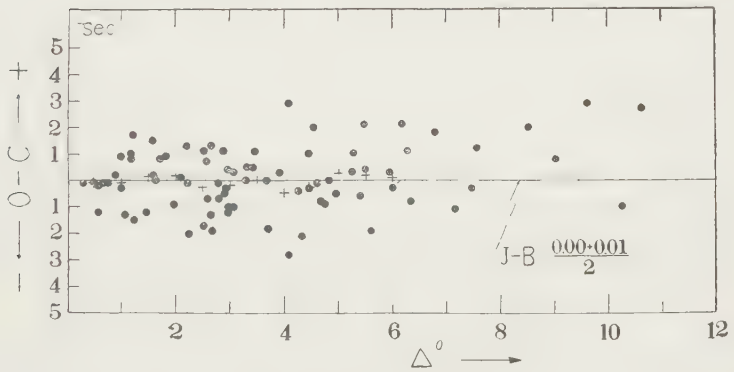

Fig. 7. The deviation graph of the earthquake of July 17, 1952.

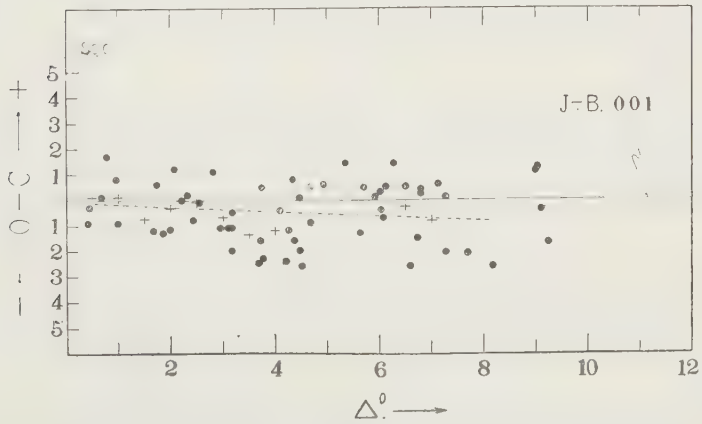

Fig. 8. The deviation graph of the earthquake of September 29, 1955.

are shown. The focal depths of these earthquakes are estimated as 70 km for the former and 90–100 km for the latter. As seen in these figures, their deviation graphs show the parallel running to the corresponding J.-B. curve or the monotonous but slight variation. Namely, the systematic variations of deviation with distance seen in the normal earthquakes are not observed in the case of the earthquakes of the deeper focal depth than about 70 km. If this is the case, the low-velocity layer should reach its minimum velocity at about 70 km, which is shallower compared with that in North America.

Thus, the existence of the low-velocity layer seems to be possible also in Japan, but it is noted that the state of the low-velocity layer, if existing, differs somewhat from those in North America and in Europe (**9**). Accordingly, we may safely presume the regional difference of the mantle's structure down to some considerable depth, including the low-velocity layer.

5. Summary

Seven normal earthquakes were analysed to investigate the structure of the uppermost part of the mantle, including the problem of existence of low-velocity layer. The results arrived at will be summarized as follows:

i) 8.0 km/sec was obtained as the *P*-velocity at the mantle's surface in the present analysis too.

ii) The existence of the low-velocity layer seems possible also in Japan. Accordingly, some parts of Summary in our previous article (**1**) should be corrected. But the state of the low-velocity layer in Japan will, if existing, differ somewhat from that in North America and in Europe, as have been presumed in our previous article cited above.

iii) The structure at deeper part than about 100 km-depth from the surface seems to coincide with that of Jeffreys-Bullen (**10**).

iv) The regional difference in the mantle's structure will be presumed down to some considerable depth, including the low-velocity layer.

Aknowledgment

The writer wishes to express his hearty gratitude to Prof. E. Nishimura for his kind guidance throughout the present investigation. The cost for the present study was partly defrayed by a grant-in-aid for Scientific Research of the Ministry of Education.

REFERENCES

1. Y. Kishimoto, Seismometric investigation of the earth's interior, Part III. On the structure of the earth's mantle (I). Mem. Coll. Science, Kyoto Univ., A, **28** (1956), 117–142.
2. B. Gutenberg, Low-velocity layers in the earth's mantle. Bull. Geol. Soc. Amer., **65** (1954), 337–348.
3. H. Jeffreys, On the Burton-on-Trent Explosion of 1944 November 27. Mon. Not. Roy. Astr. Soc., Geophys. Suppl., **5** (1947), 99–104.

4. I. LEHMANN, The times of P and S in Northern America. Estratto da Annali di Geofisica, **8** (1955), 351–370.
5. Y. KISHIMOTO, Seismometric investigation of the earth's interior, Part II. On the structure of the earth's crust. Mem. Coll. Science, Kyoto Univ., A, **27** (1955), 243–288.
6. T. NISHITAKE, Elasticity at high pressure and the earth's mantle. Mem. Coll. Science, Kyoto Univ., A, (1958), (in press).
7. A. KAMITSUKI, On the seismic waves reflected at the Mohorovicić discontinuity (II). Mem. Coll. Science, Kyoto Univ., A. (1958), (in press).
8. Y. KISHIMOTO, On a 13°-discontinuity of the earth's mantle. Zisin, 2nd Ser., **5** (1951), 7–12 (in Japanese).
9. I. LEHMANN, P and S at distances smaller than 25°. Trans. Amer. Geophys. Union, **34** (1953), 477–483.
10. H. JEFFREYS, The times of P, S and SKS, and the velocities of P and S. Mon. Not. Roy. Astr. Soc., Geophys. Suppl., **4** (1939), 498–533.

INDEX OF AUTHORS TO VOLUME XXVIII

PAGE

Asai, K. (see **Seto, T., Asai, K. Mito, A.**) 1

Harada, K. and **Sakai, T.**—The Effect of Electric Field upon the Structure of Thin Films of Some Dipolar Long-chain Molecules. 283

Hosoyama, K.—On the Observation of Secular Phenomena of the Tilting Motion of Ground. 253

Ichinohe, T.—Study on Change of Gravity with Time. Part III. On the Tidal Factor of Gravity. 11

Kamitsuki, A.—On the Seismic Waves reflected at the Mohorovičić Discontinuity (I) 143

Kishimoto, Y.—Seismometric Investigation of the Earth's Interior (III). 117

Kishimoto, Y.—Seismometric Investigation of the Earth's Interior. Part IV. On the Structure of the Earth's Mantle (II) 391

Kômura, S.—A Consideration about the Mechanism of Occurrence of Large-scale Earthquakes, I. 363

Kômura, S.—A Consideration about the Mechanism of Occurrence of Large-scale Earthquakes, II. 379

Mikumo, T.—Precise Seismometric Observations in the Epicentral Region of Local Shocks. 161

Mito, A. (see **Seto, T., Asai, K.** and **Mito, A.**) 1

Muto, J. and **Okano, K.**—An Electromagnetic Isotope Separator. 337

Nishitake, T.—Elastic Properties of Rocks with Relation to the Earth's Interior. . . 73

Okabe, S.—On Some Relations between the Hot Spring and Radioactivity. 39

Okabe, S.—Time Variation of the Atmospheric Radon Content near the Ground Surface with Relation to Some Geophysical Phenomena. 99

Okabe, S.—On Some Relation between Atmospheric Ions and Natural Radioactivity. 231

Okano, K. (see **Muto, J.** and **Okano, K.**) 337

Sasaki, T. (see **Harada, K.** and **Sasaki, T.**) 283

Seto, T., Asai, K. and **Mito, A.**—On the "Triple Melting" of Tripalmitin. 1

Takahashi, I., Watanabe, T. and **Tanimoto, K.**—Diffraction of Electromagnetic Waves by a Circular Cylinder of Infinite Length. 209

Takahashi, I. and **Watanabe, T.**—Transient Phenomena in the Wave Guide. . . . 221

Takemoto, S.—The Complex Dielectric Constant and Permeability of Ni-Cd Ferrite System at Microwave Frequencies. 327

Tanimoto, K. (see **Takahashi, I., Watanabe, T.** and **Tanimoto, K.**). 209

Watanabe, T. (see **Takahashi, I., Watanabe, T.** and **Tanimoto, K.**) 209

Watanabe, T. (see **Takahashi, I.** and **Watanabe, T.**) 221

Watanabe, T.—Introduction of the Translational Operator in Frequency Domain and Treatment of Certain Linear Differential Equations, I. 293

Watanabe, T.—Introduction of the Translational Operator in Frequency Domain and Treatment of Certain Linear Differential Equations, II. 311

CONTENTS

The Effect of Electric Field upon the Structure of Thin Films of Some Dipolar Long-chain Molecules

By *K. Harada* and *T. Sakai* 283

Introduction of the Translational Operator in Frequency Domain and Treatment of Certain Linear Differential Equations, I.

By *T. Watanabe* 293

Introduction of the Translational Operator in Frequency Domain and Treatment of Certain Linear Differential Equations, II.

By *T. Watanabe* 311

The Complex Dielectric Constant and Permeability of Ni-Cd Ferrite System at Microwave Frequencies

By *S. Takemoto* 327

An Electromagnetic Isotope Separator

By *J. Muto* and *K. Okano* 337

A Consideration about the Mechanism of Occurrence of Large-scale Earthquakes, I.

By *S. Kômura* 363

A Consideration about the Mechanism of Occurrence of Large-scale Earthquakes, II.

By *S. Kômura* 379

Seismometric Investigation of the Earth's Interior. Part IV. On the Structure of the Earth's Mantle (II).

By *Y. Kishimoto* 391

Printed by NIPPON INSATSU SHUPPAN

Fukushima, Osaka